

**PROCESS BEHAVIOR OF FLOWER-LIKE AG-ZNO
MICRO/NANOSTRUCTURES IN UV-VISIBLE LIGHT PHOTOCATALYTIC
AND ANTIBACTERIAL ACTIVITY**

QUEK JIAN AI

**A project report submitted in partial fulfilment of the
requirements for the award of the degree of Bachelor of Engineering
(Hons) Environmental Engineering**

**Faculty of Engineering and Green Technology
Universiti Tunku Abdul Rahman**

May 2017

DECLARATION

I hereby declare that this project report is based on my original work except for citations and quotations which have been duly acknowledged. I also declare that it has not been previously and concurrently submitted for any other degree or award at UTAR or other institutions.

Signature : _____

Name : Quek Jian Ai

ID No. : 12AGB02864

Date : _____

APPROVAL FOR SUBMISSION

I certify that this project report entitled “**PROCESS BEHAVIOR OF FLOWER-LIKE AG-ZNO MICRO/NANOSTRUCTURES IN UV-VISIBLE LIGHT PHOTOCATALYTIC AND ANTIBACTERIAL ACTIVITY**” was prepared by **QUEK JIAN AI** has met the required standard for submission in partial fulfillment of the requirements for the award of Bachelor of Engineering (Hons) Environmental Engineering at Universiti Tunku Abdul Rahman.

Approved by,

Signature : _____

Supervisor : Dr. Lam Sze Mun

Date : _____

The copyright of this report belongs to the author under the terms of the copyright Act 1987 as qualified by Intellectual Property Policy of University Tunku Abdul Rahman. Due acknowledgement shall always be made of the use of any material contained in, or derived from, this report.

© 2017, Quek Jian Ai. All right reserved

ACKNOWLEDGEMENTS

I would like to thank everyone who had contributed to the successful compilation of this research project. I would first like to express my gratitude to my research supervisor, Dr. Lam Sze Mun for the constant and invaluable advice, guidance and her exceptional patience throughout the development of this research. Furthermore, I would also like to thank Dr. Sin Jin Chung for his support for this research.

My sincere gratitude goes towards my university, Universiti Tunku Abdul Rahman (UTAR) specifically the Faculty of Engineering and Green Technology in giving me this opportunity to conduct this research project. In addition, I would also like to thank the lab officers whom had continuously cater to my experiment needs.

Finally, I would like to give my heartfelt gratitude to my family members and friends for their unwavering physical and mental support throughout the duration of this project. I would like to use this opportunity to thank Christina Previtha a/p John Devasahayam, Kee Shin Yiing and Ng Suk Ting for their assistance in experimental works and late nights in the laboratory during this research project.

**PROCESS BEHAVIOR OF FLOWER-LIKE AG-ZNO
MICRO/NANOSTRUCTURES IN UV-VISIBLE LIGHT PHOTOCATALYTIC
AND ANTIBACTERIAL ACTIVITY**

ABSTRACT

Wastewater effluents which contain Fast Green (FG) dye and *Escherichia coli* (*E.coli*) exhibited human health hazards and significant researches were committed toward it. Comprehensive treatment methods were developed and amongst them, heterogeneous photocatalyst integrating silver doped zinc oxide (Ag-ZnO) as potential wastewater treatment. In this study, Ag-ZnO photocatalyst was synthesized with co-precipitation-photodeposition methods. Characterization tests such as field-emission scanning electron microscopy (FESEM), UV-visible diffuse reflectance spectroscopy (UV-Vis DRS) and photoluminescence (PL) analysis were conducted. FESEM analysis identified as-produced Ag-ZnO as 3D micro/nanoflowers structures and UV-Vis DRS analysis identified the reduction in band gap of Ag-ZnO samples. Furthermore, PL analysis revealed Ag attachment onto ZnO had low emission peak. As-synthesized 5.0 wt% Ag-ZnO also exhibited superior photocatalytic degradation of FG dye compared to commercial ZnO, commercial TiO₂, pure ZnO and different Ag loadings of Ag-ZnO under 240 min of UV-Vis irradiation. Moreover, 5.0 wt% Ag-ZnO settled first in the sedimentation test. Initial dye concentration and solution pH were tested for the degradation of FG dye. Under optimized condition of 2.5 ppm FG concentration and natural pH of pH 6.65, complete photocatalytic degradation and mineralization of FG dye was attained under 240 min. The investigation of active species roles had demonstrated that superoxide radicals anions ($\bullet\text{O}_2^-$) and photogenerated holes (h_{VB}^+) played major roles in the photocatalytic reaction, while hydroxyl ($\bullet\text{OH}$) radicals showed a lesser extent. Besides that, antibacterial response screening was also tested under 180 min with 5.0 wt% Ag-ZnO. Under UV-Vis light, 10^7 of *E.coli* colonies were disinfected. Lastly, membrane integrity assay was conducted and its result observed that 5.0 wt% Ag-ZnO produced the highest leakage of DNA absorbance within 180 min under UV-Vis light.

TABLE OF CONTENTS

DECLARATION	ii
APPROVAL OF SUBMISSION	iii
ACKNOWLEDGEMENTS	v
ABSTRACT	vi
TABLE OF CONTENTS	vii
LIST OF TABLES	x
LIST OF FIGURES	xi
LIST OF SYMBOLS	xiv
LIST OF ABBREVIATIONS	xvii
LIST OF APPENDICES	xix

CHAPTER

1.	INTRODUCTION	1
	1.1 Conventional Wastewater Effluents Treatment	1
	1.2 Heterogeneous Photocatalysis	2
	1.3 Problem Statements	3
	1.4 Objectives	4
	1.5 Scope of Study	4
2.	LITERATURE REVIEW	6
	2.1 Wastewater Effluents	6
	2.2 Conventional Methods for Wastewater Effluents	8
	2.3 Advanced Oxidation Processes (AOPs)	10

2.3.1	Fundamental of Heterogeneous Photocatalytic Process	13
2.3.2	Zinc Oxide Properties	14
2.3.2.1	Synthesis of ZnO Micro/nanostructures	16
2.4	Improvement of ZnO via Noble Metal Doping	21
2.5	Effect of Process Parameters	25
2.5.1	Initial Dye Concentration	25
2.5.2	Solution pH	26
2.6	Antibacterial Properties of Ag doped ZnO	28
2.7	Summary	31
3.	RESEARCH METHODOLOGY	32
3.1	Materials and Chemicals	33
3.2	Apparatus	34
3.2.1	UV-Vis Light Irradiation Experiment Apparatus	34
3.3	Analytical Procedures	35
3.3.1	UV-Vis Spectrophotometer Analysis	35
3.3.2	Chemical Oxygen Demand (COD) Analysis	36
3.4	Preparation of Photocatalyst	37
3.4.1	Preparation of ZnO Flower-Like Photocatalyst	37
3.4.2	Preparation of Ag doped ZnO	38
3.5	Characterization of the photocatalyst	39
3.5.1	Crystal Phases Analysis	39
3.5.2	Morphological Analysis	39
3.5.3	Elemental Analysis	39
3.5.4	UV-Vis Absorption Analysis	40
3.5.5	Photoluminescence Analysis	40
3.6	Photoactivity of Photocatalyst under the UV-Vis Light Irradiation	41
3.7	Process Parameters	42
3.7.1	Initial Dye Concentration	42
3.7.2	Solution pH effect	42
3.8	Detection of Radical Species	42
3.9	Antibacterial Studies	43

3.9.1	Preparation of Bacterial Studies	43
3.9.2	Screening for Antibacterial Response	44
3.9.3	Membrane Integrity Assay	44
4.	RESULTS AND DISCUSSION	45
4.1	Characterization of the Photocatalyst	45
4.1.1	XRD Analysis of the Developed Photocatalysts	46
4.1.2	Morphological Analysis	47
4.1.3	Elemental Analysis	49
4.1.4	UV-Vis Absorption Analysis	50
4.1.5	Photoluminescence Analysis	52
4.2	Photoactivity of Photocatalyst under the UV-Vis Light Irradiation	53
4.3	Process Parameters	59
4.3.1	Initial Dye Concentration	59
4.3.2	Solution pH Effect	61
4.4	Mineralization Study	65
4.5	Detection of Free Radicals	66
4.6	Antibacterial Study	69
4.6.1	Screening for Antibacterial Response	69
4.6.2	Membrane Integrity Assay	71
5.	CONCLUSION AND RECOMMENDATIONS	75
5.1	Conclusions	75
5.2	Recommendations	77
	REFERENCES	78
	APPENDICES	105
	PUBLICATION	108

LIST OF TABLES

TABLE	TITLE	PAGE
2.1	The Redox Potential of a Number of Oxidants (Belgiorno, Naddeo and Rizzo, 2011).	11
2.2	The Position of Conduction and Valence Band in Some Common Semiconductor Photocatalyst at pH 1 (Lam, et al., 2012).	12
2.3	Synthesis of ZnO Micro/nanostructures.	19
	Synthesis of ZnO Micro/nanostructures (Continued).	20
2.4	Synthesis of Noble Metal-doped ZnO Micro/nanostructures.	23
	Synthesis of Noble Metal-doped ZnO Micro/nanostructures (Continued).	24
2.5	Effect of Solution pH Parameter on Photocatalytic Degradation of Organic Pollutant.	27
2.6	Photocatalytic Disinfection of Different Photocatalyst towards Diverse Bacteria Species.	29
3.1	List of Chemicals Used.	33
4.1	Comparison Survey of the Degradation of Dye by UV-Vis Light Photocatalysis.	64
4.2	Comparison Survey of the Antibacterial Response of <i>E.coli</i> by UV-Vis Light Photocatalysis.	74

LIST OF FIGURES

FIGURE	TITLE	PAGE
2.1	Chemical Structure of FG (Mittal, Kaur and Mittal, 2009).	7
2.2	The Wurtzite ZnO Crystal Structure (Samadi, et al., 2016).	15
2.3	Photocatalytic Process of MO and Ag-ZnO (Kumar, et al., 2015).	21
2.4	Migration of e_{CB}^- from Ag Nanowires to ZnO (Liu, et al., 2012).	22
3.1	Flowchart of Research Methods Involved in This Study.	32
3.2	Experimental Setup for Photocatalytic Process.	34
3.3	Schematic Diagram of Photocatalytic System Experimental Setup.	35
3.4	Preparation of ZnO Flower-Like Photocatalyst.	37
3.5	Preparation of Ag doped ZnO Photocatalyst.	38
4.1	XRD Patterns of Pure ZnO and Ag-ZnO with Different Ag Doping Loadings. Inset is the Magnified Region of (002) Peak.	47
4.2	FESEM Images under 10,000x Magnification of (a) Pure ZnO, (b) 2.5 wt% Ag-ZnO, (c) 5.0 wt% Ag-ZnO and (d) 10.0 wt% Ag-ZnO.	48
4.3	Schematic Diagram of Proposed Growth Mechanism of	49

Flower-Like ZnO Micro/nanostructures.

4.4	EDX Spectra for (a) pure ZnO, (b) 2.5 wt% Ag-ZnO, (c) 5.0 wt% Ag-ZnO and (d) 10.0 wt% Ag-ZnO.	50
4.5	UV-Vis DRS Spectra Pure ZnO and Ag-ZnO with Different Ag Doping Loadings.	51
4.6	PL Spectra of Pure ZnO and Ag-ZnO with Different Ag Loadings.	53
4.7	Preliminary Photocatalysis Studies Using Various Photocatalytic Conditions ([FG] = 5.0 mg/L; [Photocatalyst] = 1 g/L; pH = 6.65).	54
4.8	(a) Absorption Spectra of Photocatalytic Degradation of FG Dye over Time at Optimized Conditions and (b) Color Change for Photocatalytic Degradation of FG Dye over Time Using 5.0 wt% Ag-ZnO ([FG] = 5 mg/L; pH = 6.65; [5.0 wt% Ag-ZnO] = 1.0 g/L).	56
4.9	Sedimentation Test of Commercial TiO ₂ , Commercial ZnO, Pure ZnO and 5.0 wt% Ag-ZnO over Time.	58
4.10	Effect of Initial Dye Concentration on the Photocatalytic Degradation of FG Dye ([5.0 wt% Ag-ZnO] = 1.0 g/L; pH = 6.65).	59
4.11	Effect of Solution pH on the Photocatalytic Degradation of FG Dye ([5.0 wt% Ag-ZnO] = 1.0 g/L; [FG] = 2.5 ppm).	62
4.12	Photocatalytic Mineralization and Degradation of FG Dye ([5.0 wt% Ag-ZnO] = 1.0 g/L; [FG] = 2.5 ppm; pH = 6.65).	65
4.13	Effect of Radical Scavengers on the Photocatalytic Degradation of FG Dye ([5.0 wt% Ag-ZnO] = 1.0 g/L; [FG] = 2.5 ppm; pH = 6.65).	66

4.14	Schematic Diagram of Proposed UV-Vis Photocatalytic Mechanism of FG Dye over 5.0 wt% Ag-ZnO Photocatalyst.	68
4.15	Screening for Antibacterial Response under (a) Photolysis, (b) Dark Absorption and Photocatalytic Activities with (c) Pure ZnO and (d) 5.0 wt% Ag-ZnO over Time.	70
4.16	Membrane Integrity Assay Analysis under Different Conditions.	71
4.17	Schematic Diagram of Photocatalytic Disinfection Mechanism of <i>E.coli</i> under UV-Vis illumination.	73

LIST OF SYMBOLS

°C	Degree Celsius
μm	Micrometer
•OH	Hydroxyl
2θ	Two Theta
Å	Ångström
Ag	Gold
Ag ⁺	Silver Ions
Ag ₂ S	Silver Sulfide
Ag ₃ PO ₄	Silver Phosphate
Ag-CuO/TiO ₂	Silver Doped Copper Oxide and Titanium Dioxide Composites
Ag-MgO	Silver doped Magnesium Oxide
AgNO ₃	Silver Nitrate
Ag-ZnO	Silver doped ZnO
Ag-ZnO/g-C ₃ N ₄	Silver doped Composite of Zinc Oxide and Graphitic Carbon Nitride
Au-ZnO	Gold doped Zinc Oxide
B	Boron
Bi ₂ WO ₆	Bismuth Tungstate
BiOBr	Bismuth Oxybromide
BiVO ₄	Bismuth Vanadate
BQ	1,4-Benzoquinone
Br	Bromine
CdS	Cadmium Sulphide
Cd-ZnO	Cadmium doped Zinc Oxide
Cl ₂	Chlorine

Co	Cobalt
CO ₂	Carbon Dioxide
Cr(VI)	Hexavalent Chromium
Cu	Copper
CuK α	Graphite Monochromatic Copper Radiation
e_{CB}^-	Electron
E _f	Fermi Energy Level Equilibration
Eu-ZnO	Europium doped Zinc Oxide
eV	Electron Volt
F ₂	Flourine
Fe(III)	Iron (III)
Fe ₂ O ₃	Iron(III) Oxide
h	hour
HO ₂ \cdot^-	Hydroperoxyl
H ₂ O ₂	Hydrogen Peroxide
HNO ₃	Nitric acid
HOCl	Hypochlorous Acid
$h\nu$	Energy
h_{VB}^+	Reactive Hole
KI	Potassium Iodide
L	Liter
M	Mol
min	Minute
M Ω ·cm	Megaohm·centimeter
Na ⁺	Sodium Ions
NaBiO ₃	Sodium Bismuthate
NaCl	Sodium Chloride
NaOH	Sodium Hydroxide
nm	Nanometer
NO ₃ $^-$	Nitrate Ions
O	Oxygen Element
O ₂	Oxygen gas
O ₂ \cdot^-	Superoxide Radicals Anions

O ₃	Ozone
OH ⁻	Hydroxyl Ions
Pa	Pascal
Pd	Palladium
PdO	Palladium Oxide
Pd-ZnO	Palladium doped Zinc Oxide
Pt	Platinum
Se-ZnO	Selenium doped Zinc Oxide and Graphitic Carbon Nitride
SiO ₂	Silicon Dioxide
SnO ₂	Tin Dioxide
Sn-ZnO	Tin doped Zinc Oxide
Ta-ZnO	Tantalum doped Zinc Oxide
TiO ₂	Titanium Dioxide
TiO ₂ /ZnO	Composite of Titanium Dioxide and Zinc Oxide
W	Watt
WO ₃	Tungsten Trioxide
WO ₃ -Ag-ZnO	Dual Tungsten Trioxide and Silver doped Zinc Oxide
Zn	Zinc Element
Zn(NO ₃) ₂ ·6H ₂ O	Zinc Nitrate Hexahydrate
Zn ²⁺	Zinc Ions
ZnO	Zinc Oxide
ZnO/SiC	Zinc Oxide and Silicon Carbide Composite
ZnS	Zinc Sulfide
ZrO ₂	Zirconium Dioxide

LIST OF ABBREVIATIONS

1D	One Dimensional
2D	Two Dimensional
3D	Three Dimensional
Ag	Silver
AOPs	Advanced Oxidation Processes
BOD	Biochemical Oxygen Demand
CB	Conduction Band
CE	Cellulose Acetate
COD	Chemical Oxygen Demand
DI	Distilled Water
DNA	Deoxyribonucleic Acid
<i>E.coli</i>	<i>Escherichia Coli</i>
EDCs	Endocrine Disrupting Chemicals
EDX	Energy Dispersive X-Ray
Eq.	Equation
FD&C	Food, Drugs and Cosmetic
FEGT, UTAR	Faculty of Engineering and Green Technology, Universiti Tunku Abdul Rahman
FESEM	Field-Emission Scanning Electron Microscopy
FG	Fast Green
IWA	International Water Association
JCPDS	Joint Committee on Powder Diffraction Standards
LD ₅₀	Lethal Dose 50
MB	Methylene Blue
MeO	Methyl Orange

MO	Mordant Orange
NPs	Nanoparticles
pH _{pzc}	pH in Point Zero Charge
PL	Photoluminescence
PPCPs	Pharmaceutical And Personal Care Products
QreC	Quality Reagent Chemical
RhB	Rhodamine B
ROS	Reactive Oxygen Species
SCR	Space-Charge Region
USD	United States Dollar
USM	University Sains Malaysia
UV-Vis	Ultraviolet-Visible
UV-Vis DRS	UV-Visible Diffuse Reflectance Spectroscopy
VB	Valence Band
VOCs	Volatile Organic Compounds
wt. %	Weight percent
XRD	X-Ray Diffraction

LIST OF APPENDICES

APPENDIX	TITLE	PAGE
A	National Water Quality Standards.	105
B	Malaysian Environmental Quality (Industrial Effluents) Regulation 2009 Fifth Schedule [Paragraph 11(1)(a)].	106
C	Calibration Curve on the FG Dye at Natural pH.	107

CHAPTER 1

INTRODUCTION

1.1 Conventional Wastewater Effluents Treatment

According to the International Water Association (IWA), it was projected nearly 7 million m³/year of wastewater effluents would be produced in Malaysia by 2020 (Ujang and Henze, 2006). These effluents produced in Malaysia were required to comply with the Environmental Quality Act 1974 to protect the economic resource potentials, viable aquatic ecosystem, public health and welfare before released to environment. Wastewater effluents contaminated with high concentration of synthetic dyes and harmful bacteria were required to be treated before released to the environment. Synthetic dyes and harmful bacteria were reported to cause human health deterioration and permanent environmental damage (Amin, Hameid and Elsttar, 2010; Kornacki, 2010; Ghaly, et al., 2013). The elimination of these wastewaters was vital to ensure safe and healthy environment.

There were many conventional methods for wastewater treatment and were categorized into three main parts such as physical, biological and chemical. Each of these methods varied in treating wastewater effluent. The physical methods were used to transfer the contaminant from liquid phase to solid phase. Examples of conventional physical methods include adsorption, coagulation and flocculation, sedimentation, and filtration (Lewinsky, 2007). Biological methods differed by using microbial activities for its treatment processes and involve majorly in aerobic and anaerobic system (Erkurt and Arshad, 2010), while chemical methods deal with chemical reactions such as ion exchange treatment, electrochemical, chemical

disinfections and advanced oxidation processes (AOPs) (Nawaz and Ahsan, 2014; Cheremisinoff, 2002).

In recent times, AOPs had gain credit as a promising treatment for wastewater as it was able to mineralize dye molecules into harmless and simple molecules by producing hydroxyl ($\bullet\text{OH}$) radicals (Belgiorno, Naddeo and Rizzo, 2011). Generated $\bullet\text{OH}$ radicals were able to remove large amount of different chemical form of micropollutants at a shorter time as it has a high reaction constants of 10^9 L/mol.s (Tokumura, et al., 2016). AOPs had the edge in dye treatment technologies as many conventional methods were not able to degrade recalcitrant pollutant and have limitation of mass transfer due to usage of solid adsorbent (Chakma, Das and Moholkar, 2015).

1.2 Heterogeneous Photocatalysis

Heterogeneous photocatalysis process was progressively recognized as an important subpart of the AOPs techniques as it had the ability for destruction of water-soluble organic in low concentration (Cheng, et al., 2016). In the heterogeneous photocatalyst process, semiconductor materials such as zinc oxide (ZnO), titanium dioxide (TiO_2) and cadmium sulphide (CdS) was illuminated by solar, ultraviolet (UV), visible light or ultraviolet-visible (UV-Vis) to promote the electron from valence band (VB) to conduction band (CB) in order to produce positively charged hole. The positive charged hole will then react with water and produce $\bullet\text{OH}$ radicals. The reactive radicals would then degrade the targeted pollutant.

As stated by Ariffin and Sulaiman (2015) approximately 72% of the 473 Malaysian rivers monitored by the Department of Environment were identified as high polluted. Therefore in Malaysia, heterogeneous photocatalyst process can be greatly optimized as it had a high effectiveness against a broad range of pollutants. Heterogeneous photocatalyst was identified as an ideal treatment for hazardous, refractory and non-biodegradable pollutants by Parsons (2004).

1.3 Problem Statements

Identification of the model pollutant and bacterium need to be address in this study. Fast Green (FG) dye was identified as the model pollutant as it was hazardous and it affected humans' health due to its carcinogenic, teratogenic and mutagenic traits (Li, et al., 2015a). This particular dye triggered eye and skin irritation and acted as neurotransmitter inhibition. The model bacterium was recognized to be *Escherichia Coli* (*E.coli*). *E.coli* was able to cause hazardous health problems such as diarrhea and gastroenteritis upon consumption.

In order to remove contaminants, heterogeneous photocatalyst was suggested and ZnO was chosen as its semiconductor as it reaped more benefits compared to TiO₂. ZnO had similar band gap energy with TiO₂. It was also able to absorb a wide range of solar spectrum and more quanta of light with a cheaper cost compared to TiO₂ in a large scale wastewater treatment (Lee, et al., 2016). However, its limitation to fast recombination of reactive hole (h_{VB}^+) and electron (e_{CB}^-) pair required to be fixed (Gomez-Solis, et al., 2015).

With such limitation, doping technique was required and ZnO was doped with a noble metal as it was able to extend light absorption, create interaction with visible light, facilitate charge carriers, hinder recombination of electron-hole pairs and improve charge separation thus improving the photocatalytic performance. Silver (Ag) was chosen as the noble metal dopant due to its traits as stable, non-toxic and economical with the highest electrical conductivity among all noble metals (Liu, Wei and Gao, 2015).

Usage of sunlight irradiation and its correlation in this study was needed to be done to see its environmental feasibility. In the energy distribution of solar spectrum, around 54.3%, 38.9% and 6.8% of the sunlight at earth were located approximately at the near infrared (760-3000 nm), visible (400-760 nm) and UV (less than 400 nm) respectively according to Cui, et al. (2015). With the high light harvesting efficiency by noble metal doped semiconductor, the photocatalysis process can be done under the sun which was an inexhaustible and free source. In Malaysia, there was an

average of 6 h per day of sunshine according to Ahmad et al., (2013) and thus usage of sunlight for photocatalysis process would be feasible in Malaysia.

1.4 Objectives

The specific objectives are:

1. To synthesize 3-dimensional (3D) micro/nanostructure flower-like Ag-doped ZnO using a co-precipitation-photodeposition method.
2. To characterize the chemical, physical and optical properties of synthesized photocatalyst using various characterization techniques.
3. To evaluate UV-Vis degradation of FG dye using the developed photocatalyst.
4. To examine antibacterial activities of as-synthesized photocatalyst towards *E.coli*.

1.5 Scope of Study

The scope of study involved the photocatalyst preparation, photocatalyst characterization, photocatalyst photoactivity, process parameters, detection of radical species, antibacterial activities. The preparation of ZnO in flower-like shape will be done using co-precipitation method and its Ag metal-doping technique was done with photodeposition method. The characterization analyses of photocatalyst will be performed to examine the physical-chemical properties of the developed photocatalyst. Each of these characterization analyses will help in determination of the effectiveness and ineffectiveness of photocatalyst. Under the influence of UV-Vis

light irradiation, the performance of photocatalyst will also be examined. Using FG dye degradation, each process variable such as initial dye concentration and optimum pH was selected based on reports in literature and through process of trial and error. The detection of radical species allowed the monitoring of the radical reaction within the FG dye. Examination of screening for antibacterial response and membrane integrity assay will be conducted towards *E.coli* to determine its antibacterial property.

CHAPTER 2

LITERATURE REVIEW

2.1 Wastewater Effluents

In this 21st century, water is an important natural resource in the world and its scarcity would cause frightening challenges for the growing 7 billion populations on Earth. The growing concern of clean water availability had amplified the significance of contaminants removal from wastewater. In Malaysia, this growing concern was applied through Environmental Quality Act 1974 which regulated the wastewater standard for discharge into environment.

Wastewater effluents which consist of hazardous pathogens and synthetic dye components in high concentration would not be able to comply with the Environmental Quality Act and needed to be treated before released. Wastewater effluents had optimum conditions for bacteria to grow and reproduce quickly with available nutrients (Spellman, 2011). Bacteria present in the wastewater were mostly pathogenic towards human and can be transmitted by waterborne route to cause enteric infection. Examples of these infections were typhoid fever, cholera and shigellosis (Bitton, 2005). *E.coli* was a prominent pathogenic bacteria present in the wastewater and it represented as the model bacterium in this study. Its traits were such as Gram-negative, short, rod-shaped bacterium and difficult to be manage as it had high acid tolerance. A Gram-negative bacterium had thin peptidoglycan cell

walls made up of polysaccharide backbone (Zyoud, et al., 2016). *E.coli* was also a remarkable bacterium to be used for studies as it was readily accessible, benign and able to grow readily on chemically defined media (Berg, 2004). It was a motile bacterium where it would swim to a favorable environment for survival. As reported by Kornacki (2010) and Hales (2015), *E.coli* infections such as gastroenteritis, neonatal meningitis, severe bloody diarrhea, kidney failure had costs USD \$300 to USD \$700 million annually in the United States.

Besides that, wastewater effluents were caused by an estimation 5 to 10% of dye discharged to the environment (Yang, et al., 2016). Synthetic dyes would stain the surrounding environment and block sunlight penetration into water surface thus increasing the biochemical oxygen demand (BOD) of the receiving waters (Ghaly, et al., 2013).

FG dye was tested as it was able to represent the model pollutant for dyed wastewater. It was widely used in candy coating, ice creams, drinks, toothpaste, health care and skin care products as they retained a brilliant color. FG was chemically known as the 4,4'-bis-(N-(ethyl-3-sulphobenzyl)-amino-2-sulpho-4-hydroxy-fuchsonlum with a molecular formula of $C_{37}H_{34}N_2O_{10}S_3Na_2$ and molecular weight of 808.86 g/mol. The chemical structure of FG was shown as below.

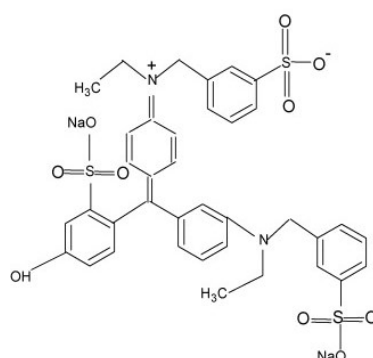


Figure 2.1: Chemical Structure of FG (Mittal, Kaur and Mittal, 2009).

According to Tahir, et al. (2010), they identified that FG was highly toxic as it caused eye and skin irritation including irritation in the upper respiratory tract. Besides that, it also acted a presynaptic locus which inhibited the release of neurotransmitter in animal or human nervous system. According to a study done by Amin, Hameid and Elsttar (2010), FG was able to alter vital organs' functions such as liver and kidney at low dosage in *Rattus Norvegicus sp.* albino rats. Due to its high toxicity, the European Union countries had prohibited its edible use in the food, drugs and cosmetic (FD&C) industries. Wastewater was often measured using the interim national water quality standards shown in Appendix A to classify itself in the classes of contaminant levels (Department of Environmental Ministry of Natural Resources and Environment, 2012).

2.2 Conventional Methods for Wastewater Effluents

Conventional treatments for these effluents were categorized into three parts which were physical, chemical and biological. Each of these methods varied in effectively effluent treatment.

Physical treatment method did not involve any chemical and biological transformation of the effluents. They were normally used prior to the biological and chemical treatment to reduce the interference of pollutant to the next system (Alley, 2007). Examples of the physical dye treatment methods were adsorption, coagulation, flocculation, sedimentation and filtration (Lewinsky, 2007). In an adsorption study done by Lin, et al. (2016), microsphere adsorbent based on monochloroacetic acid modified epichlorohydrin cross-linked carboxymethyl cellulose was used to adsorb 50 mg/L of Orange II and methylene blue (MB) dyes and showed that 98.54% of MB and 83.07% of Orange II was desorbed within 20

min. For bacterial treatment, Lemma, et al. (2016) had proposed nylon-6 nanofibrous membrane technology which resulted in to reduction of 6.6 log unit of *Flavobacterium jonsoniae sp.* but had a sharp increase of flow resistance as filter bed was clogged after retrieving 50 mL filtrate. Despite its high elimination percentage, the treatment operation period require 18 months for improved efficiency of filter bed. Physical treatment may not be practical as bacteria and dyes were noxious in nature and transfer of dye from a liquid to solid phase might create secondary pollutants (Asano, Burton and Leverence, 2007).

Biological treatments can be described as treatments which used microbial activities to convert pollutants to carbon dioxide (CO₂), water and energy. The biological treatments were separated into two different methods which were aerobic and anaerobic. Examples of the microorganisms used in this effluent treatment were fungi and bacteria. As reported by Chandrasena, et al. (2014), the reduction of *E.coli* from storm water was 1.7 log unit of *E.coli* via biofilters made of *Leptospermum continentale sp.* plant. The biofilters systems however were dependent on the weather where its performance was reduced during dry period due to high transpiration losses. On the contrary, bacterial anaerobic treatment done by Cao, et al. (2013) showed that *Shewanella oneidensis sp.* was able to remove 0.1 mmol/L methyl orange (MeO) dye at 35 °C in pH 7 after 1.5 h. The study showed that anaerobic treatment was dependent on the temperature and pH. Biological treatment was not suitable treatment for wastewater as they present many factors to consider.

Another treatment method which involved chemical reaction was chemical treatment. Examples of chemical treatment were ion exchange treatment, electrochemical method and AOPs. A study conducted by Akhigbe, Ouki and Saroj (2016) showed that fixed bed system using Ag modified zeolite was able to remove *E.coli* completely after 570 min of operation but was stopped after 7920 min due to bed clogging. Meanwhile, 100% elimination of 20 ppm of MeO was done via

electrochemical flow-cell in 150 min by Redha, et al. (2017). The complete elimination was conducted using 37.5 kWh/m³ of electrical energy, similar to the electrical consumption of a sludge handling operation plant (Milazzo, 1979). According to Nawaz and Ahsan (2014), these methods were quick, effective and compact but not economical due to high chemical and operation cost with complex sludge generation. Among these chemical treatment methods, AOPs had gained prominence as treatment system in urban wastewater treatment after the imposition of European Union Council Directive 91/271/EEC which wastewater collecting and treatment system after the 31st of December 2005 were obliged to use AOPs in their treatment facilities (Lofrano, 2012).

2.3 Advanced Oxidation Processes (AOPs)

AOPs were a chemical treatment process which were able to mineralize pollutants into simple, relatively harmless and inorganic molecules by producing highly reactive •OH radicals. Its major conversion were visualized as carbon into CO₂, hydrogen to water, nitrogen to nitrates, phosphorus to phosphates or phosphoric acids, sulphur to sulphates and halogen to halogen acids as stated by Belgiorno, Naddeo and Rizzo (2011). AOPs can be applied in drinking water, wastewater, air and solid treatment which consist of contaminants such as herbicides, pesticide, volatile organic compounds (VOCs), endocrine disrupting chemicals (EDCs), pharmaceutical and personal care products (PPCPs) and taste and odor causing compound (American Water Works Association and American Society of Civil Engineers, 2012; Moussavi, et al., 2014; Qian, et al., 2016; Xiang, Fang and Shang, 2016; Antonopoulou, et al., 2014). •OH radicals were used in AOPs as they were powerful oxidant, highly reactive, thus short-lived and relatively a non-selective electrophilic oxidizing agent along with ease of production under natural water

conditions (Suzuki, Araki and Yamamoto, 2015). Table 2.1 showed the redox potential of oxidants and $\bullet\text{OH}$ shown was the second highest thermodynamic oxidation potential after F_2 .

Table 2.1: The Redox Potential of a Number of Oxidants (Belgiorno, Naddeo and Rizzo, 2011).

Oxidant Name	Oxidant Symbol	Redox potential, V vs NHE
Flourine	F_2	3.03
Hydroxide radical	$\bullet\text{OH}$	2.80
Ozone	O_3	2.07
Hydrogen Peroxide	H_2O_2	1.78
Hypochlorous acid	HOCl	1.49
Chlorine	Cl_2	1.36

According to Cheng, et al. (2016), AOPs can be divided into four techniques for generation of $\bullet\text{OH}$ radicals such as Fenton oxidations, photocatalysis, plasma oxidation and ozonation. Photocatalysis were focused as they had gained popularity in treating wastewaters. Photocatalysis was explained as a photoreaction acceleration process with the presence of photocatalyst. Heterogeneous photocatalysis was a subpart of the photocatalysis process. It was a process where semiconductors in Table 2.2 illuminated under UV or solar irradiation in contact with an oxidizing agent would produce e_{CB}^- that form reactive $\bullet\text{OH}$ radicals and superoxide radicals anions ($\text{O}_2^{\bullet-}$). $\text{O}_2^{\bullet-}$ radicals would further produce more $\bullet\text{OH}$ radicals when in contact with water. This photocatalysis process was viewed as the most promising environmental remediation technology as it can harness solar power in the form of solar photons (Cheng, et al., 2016). With solar harnessing ability, heterogeneous photocatalysis will become an economically viable process particularly in large-scale aqueous-phase application (Borges, et al., 2016).

According to Rodríguez, et al. (2016), usage of solar energy would also reduce the overall environmental impact of dye treatment process.

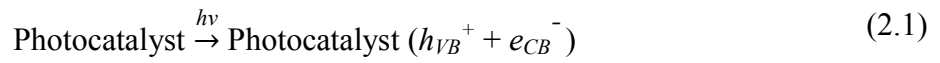
AOPs were remarked as an attractive alternative as they were capable to remove recalcitrant organic compounds, mineralize pollutants into harmless molecules and less susceptible to toxic chemical stated by Belgiorno, Naddeo and Rizzo (2011). Heterogeneous photocatalyst gained its momentum in the wastewater treatment process as it was able to perform in ambient temperature and pressure, complete oxidation of pollutant, reuse photocatalyst and use solar photon for photocatalyst. Despite its advantages, heterogeneous photocatalyst had problems with their electron-hole pair recombination which reduced its photocatalytic degradation efficiency (Malato, et al., 2009).

Table 2.2: The Position of Conduction and Valence Band in Some Common Semiconductor Photocatalyst at pH 1 (Lam, et al., 2012).

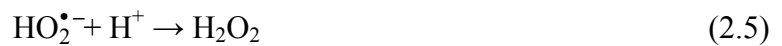
Semiconductors	VB (V vs NHE \pm 0.1 V)	CB (V vs NHE \pm 0.1 V)	E_g (eV)
ZrO ₂	+ 4.0	- 1.0	5.0
SnO ₂	+ 4.1	+ 0.3	3.8
ZnS	+ 1.4	- 2.3	3.7
ZnO	+ 3.0	- 0.2	3.2
TiO ₂	+ 3.1	- 0.1	3.2
WO ₃	+ 3.0	+ 0.2	2.8
CdS	+ 2.1	- 0.4	2.5
Fe ₂ O ₃	+ 2.9	+ 0.6	2.3

2.3.1 Fundamental of Heterogeneous Photocatalytic Process

Heterogeneous photocatalytic process can be explained from the start when semiconductors adsorb light irradiation with equal or greater energy ($h\nu$) than semiconductor band gap energy. This photon absorption process was also known as charge-carrier generation. It will create an excitation and transfer the e_{CB}^- from the VB to CB which would lead to the generation of h_{VB}^+ in VB as shown in the Eq. (2.1) (Samadi, et al., 2016; Lam, et al., 2012).



After charge-carrier generation step, the charge-carrier trapping process would begin by having h_{VB}^+ and e_{CB}^- pair trapped by its scavengers. Recombination of the h_{VB}^+ and e_{CB}^- pair should be inhibited as it would lead to the reduction of photocatalytic process. The positive h_{VB}^+ acted as a strong oxidant that can oxidize dye with bacteria and react with electron donors such as water, hydroxyl ions (OH) to form $\bullet\text{OH}$ radicals. On the contrary, the trapped e_{CB}^- will be scavenged by oxygen (O_2) as an electron acceptor and produce $\text{O}_2^{\bullet-}$ which would further lead to formation of $\bullet\text{OH}$ radicals together with hydroperoxyl ($\text{HO}_2^{\bullet-}$) and hydrogen peroxide (H_2O_2). The whole process was illustrated from Eqs. (2.2) till (2.6).



If charge-carrier recombination happened in the second step, heat would be produced as shown in Eq. (2.7) due to competition between h_{VB}^+ and e_{CB}^- with charge transfer.



Finally, photocatalytic degradation would occur where the $\bullet\text{OH}$ radicals will decompose the harmful compound such as bacteria and recalcitrant dyes to harmless product as presented in Eq. (2.8). Photocatalyst would return to the same amount as before addition to the system after contact with O_2 as displayed in Eq. (2.9).



2.3.2 Zinc Oxide Properties

ZnO was an outstanding photocatalyst for wastewater treatment among an array of semiconductors provided in Table 2.2. This was because of its unique physical and chemical properties such as its adjustable morphologies, high reaction activity, biocompatibility, thermal stability and non-toxicity (Samadi, et al., 2016; Cao, Chen and Qi, 2015). Besides that, it also had a wide direct band gap of ~ 3.2 eV at room temperature and large exciton binding energy of near to 60 meV.

Crystal structure of ZnO existed in rock-salt, wurtzite and zinc-blende. Though there were three types of crystal structure, wurtzite was normally present at ambient temperature and pressure. Figure 2.2 shows the wurtzite ZnO crystal structure. The Zn-O bonds possessed a strong ionic bond thus making ZnO an ionic and a covalent compound (Jagadish and Pearton, 2006). The coordination of the wurtzite ZnO would be responsible for crystal growth and defect generation. Figures 2.2a and b showed the top view of the structure, respectively ZnO primitive unit cells which were bordered with thicker black lines while the blue and red pyramid

and triangle shape shows that one zinc (Zn) atoms were attached to three oxygen (O) atoms.

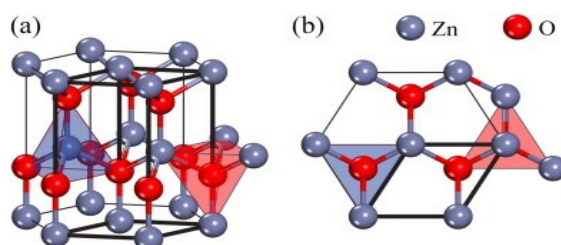


Figure 2.2: The Wurtzite ZnO Crystal Structure (Samadi, et al., 2016).

ZnO was used as an innovative and lower cost alternative compared to most employed photocatalytic semiconductor such as TiO_2 (Fatin, et al., 2012). According to Paschoalino, et al. (2012), ZnO was reported to be more efficient than TiO_2 in visible light photocatalytic degradation process of certain organic or chlorinated compounds in aqueous solution. The reason was because ZnO had the ability to absorb a wider range of the solar spectrum and more quanta of light with a threshold of 425 nm (Lee, et al., 2016).

Examples of the application of ZnO in water purification were real textile effluent, tannery sludge and biomedical waste. As reported by Souza, et al. (2016), ZnO had 96.98 % of chemical oxygen demand (COD) reduction of real textile effluent with irradiation time of 300 min. The photocatalytic degradation of real textile effluent was aided with 250 W mercury vapor lamp at pH 3.0. At the same time, ZnO had a degradation efficiency of 86 % of 250 mg/L of green hexavalent chromium (Cr(VI)) ions produced in tannery industry under 180 min of 500 W UV lamp irradiation (Liu, et al., 2016a).

While in biomedical waste study done by Zijno, et al. (2015), it was reported that ZnO nanoparticles (NPs) promoted more reactive oxygen species compared to TiO₂ NPs to reduce equivalent amount of Caco-2 cells. The principal downside of ZnO was its fast recombination of photogenerated charges (Gomez-Solis, et al., 2015).

2.3.2.1 Synthesis of ZnO Micro/nanostructures

Synthesis of different ZnO micro/nanostructures forms were manipulated for better photocatalytic reaction towards wastewater effluents. The photocatalytic activities of ZnO were dependent on surface-volume ratio and porosity of the active layer (Chang, et al., 2013). The increase in surface-to-volume ratio and porosity of active layer would increase the movement of e_{CB}^- transfer from semiconductor to oxidize dye molecules (Lam, et al., 2012). The study of Lai, Meng and Yu (2010) stated that higher surface area would reduce recombination of h_{VB}^+ and e_{CB}^- pairs as mean free path was reduced to micro/nanoscale and h_{VB}^+ and e_{CB}^- pair could easily travel to ZnO surface for photocatalysis reaction. Therefore, morphology modification with higher surface-volume ratio was required to counter the drawback of charge carrier recombination problem.

There were three types of micro/nanostructures of ZnO such as one dimensional (1D), two dimensional (2D), and three dimensional (3D). First, 1D ZnO micro/nanostructures were non-toxic and chemically stable (Chu and Liu, 2008). Examples of micro/nanostructures of 1D ZnO were rod-like, wire-like, helix-like, micro/nanoneedles, micro/nanocombs and belt-like (Panda and Tseng, 2012; Amornpitoksuk, et al., 2012). Kayaci, et al. (2014) tested needle-like 1D ZnO under the growth condition of dynamic vacuum condition with 18.8 μM of MB in 60 min

of 300 W UV light exposure resulted 47% of MB degradation only. Furthermore, a degradation efficiency of 62% of MB was also reported in Lee, et al. (2015) study with the aid of 20 W black light using rod-like 1D ZnO structures in 240 min. In spite of its merits, production of 1D ZnO micro/nanostructure often had restricted growth conditions such as temperature, pressure, atmosphere and substrates (Udom, et al., 2013).

Alternatively, 2D ZnO micro/nanostructures combine unique sheet-like morphology and porous structures to increase their potential in photodegradation efficiency compared to the 1D ZnO structure (Huang et al., 2011). Examples of 2D ZnO micro/nanostructures were micro/nanosheet, dendrite-like, pellet-like and micro/nanoplates (Tonezeer, et al., 2015; Al-Hardan, et al., 2012). The improved photocatalysis efficiency was due to its micro/nanometer-scale thickness and enhanced adsorption capability which allowed acceleration of photogenerated h_{VB}^+ and e_{CB}^- pairs separation (Liu, et al., 2016b). According to Liu, et al. (2016c), the degradation of 40% of phenol in 120 min with simulated solar light aid using 2D nanosheet ZnO had a better photocatalytic activity compared to ZnO NPs as ZnO nanosheets provided direct electrical pathways which accelerated the electron transport of photogenerated charges.

3D ZnO micro/nanostructures were created with combination of numerous assembled 1D and 2D ZnO micro/nanostructures as building blocks. Examples of 3D ZnO micro/nanostructures shape were coniferous urchin-like, flower, snowflakes and dandelion (Kurbanov, et al., 2016). As stated by Lu, et.al. (2011), the 3D flower-like ZnO had a better photocatalytic activity compared to 2D plate-like ZnO as 3D flower-like ZnO absorbed more O_2 due to widen space-charge region (SCR). With wider SCR, the photogenerated h_{VB}^+ and e_{CB}^- pairs were separated easily and thus the recombination of photogenerated charge carrier would be reduced. 3D ZnO micro/nanostructures also exhibited excellent photocatalytic activities as they had

larger surface area which led to higher availability of active sites (Cui, et al., 2014). Miao, et al. (2016) showed that rhodamine B (RhB) was almost degraded with efficiency of 99.19% within 45 min under UV light irradiation using rose-like 3D ZnO micro/nanostructure composed of micro/nanosheets ZnO. The high photocatalytic activity of the rose-like ZnO was due to its high void and interspaces presence which increased its surface area and was able to facilitate rapid diffusion of RhB molecules with ZnO. Zhang, Jiang and Shi (2014) also proved that 3D ZnO had higher photocatalytic performance of 60% compared to 2D ZnO as 3D ZnO had high stability against aggregation. Higher stability against aggregation characteristic allowed ZnO to be uniformly dispersed in the pollutant, thus increasing the contact of pollutant with ZnO NPs for photocatalytic activity. In short, 3D was preferred as it had wide SCR, large surface area and high stability against aggregation.

Synthesis of 3D ZnO can be done via hydrothermal (Cauda, et al., 2014), solvothermal (Yang, et al., 2011), co-precipitation (Huang, et al., 2012), sol-gel (Kanukaran, Rajeswari and Gomanthisankar, 2011) and template method (Liu, et al., 2016c). The co-precipitation method was chosen in this study as it was more cost effective, does not need sophisticated equipment, versatile and environmental friendly compared to other synthesis methods. A study done by Bordbar, et al. (2016) presented that co-precipitation would produce ZnO with lower band gap energy of 2.47 eV compared to hydrothermal (3.08 eV) and sonochemical (2.97 eV). Lower band gap permitted fast excitation of e_{CB}^- via UV-Vis irradiation which lead to increase of photocatalytic performance. The co-precipitation produced ZnO with lower photoluminescence spectra among hydrothermal and sonochemical which indicated low recombination rate between photogenerated h_{VB}^+ and e_{CB}^- pairs. Chen, et al. (2011) discovered that co-precipitation method had a 94.59% photodegradation efficiency compared to sol-gel method (86.21%) and hydrothermal (85.29%) towards MeO due to its production of small crystalline size ZnO. Table 2.3 would show the various syntheses of ZnO micro/nanostructures with different methods.

Table 2.3: Synthesis of ZnO Micro/nanostructures.

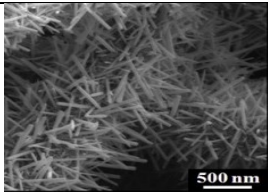
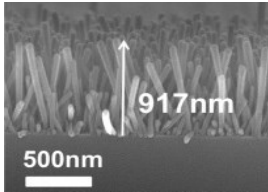
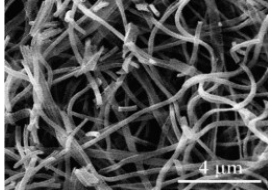
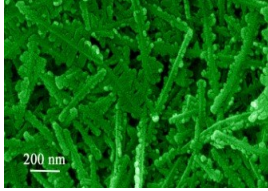
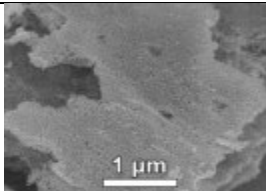
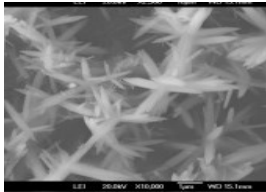
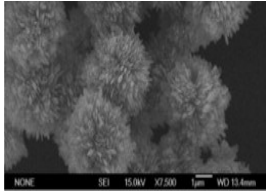
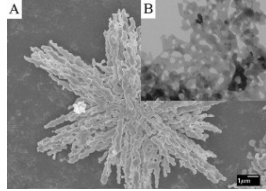
Structure Morphology	Method	Pollutant	Light Source	Treatment time (min)	Degradation (%)	FESEM/SEM	References
Nanoneedle (1D)	Atomic Deposition Layer seeds via hydrothermal	MB	300 W UV light	60	47		Kayaci, et al. (2014)
Nanorods (1D)	Seed coating and hydrothermal growth	MB	20 W black light	240	62		Lee, et al. (2015)
Nanotubes (1D)	Electrospinning	RhB	20 W UV light	180	90		Dong, et al. (2016)
Fern-like leaves (2D)	Ultrasonic	MeO	High pressure mercury lamp	180	100		Ma, et al. (2015)

Table 2.3: Synthesis of ZnO Micro/nanostructures (Continued).

Structure Morphology	Method	Pollutant	Light Source	Treatment time (min)	Degradation (%)	FESEM/SEM	References
Nanosheet (2D)	Colloidal templating	Phenol	Simulated solar light	120	40		Liu, et al. (2016c)
Flower like (3D)	Sonochemical	MB	UV light	120	100		Yu, et al. (2015)
Flower like hierarchical (3D)	Hydrothermal	RhB	UV light	50	100		Zhou, et al. (2015)
Snowflake-like multi-layered (3D)	Hydrothermal	MeO	Sunlight	210	100		Jing, et al. (2012)

2.4 Improvement of ZnO via Noble Metal Doping

ZnO had a problem with fast recombination of h_{VB}^+ and e_{CB}^- pair and it could be countered using doping method as it aided ZnO in surface area variation, lattice defects generation and band gap energy change (Bechambi, Najjar and Sayadi, 2016). Doping of ZnO can be done with noble metal, transition metal oxides, rare earth metal non-metal or metal oxide (Li, et al., 2015b). Noble metal was chosen as they act as electron sink (Chamjangali and Boroumand, 2013).

Examples of noble metal such as gold (Au), Ag, palladium (Pd) and platinum (Pt) can be used to extend the light absorption with intense interaction of visible light and facilitate charge carriers creations when doped with ZnO (Liu, Wei and Gao, 2015; Lin, et al., 2014). With higher interaction of visible light and photocatalyst which further increase the facilitation of charge carriers, the photocatalytic reactions could increase.

Figure 2.3 below showed the photocatalytic process between the pollutant such as mordant orange (MO) and Ag doped ZnO (Ag-ZnO). This explained electron excitations from VB to CB were easily trapped by Ag NPs (Kumar, et al., 2015).

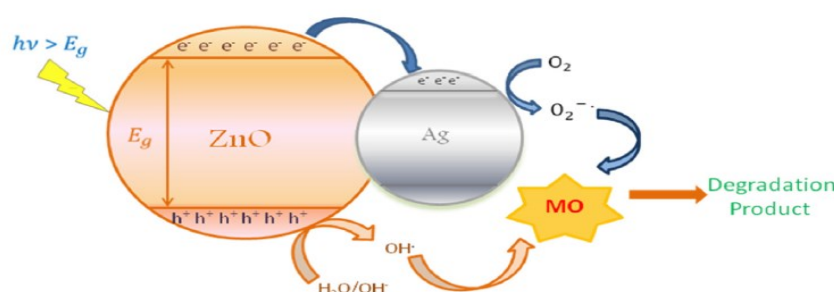


Figure 2.3: Photocatalytic Process of MO and Ag-ZnO (Kumar, et al., 2015).

Figure 2.4 depicted the migration of e_{CB}^- from Ag nanowires to ZnO. As shown in figure, the bottom energy level of the CB was higher than Fermi energy level equilibration (E_f) so potential energy would drive e_{CB}^- from Ag nanowires to ZnO. The figure concluded that Ag acted as an electron sinks and was able to reduce recombination of photoinduced e_{CB}^- , thus prolonged the lifetime of photogenerated h_{VB}^+ and e_{CB}^- pairs.

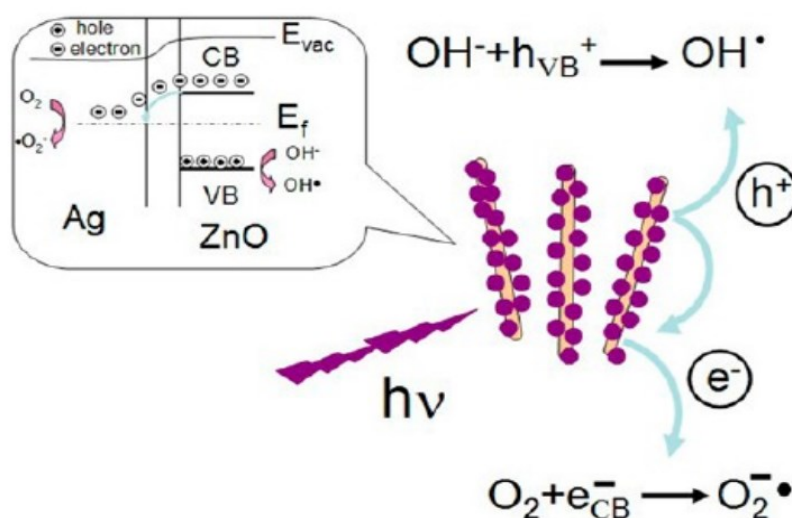


Figure 2.4: Migration of e_{CB}^- from Ag Nanowires to ZnO (Liu, et al., 2012).

Ag metal was suitable to be used as a dopant. As stated by Liu, Wei and Gao (2015), Ag was a stable, non-toxic, cheapest and had highest electrical conductivity among all noble metals which would help in the photocatalytic properties of ZnO. Ag-ZnO can be done with photodeposition (Kuriakose, et al., 2014; Deng, et al., 2012), co-precipitation (Yildirim, Unalan and Durucan, 2013), self-assembly (Zhang, et al., 2010) and ultrasonic (Liu, et al, 2012). The simple and cost effective photodeposition method that utilized sunlight irradiation was chosen. The synthesis of the noble metal doped ZnO can be seen in Table 2.4.

Table 2.4: Synthesis of Noble Metal-doped ZnO Micro/nanostructures.

Noble Metal	Structure Morphology	Method	Pollutant	Light Source	Treatment time (min)	Degradation (%)		References
						Doped ZnO	Pure ZnO	
Ag	Pompon-like nanocomposites	Heterothermal and photodeposition	MeO	8 W light tube and high pressure mercury lamp	120	99.1	57.9	Cheng, et al. (2013)
Ag	Porous flower-like	Hydrothermal and Photodeposition	RhB	500 W Xenon and high pressure mercury lamp	120	79	21	Liang, et al. (2015)
Ag	Spindle – like heterostructures	Surface modification	MB	15 W UV and high pressure mercury lamp	60	83.5	43.2	Zhang, et al. (2014)
Au	Cobblestone-like	Mild Non-aqueous	RhB	16 W UV light tube	150	100	55	Hou (2015)
Au	Natural flower like	Double Impregnation	Phenol	Simulated solar light	120	77.5	2.5	Silva, et al. (2014)

Table 2.4: Synthesis of Noble Metal-doped ZnO Micro/nanostructures (Continued).

Noble Metal	Structure Morphology	Method	Pollutant	Light Source	Treatment time (min)	Degradation (%)		References
						Doped ZnO	Pure ZnO	
Au	Porous coral-like	Hydrothermal	Orange II	400 mL tubular quartz reactor	180	87.4	82.1	Chen, et al. (2013)
Pd	Nanocomposites	Solvothermal	RhB	300 W high pressure mercury lamp	15	82.3	63.1	Zhang, et al. (2012)
Pd	Nanoparticles	Sol-Gel	MeO	300 W high pressure mercury lamp	60	48.2	30.2	Zhong, et al. (2012)
Pd	Nanoplates	Hydrothermal and borohydride reduction	Congo Red	100 W UV light	60	98.2	53.1	Güy, Çakar and Özacar (2016)
Pt	Nanoparticles	Direct precipitation	Nitrate	400 W high pressure mercury lamp	240	69.5	18.5	Shojaei and Golriz (2015)
Pt	Nanoparticles	Sol-Gel	Malachite green	300 W Xenon lamp	15	100	14	Mohamed, et al. (2016)
Pt	Nanoparticles	Solvothermal	MB	125 W high pressure mercury vapor lamp	120	99	75	Muñoz-Fernandez et al. (2016)

2.5 Effect of Process Parameters

Photodegradation of wastewater was influenced by several parameters such as initial dye concentration and solution pH. Investigation of the parameters needed to be done to ensure optimum photocatalytic process and operating condition for dye concentration reduction in the environment.

2.5.1 Initial Dye Concentration

In many literature reports, concentration of the initial dye had a detrimental outcome on the photocatalytic degradation efficiency (Aguilar, Garvín and Ibarz, 2016; Khaparde and Acharya, 2016; Sinha, Ahmaruzzaman and Bhattacharjee, 2014). As reported by Kusic, Koprivanac and Bozic (2013) concentration affects the absorbance of dye.

Example of initial dye concentration effect for Ag-ZnO photocatalyst was degradation of MeO concentration of 5 mg/L to 20 mg/L with catalytic loading of 0.3 g/L at pH 7. Efficiency of MeO degradation decreased when initial MeO concentration increase as disclosed by Chamjangali and Boroumand (2013). Another example of initial dye concentration effect was degradation of nonylphenol concentration in range of 2 mg/L to 7 mg/L with 1 g/L of ZnO at pH 8 showed that higher concentration of nonylphenol decrease degradation percentage (Bechambi, Najjar and Sayadi, 2016). This was due to the presence of high amount of dye pollutants blocking the active site of photocatalyst as stated by Mohamed, et al. (2016). The fixed amount active sites of the photocatalyst can accommodate a limited amount of dye molecules. This competition among the dye pollutant would happen (Lee, et al., 2016). Thus, the degradation efficiency would reduce if the amount of substrates was high as fewer •OH radicals will be available to degrade the dye molecules.

2.5.2 Solution pH

The pH of the dye would affect the photocatalyst degradation. This was because different semiconductors had their own optimum pH to work efficiently in the photocatalytic process. In Table 2.5, research works on the optimum pH were done using different photocatalysts.

Adjustment of the solution pH determines its absorption capacity and degradation efficiency of the substrates under similar conditions. The reason was attributed to dissociation species of the substrate, acidic-basic properties and the surface charge of the photocatalyst changes (Li, et al., 2016a). According to Rauf, Meetani and Hisaindee (2011), the dye adsorption was at minimum when the pH of the photocatalyst was at isoelectric charge or zero point charge. If the photocatalyst surface was at lower than isoelectric charge, the surface will be positively charged and vice versa when the photocatalyst surface was higher than isoelectric point, the surface was negatively charged.

The attraction of negatively and positively charges would promote better photocatalytic adsorption of the semiconductor surface and dye particles. If the semiconductor surface was positive and protonated, it would attract negative charged pollutant while negative semiconductor surface would attract positive charged pollutant (Zhang, et al., 2016a). Isoelectric point can be measure in pH and it was known as pH in point zero charge (pH_{pzc}). It can also be measured using pH drift method where pH of final value and pH of initial value intersected and the pH_{pzc} was shown (Bechambi, Najjar and Sayadi, 2016). Thus, the pH_{pzc} and the nature of the dye should be known to ensure optimum photocatalytic process.

Example of reports that showed photocatalyst worked best in acidic solution done by López-Muñoz, et al. (2016). They found that arsenic (III) degrade at 79% efficiency at pH 3 using TiO_2 and 150 W mercury lamp as acidic pH created positively charged TiO_2 surface which would promote the uptake of produced negatively charged arsenic (III) ions due to attraction of both charges.

Table 2.5: Effect of Solution pH Parameter on Photocatalytic Degradation of Organic Pollutant.

Photocatalyst	Pollutant	Light Source	Treatment time (min)	pH range	Optimum pH	Degradation (%)	References
Ag ₃ PO ₄	Orange II	350 W Xenon lamp	150	3 - 9	9	88.16	Li, et al. (2016a)
Ag-CuO/TiO ₂ heterostructure	2,4-Dinitrophenol	Simulated solar light irradiation	70	3 - 7	5	95.8	Zhang, et al. (2016b)
Ag-ZnO	Trypan Blue	Sunlight / UV light	120	2 - 10	10	100	Ravishankar, et al. (2016)
Bi ₂ WO ₆	RhB	300 W Xenon arc lamp	120	3.2 – 12.5	3.2	90	Zhou, et al. (2016)
Bismuth oxybromide	Ibuprofen	500 W Xenon lamp	120	2 - 12	12	100	Li, et al. (2016b)
BiVO ₄	Ibuprofen	300 W Xenon arc lamp	40	2 - 9	4.5	90	Li, et al. (2016c)
NaBiO ₃	Bisphenol A	500 W halogen lamp	60	3 - 9	3	99	Ding, Zhou and Tang (2016)
TiO ₂	Ciprofloxacin (antibiotic)	15 W UV lamp	120	3 - 9	9	90	Salma, et al. (2016)
TiO ₂	Arsenic (III)	150 W mercury lamp	180	3 - 9	3	79	López-Muñoz, et al. (2016)
ZnO/SiC composite	Phenol	500 W tungsten halogen lamp	240	2 - 12	6.65	90	Meenakshi, et al. (2016)

Besides that according to Li, et al. (2016b), bismuth oxybromide (BiOBr) worked best in alkaline ibuprofen of pH 12 with a degradation percentage of 100% under 120 min aided with 500 W of xenon lamp. The study by Li, et al. (2016b) stated that the hydrolysis of BiOBr was inhibited in acidic condition, thus anion exchange between ibuprofen and BiOBr was inhibited. Inhibition of the ibuprofen and BiOBr was caused by the repulsion between BiOBr surface and ibuprofen ions.

Concurrently, there was report that showed photocatalyst worked best in neutral pH and it showed that phenol was 90% degraded under 240 min at pH 6.65 reacted with ZnO/silicon carbide (SiC) composite and 500 W tungsten halogen lamp as the pH_{pzc} of ZnO/SiC was 8.84. The optimum pH value of 6.65 would be less than pH_{pzc} and repulsion between the phenol ions and ZnO/SiC surface was null and adsorption of the phenol ion to the surface could happen at a faster period. Hence, the pH_{pzc} and the nature of the dye should be known to ensure optimum photocatalytic process.

2.6 Antibacterial Properties of Ag doped ZnO

As stated by Kanematsu and Barry (2015), photocatalyst such as Ag-ZnO was classified antibacterial as it had disinfection and bacterial growth inhibition effect. Disinfection can be defined as a process when the microbial population decreased to a harmless level towards environment and human while bacterial growth inhibition effect involved the manipulation of bacterial growth. Table 2.6 would demonstrate different photocatalyst with antibacterial studies.

It was stated that Ag-ZnO had disinfection effect as they were able to produce intracellular reactive oxygen species (ROS) such as $\bullet OH$ and $O_2^{\bullet -}$ radicals when activated by UV-Vis light irradiation (Podporska-Caroll, et al., 2017). The ROS would then inflict oxidative stress towards the bacterial cell. Oxidative stress damaged the bacterial cell wall and decomposed the cellular materials in the bacteria.

Table 2.6: Photocatalytic Disinfection of Different Photocatalyst towards Diverse Bacteria Species.

Dopant	Photocatalyst	Bacteria Sp.	Light Source	Treatment time (min)	Photocatalyst Loading (g/L)	Log reduction of cells	References
-	TiO ₂	<i>Klebsiella pneumoniae</i>	15-W full-spectrum light source	30	10	10 ⁵	Kőrösia, et al. (2016)
-	TiO ₂	<i>Pseudomonas aeruginosa</i>	UV-A	150	0.5	10 ³	Wang, et al. (2013)
-	ZnO	<i>E.coli</i>	Solar simulator	60	1	10 ³	Zyoud, et al. (2016)
Ag	TiO ₂	<i>Pseudomonas aeruginosa</i>	Fluorescent	120	0.2	10 ³	Barudin, et al. (2014)
Ag	ZnO	<i>Vibrio cholerae 569B</i>	Sunlight	60	0.5	10 ⁶	Das, et al. (2015)
B	BiOBr	<i>E.coli</i>	15 W fluorescent	120	1	10 ⁵	Wu, et al. (2016)
C/Br	TiO ₂	<i>Staphylococcus aureus</i>	Fluorescent tubes	120	8	10 ²	Wang, Xue and Yang (2014)
Co	SiO ₂	<i>Staphylococcus aureus</i>	8 W UV	240	0.006	10 ³	Talebian and Zare (2014)
Cu	Ag ₂ S	<i>Enterococcus faecalis</i>	125 W UV	180	10	10	Fakhri, et al. (2015)
PdO	TiO ₂	<i>E.coli</i>	300 W Xenon arc	100	1	10 ⁷	Liu, et.al (2014)

Damage to the bacteria would reduce the survivability of bacteria in the medium down to safe standards. According to Elango, et al. (2017), Ag-ZnO was able to inflict more oxidative stress towards the bacterial cells compared to pure ZnO due to presence of Ag dopant. Ravichandran, et al. (2015) showed that the presence of Ag would enhance the photocatalytic disinfection reaction as the substitutional assimilation of silver ion (Ag^+) into zinc ion (Zn^{2+}) sites would create more Zn^{2+} ions to occupy the interstitial position of ZnO as Ag^+ ionic radii (0.126 nm) was higher than Zn^{2+} (0.074 nm). The Ag NPs attached to ZnO had the ability to interrelate the bacteria cells building elements which changed to bacterial structure. When Ag NPs reacted with deoxyribonucleic acid (DNA) molecules, bacteria would condensed their DNA form to protect itself which lead to loss of DNA replication ability and inactivation of cellular proteins (Adhikari, et al., 2015).

The as-produced photocatalyst was able to fulfill the growth inhibition property too as Ag dopant was able to manipulate the bacterial growth with loss of bacterial DNA replication ability. Zhu, et al. (2016a) studies indicated that 1×10^6 CFU/mL of *E.coli* was inhibited after 24 h with presence of 40 mg/L of Ag-ZnO. This was because Ag-ZnO was able to inhibit the bacteria growth. Moreover, Esparza-González, et al. (2016) study described that medium contained 400 $\mu\text{g/mL}$ of ZnO after 18 h also able to inhibit bacterial growth as ZnO NPs had interacted and broke down bacterial protective membrane and peptidoglycan layer thus resulted to bacterial inhibition. The combination of Ag dopant and ZnO would result into a highly potent antibacterial material.

The administration of Ag-ZnO was discovered to be lethal towards bacteria but harmless to human. This was because ZnO was able to diffuse Zn^{2+} ions into drinking water act as an effective nutrient towards human therefore these ions are safe to consume (Tankhiwale and Bajpai, 2012). Pattwatt, et al. (2011) also stated that the Ag NPs was found to be non-toxic during the dermal, oral and ocular toxicity test with mice. Their result showed that the lethal dose 50 (LD_{50}) was found to be 5000 mg/kg of body weight which considered low toxicity. According to the Malaysian Environmental Quality (Industrial Effluents) Regulation 2009 Fifth

Schedule [Paragraph 11(1)(a)], the acceptable conditions for the Ag released into the environment was 0.1 mg/L in standard A while 1.0 mg/L in standard B (Department of Environmental Ministry of Natural Resources and Environment, 2010). The Malaysian regulation was showed in Appendix B.

2.7 Summary

Popularity of synthetic dyes industries were shown despite their characteristic as carcinogenic, teratogenic and mutagenic. Conventional methods for wastewater treatment such as physical, chemical and biological were used. Among all wastewater treatment, heterogeneous photocatalyst under AOPs would be able to mineralize the pollutants into harmless product by using $\bullet\text{OH}$ radicals. ZnO was selected among the semiconductor in heterogeneous photocatalyst. It was able to absorb a wide range of solar spectrum and had a better degradation percentage compared to TiO_2 . The only downside of ZnO was its fast recombination of photogenerated charge carriers that can be minimized by 3D morphological modification and Ag metal doping. The photocatalytic efficiency of the Ag-ZnO was manipulated using two process parameter such as initial dye concentration and solution pH. Ag-ZnO was classified as antibacterial photocatalyst as it can disinfect and inhibit growth of bacterial cell. Lastly, there was no report on the photocatalytic process behavior of Ag-ZnO on FG dye degradation and *E.coli* disinfection in aqueous solution in the literatures review.

CHAPTER 3

RESEARCH METHODOLOGY

In this chapter, the experimental set-up and research methods were shown. It consists of 10 different parts which were materials and chemicals, apparatus, analytical procedures, photocatalyst preparation, photocatalyst characterization, photocatalyst photoactivity, process parameters, mineralization, detection of radical species and antibacterial studies. Figure 3.1 showed a brief section of the research methods employed.

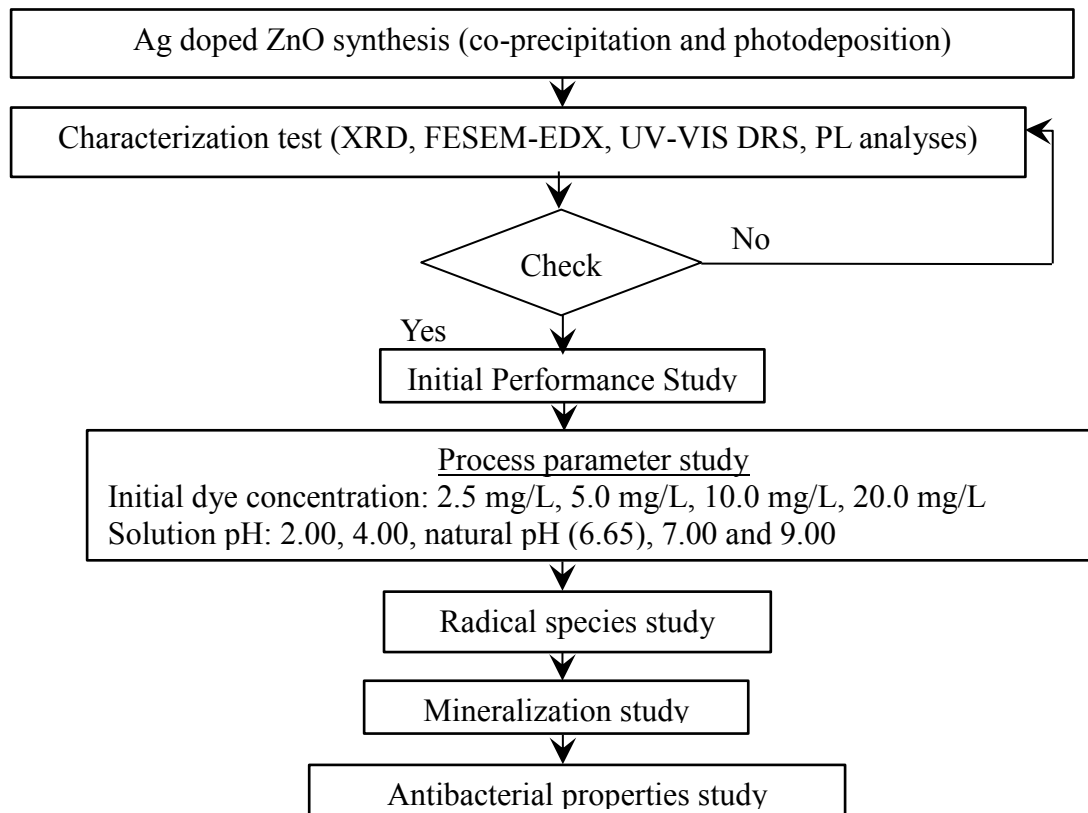


Figure 3.1: Flowchart of Research Methods Involved in This Study.

3.1 Materials and Chemicals

All of the chemicals used were graded analytically and used without any further purification. Distilled water (DI) generated from *Favorit WaterStill* distillation system with resistivity of 0.3 M Ω ·cm was used to prepare the dye solution through dissolution of certain amount of stock solution. The chemicals used were listed in Table 3.1.

Table 3.1: List of Chemicals Used.

Chemical	Purpose	Purity (%)	Source
Zinc nitrate hexahydrate (Zn(NO₃)₂·6H₂O)	Photocatalyst preparation	> 99	Quality Reagent Chemical (QreC)
Sodium Hydroxide (NaOH)	Photocatalyst preparation and pH adjuster	> 99	R&M Chemicals
Silver Nitrate (AgNO₃)	Photocatalyst preparation	> 99	R&M Chemicals
Trisodium Citrate	Photocatalyst preparation	>98	Sigma-Aldrich
Fast Green (FG) Dye	Model Dye	> 99	Fluka Chemical
Nitric acid (HNO₃)	pH adjuster	65	Quality Reagent Chemical (QreC)
Isopropanol	•OH scavenger in radical scavenger test	> 99	Bendosen Chemical
1,4-benzoquinone (BQ)	•O ₂ ⁻ scavenger in radical scavenger test	>98	ACROS Chemicals
Potassium Iodide (KI)	h_{VB}^+ scavenger in radical scavenger test	>99	Ajax Chemicals
Commercial TiO₂	Photocatalyst comparison	> 99	ACROS Chemicals
Commercial ZnO	Photocatalyst comparison	> 99	ACROS Chemicals
HR COD reagent	Mineralization test	-	Hach
Sodium Chloride (NaCl)	Saline water preparation	>99	Merck
Nutrient broth	Antibacterial study	-	Merck
Nutrient agar	Antibacterial study	-	Merck

3.2 Apparatus

3.2.1 UV-Vis Light Irradiation Experiment Apparatus

An acrylic black box was used in the photocatalytic reaction using the synthesized photocatalyst towards a dye solution. The box was used to ensure there was no other light source penetration from outside or vice versa. Outside light penetration will interfere with $\bullet\text{OH}$ and $\text{O}_2^{\bullet-}$ radicals (Kansal, et al., 2013). The black box was equipped with two ventilation fans to reduce temperature and air pump with adjustable flow meter preferably 3 L/min for solution consistency. The black box was also installed with a 45 W compact fluorescent lamp (*Universal*) with a distance of 12 cm between itself and the surface of the dye tested in a 250 mL glass beaker. The electric efficient fluorescent lamp was used to give an irradiation of both UV and visible light spectrum (Lam, et al., 2013; Khademalrasool, Farbod and Talebzadeh, 2016). The intensity of the UV light was known to be less than UV-Vis light. During the photocatalytic process, a magnetic stirrer was used to ensure the homogenous distribution of dye solution. The set-up of the apparatuses was shown in Figure 3.2, while its schematic diagram was shown in Figure 3.3.

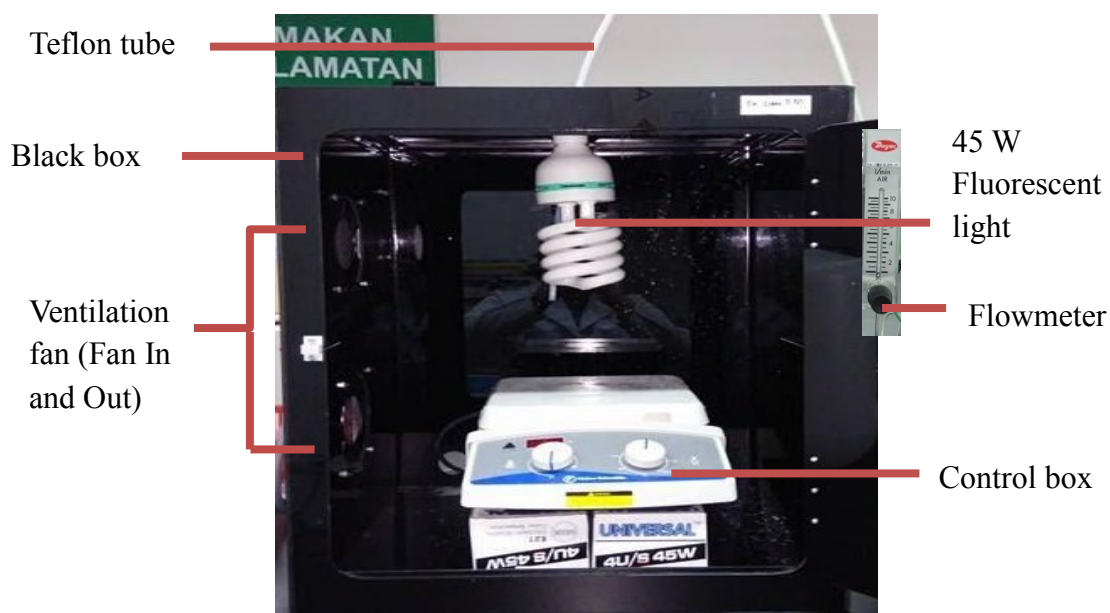


Figure 3.2: Experimental Setup for Photocatalytic Process.

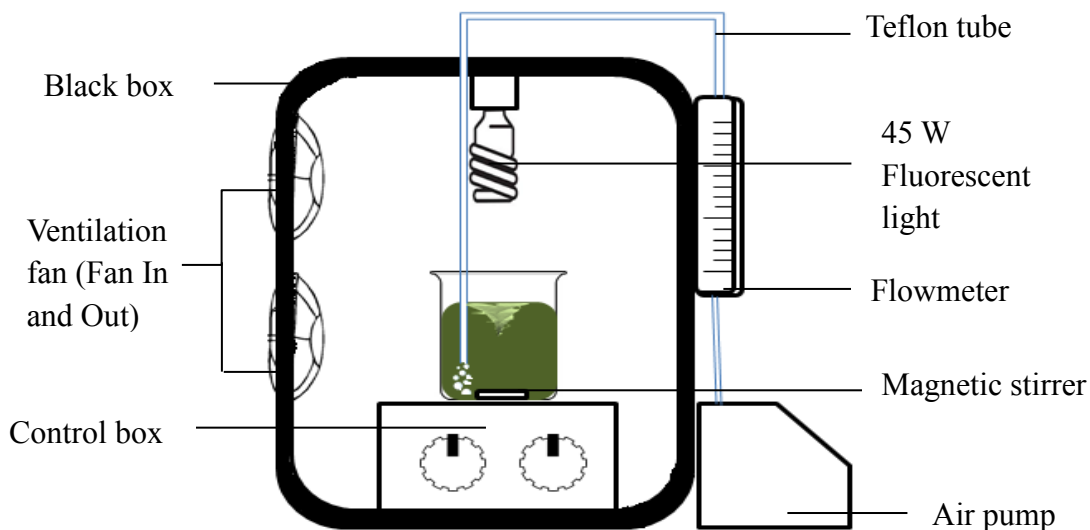


Figure 3.3: Schematic Diagram of Photocatalytic System Experimental Setup.

3.3 Analytical Procedures

3.3.1 UV-Vis Spectrophotometer Analysis

UV-Vis spectrophotometer analysis was done with a *Hach DR 6000* UV-Vis spectrophotometer to observe the dye concentration in the solution and its photocatalytic efficiency using photocatalyst. The analysis used a 1 cm internal size of rectangular cuvette and the maximum absorbance spectra of FG which was found to be wavelength of 624 nm (Sharma, McKone and Markow, 2011). The analyses were done twice and its average was used. This analysis complies with the Beer-Lambert Law which defines as the amount of light absorbed by a colored solution with suitable wavelength illuminated was directly proportional to the concentration of the colored solution. Absorbance was used as it was a quantitative amount unit of light absorbed. Eq. (3.1) showed the calculation of degradation efficiency with initial and final absorbance when Beer-Lambert law was obeyed (Ochei, 2008; Dermenci et al., 2014). A calibration curve on the FG dye was also conducted and its data was shown in Appendix C.

$$D_t (\%) = \frac{A_0 - A_t}{A_0} \quad (3.1)$$

Where:

D_t = Degradation efficiencies

A_0 = Equilibrium absorbance after adsorption-desorption equilibrium, Abs

A_t = Equilibrium absorbance after a certain irradiation time, Abs

3.3.2 Chemical Oxygen Demand (COD) Analysis

The COD analysis was used to quantify oxygen equivalent content of a sample by using potassium dichromate to oxidize the organic content of the sample. According to Sincero and Sincero (2003), the higher the COD value, the higher the polluting potential. A *Hach DRB 200* COD reactor and *Hach HR* COD digestion vials were used to do the COD analysis. The COD digestion vials which consist of potassium dichromate and sulfuric acid would be heated for 2 h. During the digestion, organic materials that were chemically oxidisable were reduced to CO_2 with concentrated sulfuric acid as a catalyst (Hunge, et al., 2017). The color of the vials would then be measured using *Hach DR 6000* UV-Vis spectrophotometer to determine the COD value. The COD analysis was repeated twice at Faculty of Engineering and Green Technology, Universiti Tunku Abdul Rahman (FEGT, UTAR). Based on Gautam, et al. (2017), the mineralization efficiency of COD was based on the following Eq. (3.2)

$$\text{Mineralization Efficiency (\%)} = \frac{C_0 - C}{C_0} \quad (3.2)$$

Where:

C_0 = Initial concentration of COD value (mg/L)

C = Final concentration of COD value (mg/L)

3.4 Preparation of Photocatalyst

3.4.1 Preparation of ZnO Flower-Like Photocatalyst

ZnO flower-like photocatalyst was synthesized using a co-precipitation method adopted by Umar, et al. (2011). Firstly, 100 mL of 0.1 M of $\text{Zn}(\text{NO}_3)_2 \cdot 6\text{H}_2\text{O}$ was prepared with the addition of 2.975 g $\text{Zn}(\text{NO}_3)_2 \cdot 6\text{H}_2\text{O}$ into 100 mL of DI. Then, 100 mL of 0.1 M of NaOH was formulated by adding 0.4 g NaOH into 100 mL of DI. Both solutions were continuously stirred afterwards. The above solution was adjusted to approximate pH 12 with addition of NaOH. The resultant mixture was stirred continuously for 30 min at room temperature. The product was reflux at 65 °C for 8 h and cooled down. White precipitate was then washed with DI and ethanol before filtered down to a filter paper. The filter paper that contains the product will then be allowed to dry in the oven at 40 °C. After drying, the dry product was placed in the muffle furnace at 550 °C for 2 h. The calcinated product was allowed to cool in a desiccator. The product was then ready. Figure 3.4 depicted the whole process synthetic process in a schematic flow diagram for ZnO flower-like photocatalyst.

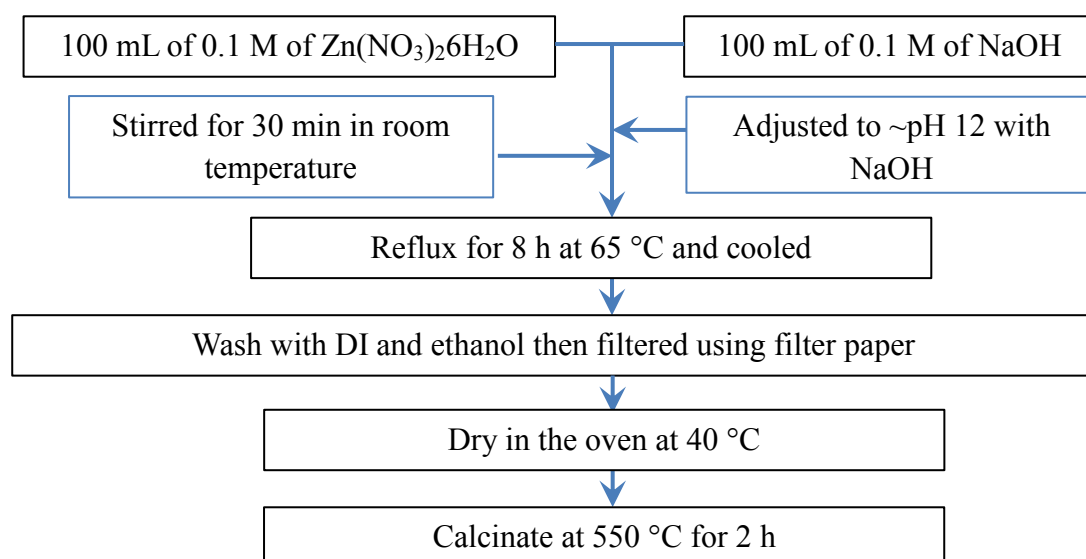


Figure 3.4: Preparation of ZnO Flower-Like Photocatalyst.

3.4.2 Preparation of Ag doped ZnO

The flower-like ZnO was doped using a photodeposition method adopted by Kuriakose, et al. (2014). The 1.5 g of dried flower-like ZnO was dispersed into 100 mL of DI under sonication. Then, the sonicated solution would be added with 20 mM of trisodium citrate and continuously stirred overnight. 2 mM of AgNO₃ was later added and agitated for 30 min in the dark. The agitated solution was further exposed to sunlight for 2 h for photodeposition process. Subsequently photodeposition process, the solution was filtered, centrifuged and washed with DI. The produced precipitates were dried in oven at 90 °C for 3 h and calcinated at 550 °C for 2 h. Figure 3.4 depict the whole process in schematic flow diagram.

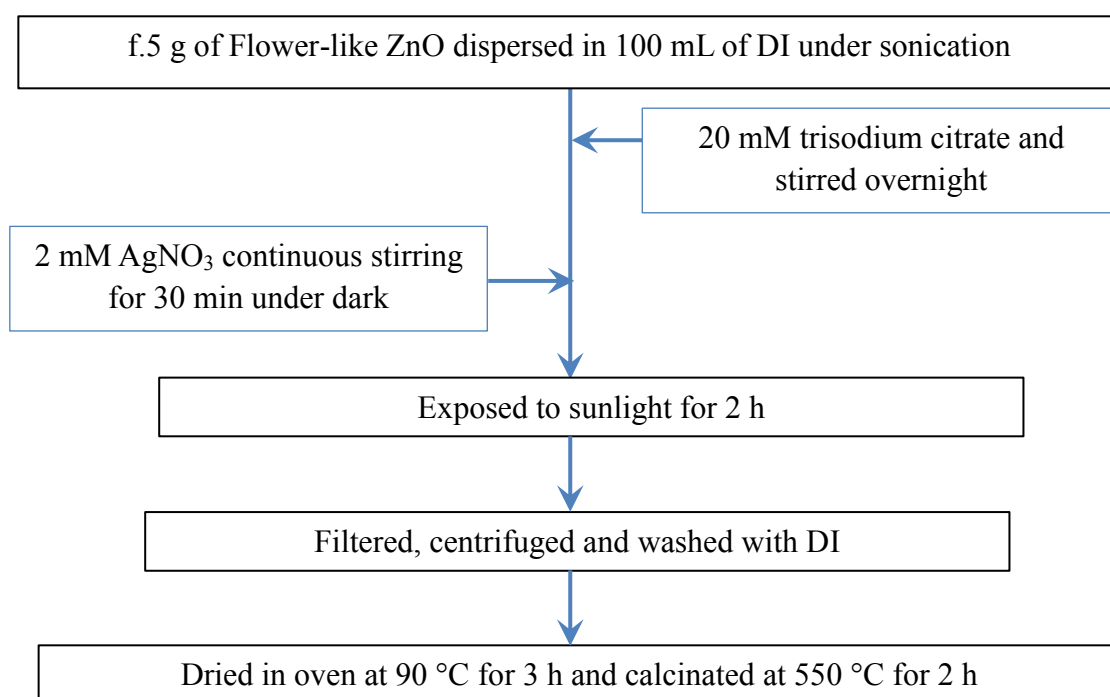


Figure 3.5: Preparation of Ag doped ZnO Photocatalyst.

3.5 Characterization of the photocatalyst

3.5.1 Crystal Phases Analysis

X-Ray Diffraction (XRD) was used to determine the crystalline structure and phase of the photocatalyst (Hernández-Ramírez and Medina-Ramírez, 2015; Saravanan, et al., 2015). This analysis was done with a *Shimadzu X-Ray Diffractometer (XRD-6000)* with a graphite monochromatic copper radiation ($\text{CuK}\alpha$) of wavelength of 1.5418 Å. The XRD analysis was carried out in School of Chemical Sciences, University Sains Malaysia (USM).

3.5.2 Morphological Analysis

Field-emission scanning electron microscopy (FESEM) was used to analyze the surface of photocatalyst (Cai, et al., 2016). Prior to the samples analysis, samples were placed with double sided carbon tape on aluminum stub to secure sample position. The sample will then be coated with Pt using *Jeol JFC-1600 Auto Fine Coater* to ensure setting of sample powders on tape. The sample will later be exposed to low vacuum of 0.1 to 10^{-4} Pa to inhibit evaporation of sample (Huebschen, et al., 2016). FESEM analysis used a *Jeol JSM 7601-f* Field Emission Scanning Electron Microscope in FEGT, UTAR.

3.5.3 Elemental Analysis

Energy Dispersive X-Ray (EDX) was used to determine elemental components and usually coupled with FESEM. EDX was a unique method that allows the discrete crystalline components identification at appropriate magnification (Ingram, 1999).

The Zn atomic percentage of the photocatalyst can be investigated with EDX (Park, et al., 2016). The analysis was done in FEGT, UTAR.

3.5.4 UV-Vis Absorption Analysis

UV-Vis absorption analysis of the proposed photocatalyst was done using a *Hach DR 6000* UV-Vis spectrophotometer which allows wavelength range analysis where its absorbance range was determined. Before the sample was used for analysis, the sample must be grounded with mortar and pestle into fine powders. The absorption edge was approximately equal to semiconductor band gap. The analysis was done by extrapolating the x- axis on a wavelength between 325 to 500 nm while the y-axis was absorption (Martin, 2015). With the relationship above, Planck relation was used to calculate the band gap shown in Eq. (3.3) (Tayade, Bajaj and Jasra, 2011). The analysis was done in FEGT, UTAR.

$$EG = hc/\lambda \quad (3.3)$$

Where:

EG = band gap energy, eV

h = Planck's constant

c = light velocity, m/s

λ = wavelength, nm

3.5.5 Photoluminescence Analysis

The photoluminescence analysis or PL analysis was done to determine the h_{VB}^+ and e_{CB}^- pair recombination properties of doped semiconductor and explain the relationship between nature of site defects and efficiency of charge carrier trapping, immigration and transfer (Anpo, 2010). The PL analysis was conducted using a *Perkin Elmer S550 Luminescence Spectrometer* at room temperature of 20 °C and

Xenon lamp as an excitation source with excitation wavelength of 325 nm (Fagan, et al., 2016). The PL analysis was carried out in School of Chemical Sciences, USM.

3.6 Photoactivity of Photocatalyst under the UV-Vis Light Irradiation

FG was used as model dye pollutant for this study. The photocatalytic activities of the synthesized Ag doped ZnO were evaluated under a compact fluorescent light. The photocatalysis process was done in a 250 mL glass beaker with a magnetic stirrer and into the black box. Former to the photocatalysis experiment, a 5 mL solution was taken out from the solution to act as a control point before dark absorption process. Dark absorption process start when mixture of dye and photocatalyst was left in the black box for 30 min for adsorption-desorption equilibrium process (Liu, Wei and Gao, 2015). After 30 min, the light source was turned on. 5 mL of sample from the beaker was taken out at certain time intervals and centrifuged for 1 h at 5000 rpm to allow the deposition of the photocatalyst to the bottom (Zhang et al., 2016c). The supernatant part of the solution in the centrifuge tube will be filtered with a cellulose acetate (CE) membrane syringe filter of 0.45 μm pore size to remove remaining suspended photocatalyst. The filtered supernatant would be analyzed using a UV-Vis spectrophotometer and a COD analyzer. The photocatalytic activities of FG will then be repeated using commercial ZnO, commercial TiO₂ and as-synthesized pure ZnO for comparison purposes under the similar experimental conditions. This analysis was done in FEGT, UTAR.

3.7 Process Parameters

3.7.1 Initial Dye Concentration

In order to evaluate the initial concentration of the photocatalysis process, the concentration of the FG dye was manipulated at constant natural pH (6.65). The basis selection of the initial dye concentration was from 2.5 mg/L to 20.0 mg/L (Lu, et al., 2016; Patil, et al., 2016; Wang, et al., 2015).

3.7.2 Solution pH effect

Evaluation of pH effect of the photocatalysis process was tested with a constant initial dye concentration of 2.5 mg/L. This parameter was manipulated using FG pH of 2.00, 4.00, 7.00 and 9.00 (Saharan, et al., 2015). The pH was adjusted with addition of 0.1 M NaOH or 0.1 M HNO₃ into the dye solution (Bechambi, Najjar and Sayadi, 2016; Odeh, Ferhod and Lafta, 2012). The natural pH of the FG dye was tested with a *Hanna HI 2550 pH/ORP & EC/TDS/NaCl Meter* with pH calibration using pH buffer solution of pH 4.00, 7.00 and 10.00. The 1000 mg/L FG dye stock solution was diluted to 10 mg/L for natural pH reading. The result of the average natural pH of four duplicated result of 10 mg/L FG dye was pH 6.65.

3.8 Detection of Radical Species

Detection of the radical species often involves generation of the test radicals and monitor of the radical reactions. The detection of the free radical was able to evaluate the photocatalytic efficiency of the synthesized photocatalyst. Radical species produced in photocatalytic reaction were •OH radicals, •O₂⁻ radicals and h_{VB}^+ . •OH radicals can be detected with isopropanol (Yang, et al., 2015). Addition of BQ acts as the •O₂⁻ scavenger (Halliwell and Gutteridge, 2015), while KI can scavenge h_{VB}^+

(Van Doorslaer et al., 2012). The addition of these scavengers will lead to a sharp decrease in the photocatalytic degradation (Schneider et al., 2016). Each scavenger added was in 2 mM concentration (Zhu, et al., 2016b).

3.9 Antibacterial Studies

During the antibacterial studies, the apparatuses and materials were autoclaved at 121 °C for 20 min with a *Hirayama HV-50* sterilizer autoclave. The experiments were conducted in an *Optimar™* vertical laminar flow clean bench to stimulate a sterile environment. The bacteria were all incubated inside *Binder* microbiological incubator and a *Memmert* shaking water baths at 37 °C.

3.9.1 Preparation of Bacterial Studies

The preparation of *E.coli* culture was assimilated using Wu, et al. (2016) method. The bacterial strain of *E.coli* (ATCC® 256922™) was inoculated into 50 mL of nutrient broth of concentration 25 g/L and later incubated for 16 h inside shaking water bath at 37 °C to reach the stationary stage of the bacteria growth. The bacterial cell was further harvested by centrifugation with a *Hermle Z236K* universal centrifuge at 5000 rpm for 10 min. The bacterial cell was washed twice with sterilized 0.9 wt% saline water and its supernatant was thrown away before finally resuspended. At the end of the preparation, the cell density was adjusted to approximately 1×10^7 colony forming unit (CFU)/mL via optical density (OD₆₀₀) measurements and dilution. The cell density adjustment was done with 1.0 OD₆₀₀ unit represent 1.5×10^8 CFU/mL formula and it was measured using a *Hach DR 6000* UV-Vis spectrophotometer at 600 nm wavelength (Salema, et al., 2013; Perlman and Laskin, 1981).

3.9.2 Screening for Antibacterial Response

Photocatalytic disinfection started with preparation of 1 mL of diluted *E.coli*. 250 mL beaker was thermostat in a water bath at 30 °C and covered with aluminum foil to prevent contamination as adopted with Zyoud, et al. (2016) technique. Next, 99 ml of 0.9 wt% saline water and diluted *E.coli* suspension was added into the beaker and heated at 37 °C for optimum bacteria growth condition. Then, 0.1 g of photocatalyst was added into the beaker and further magnetically stirred. The mixture was in the dark for 30 min. The mixture was exposed to a 45 W Universal compact fluorescent lamp for 150 min to start the photocatalytic disinfection process. The viable bacteria test was conducted using the spread plate method (Wang, et. al., 2013). Each sample was taken out from the reaction mixture at certain periods and filtered using 0.45 µm membrane filters. Successive dilution was done seven times and 0.5 mL sample from each dilution was uniformly spread on the agar plate and additional incubated at 37 °C for 24 h. Two agar plates were used for every dilution and plates were visually inspected for the effects of photocatalyst then for comparison. The control experiments were prepared in the dark with photocatalyst and UV-Vis irradiation without photocatalyst conditions.

3.9.3 Membrane Integrity Assay

While the photocatalytic disinfection experiment was conducted with control and catalytic conditions, another 5 mL of sample was taken out at identical time periods as photocatalytic disinfection sample extraction and filtered with 0.22 µm filters as done by Xu, et al. (2017). The filtrate was monitored using a *Hach DR6000* UV-Vis spectrophotometer at a 260 nm for DNA absorbance (Dasgupta and Ramalingam, 2016).

CHAPTER 4

RESULTS AND DISCUSSION

This chapter presents the results, interpretation and analyses of the existing research study. The contents of the chapter were outlined into six subsections. The first subsection was the characterization of Ag-ZnO. The section consisted of crystal phases/ structure, morphological, elemental, UV-Vis absorption and PL analyses. Next, the photoactivity of photocatalyst on the degradation of FG dye under the UV-Vis light irradiation was described in section 4.2. The process parameters such as initial dye concentration and solution pH effect were investigated in the following section 4.3. In section 4.4, photocatalysis degradation mechanism was proposed. In section 4.5, mineralization study was completed and analyzed. In addition, antibacterial response properties of Ag-ZnO was identified and detailed in this study.

4.1 Characterization of the Photocatalyst

The characterization of photocatalyst was done to investigate the chemical, physical and optical properties of the synthesized pure ZnO and Ag-ZnO as efficient photocatalyst. The photocatalysts were characterized via XRD, FESEM, EDX, UV-Vis absorption and PL analyses. The XRD analysis was used to determine the phase and crystalline structure of photocatalysts while the FESEM analysis was done to analyze pure ZnO and Ag-ZnO shape and size. Moreover, EDX analysis was prepared for elemental components determination. UV-Vis absorption analysis was used for identification of absorbance range of the photocatalysts whereas PL analysis

was conducted for determination of recombination photogenerated charge carriers of pure ZnO and Ag-ZnO.

4.1.1 XRD Analysis of the Developed Photocatalysts

Figure 4.1 displays the crystal structure of pure ZnO and Ag-ZnO samples. The XRD patterns revealed sharp peaks which indicated high degree of crystallinity of the photocatalyst. Furthermore, the XRD patterns of all samples are readily indexed with their characteristic peaks according to the Joint Committee on Powder Diffraction Standards (JCPDS). Major phases of hexagonal wurtzite ZnO (JCPDS 36-1451) were detected in pure ZnO and Ag-ZnO samples. Hexagonal wurtzite ZnO peaks correspond to their diffraction patterns of (100), (002), (101), (102), (110), (103), (200), (112) and (201) planes, respectively. Alternatively, the XRD peaks of Ag-ZnO sample were also matched closely to the characteristic peak of cubic Ag structure with diffraction patterns of (111), (200) and (400), respectively (JCPDS 04-0783). The XRD results obtained were consistent with other literature reports (Kumar, et al., 2015; Zyoud, et al., 2016; Souza, et al., 2016; Yang, et al., 2015; Deng, et al., 2012; Pant, et al., 2016; Ravishankar, et al., 2014; Saravanan, et al., 2013). No additional crystalline impurities were detected in the XRD patterns, indicating the phase purity of ZnO and Ag-ZnO products. To determine possible substitution of Zn ions with Ag ions in Ag-ZnO, the angle shift of 2θ for the ZnO characteristic peak of (002) as a function of Ag doping was displayed. Slight deviation of lattice parameters to lower 2θ values of Ag-ZnO samples from individual ZnO and Ag were observed. The positional shift to lower 2θ occurred due to different ionic size of Ag^+ (1.26 Å) and Zn^{2+} (0.74 Å) ions (Yildirim, Unalan and Durucan, 2013; Hu, et al., 2013; Khan, et al., 2015). It was clear that the lattice enlargement was due to substitution of Ag^+ ions into ZnO lattice. Hence, the XRD analyses detected hexagonal wurtzite ZnO and cubic Ag from photocatalyst samples and lattice enlargement in ZnO lattice.

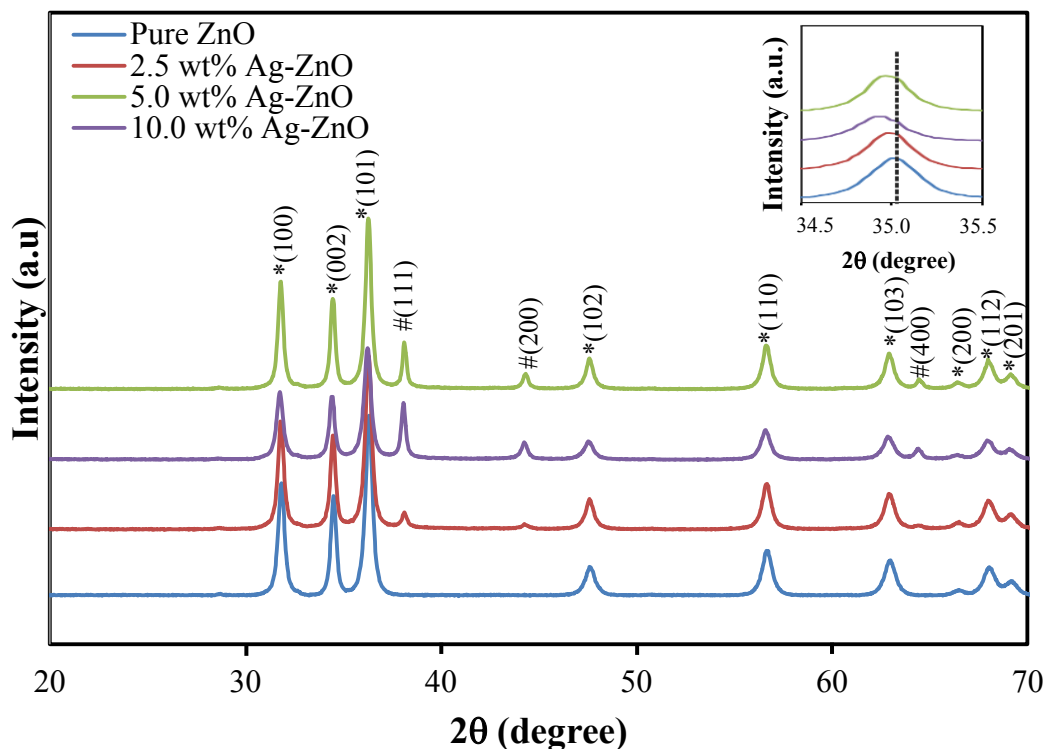


Figure 4.1: XRD Patterns of Pure ZnO and Ag-ZnO with Different Ag Doping Loadings. Inset is the Magnified Region of (002) Peak.

4.1.2 Morphological Analysis

Figures 4.2a-d exhibit the FESEM images of the as-synthesized pure ZnO and Ag-ZnO samples prepared at different Ag wt%. In the Figure 4.2a, the panoramic morphologies of the as-synthesized photocatalyst are displayed in a 3D flower-like shape. The 3D flower-like products were displayed as not uniform and varied in sizes from 700 nm to 3.5 μm diameter. Moreover, the samples still maintained their micro/nanoflowers shape after the interferences of Ag NPs onto ZnO (Figures 4.2b-d). It indicated that the attachment of Ag NPs to the ZnO were not able to change the flower-like ZnO morphology.

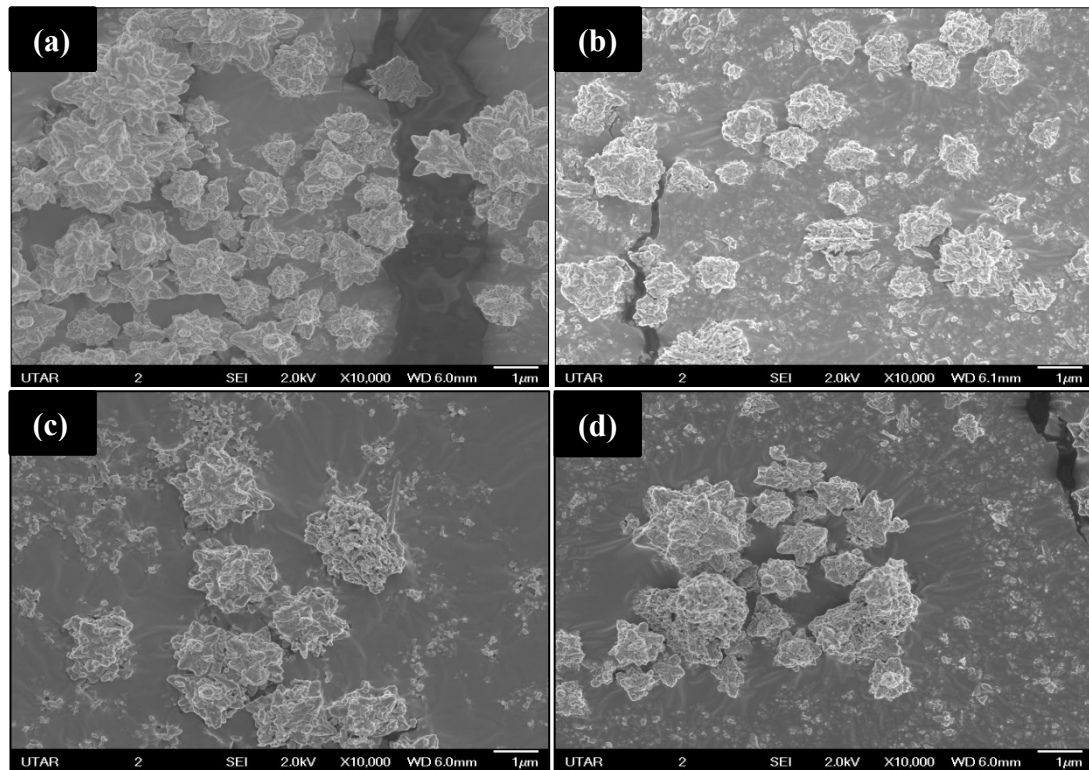
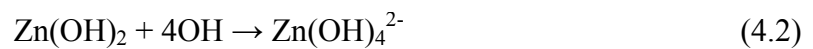


Figure 4.2: FESEM Images under 10,000x Magnification of (a) Pure ZnO, (b) 2.5 wt% Ag-ZnO, (c) 5.0 wt% Ag-ZnO and (d) 10.0 wt% Ag-ZnO.

Based on the FESEM observation, the growth micro/nanoflowers ZnO micro/nanostructures can be proposed based on the subsequent chemical reactions involved and its crystal growth habits (Yu, et al., 2015; Huang, et al, 2010). The reaction processes can be expressed in Eqs. (4.1) till (4.3):



The reaction in Eq. (4.1) started when NaOH was introduced into the Zn^{2+} solution to produce $\text{Zn}(\text{OH})_2$. During the reaction process in Eq. (4.2), heat was provided to ensure that the $\text{Zn}(\text{OH})_2$ precipitates broke down to form $\text{Zn}(\text{OH})_4^{2-}$ ions. As time passed, ZnO nuclei would be formed from dehydration of $\text{Zn}(\text{OH})_4^{2-}$ ions. ZnO nuclei would act as the building blocks for the construction of 3D ZnO hierarchical micro/nanostructures as shown in Figure 4.3. During co-precipitation method, low temperature of 65°C was used during synthesis stage. The co-

precipitation method resulted to slow evolution of nucleation and growth mechanism of ZnO micro/nanostructure for thermodynamically stability. These processes were mainly due to the behaviour of crystal structure to aggregate easily through the lowest energy path. The multinuclei aggregates later served as the initial central sites for bi-dimensional ZnO micro/nanostructure growth. Finally, the multinuclei aggregates at the centre of micro/nanostructure formed flower-like shape with randomly distributed mono-crystalline petals. In this current study, the 3D flower-like Ag-ZnO was fabricated under low temperature without any surfactant.

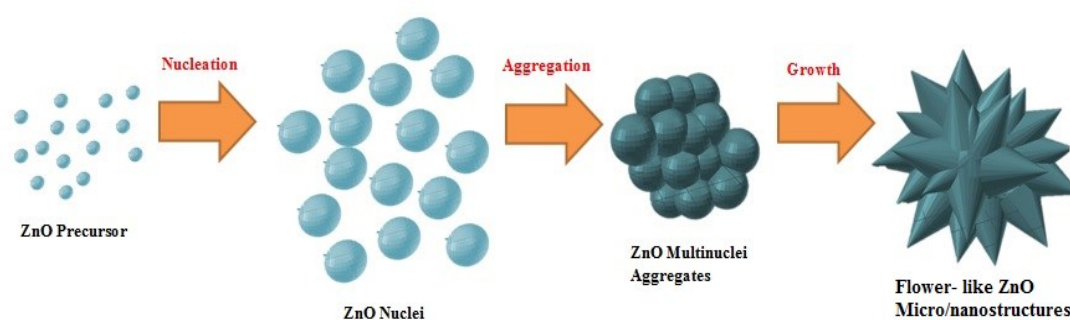


Figure 4.3: Schematic Diagram of Proposed Growth Mechanism of Flower-Like ZnO Micro/nanostructures.

4.1.3 Elemental Analysis

The elemental analysis of pure ZnO and Ag-ZnO samples were identified using EDX analysis as shown in Figures 4.4(a)-(d). In the EDX mapping, the Zn and O peaks can be easily observed in pure ZnO sample, while Ag, Zn and O peaks were found in Ag-ZnO sample. The presence of Ag, Zn and O peaks indicated that the Ag dopant was successfully incorporated into the ZnO. In addition, the escalating peaks of Ag were seen when the Ag wt% in the sample increased. The escalating peak of Ag element can be seen by comparing the peak of Zn element at 1 keV with Ag peak at 3 keV. The weight ratio of Zn element: Ag element reduced from 8:1 in 2.5 wt% Ag-ZnO sample to 6:1 in 5.0 wt% Ag-ZnO sample and further decrease to 1:1 in 10.0 wt% Ag-ZnO sample upon addition of Ag loading to the flower-like

micro/nanostructure ZnO. The comparison of weight ratio in EDX was similarly done by Zhang, et al. (2011). It was confirmed that the presence of Ag metal on the surface of ZnO.

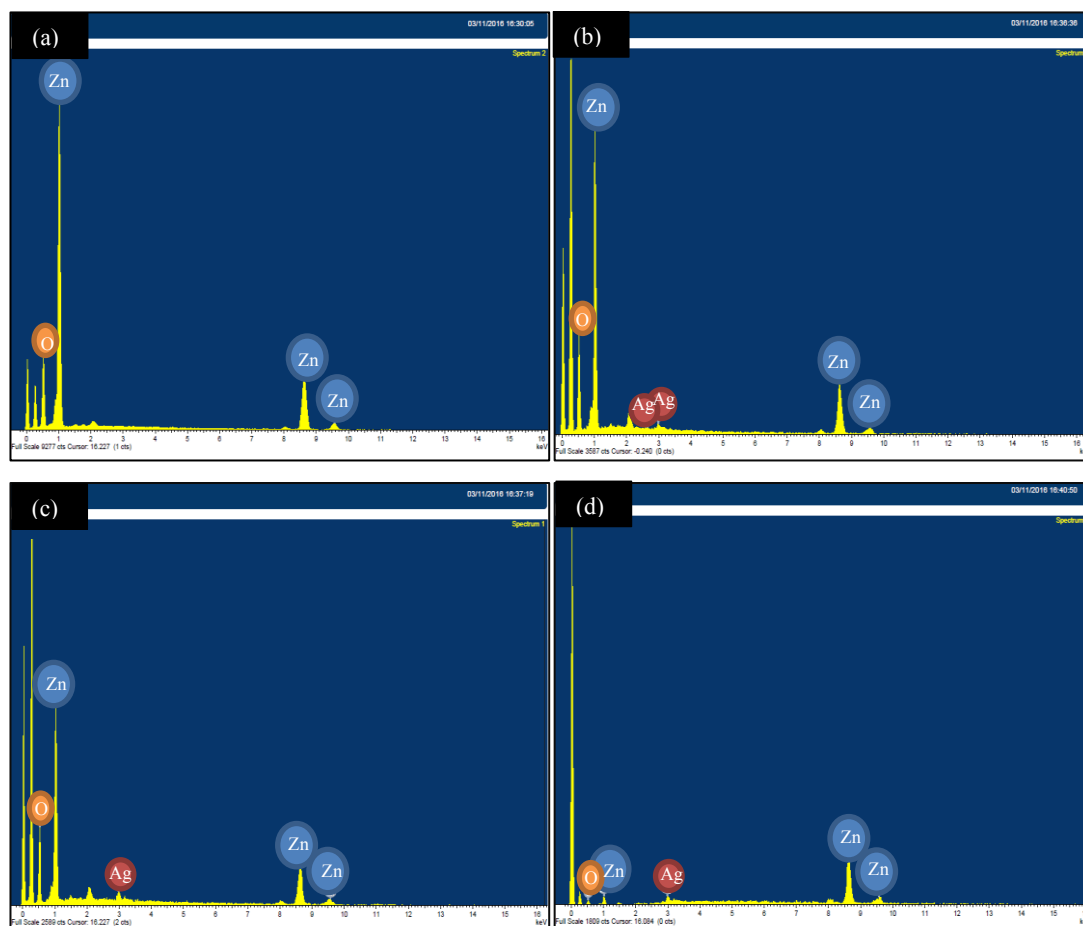


Figure 4.4: EDX Spectra for (a) pure ZnO, (b) 2.5 wt% Ag-ZnO, (c) 5.0 wt% Ag-ZnO and (d) 10.0 wt% Ag-ZnO.

4.1.4 UV-Vis Absorption Analysis

Figure 4.5 displays UV-Vis DRS spectra as a function of wavelength for pure ZnO and different Ag loadings of Ag-ZnO photocatalyst. Modification of micro/nanoflowers ZnO with Ag dopant significantly increased the light absorption

property of the photocatalyst sample. It was noticed that light absorption of all Ag-ZnO samples in the visible light range was higher than pure ZnO. Moreover, the light absorption increased with the increase of Ag loadings. A slight red shift of the optical absorption edge was seen in all doped products compared to pure ZnO. This phenomenon implicated that Ag-ZnO composites can absorb more energy, which would benefit the photocatalytic activity (Liang, et al., 2015).

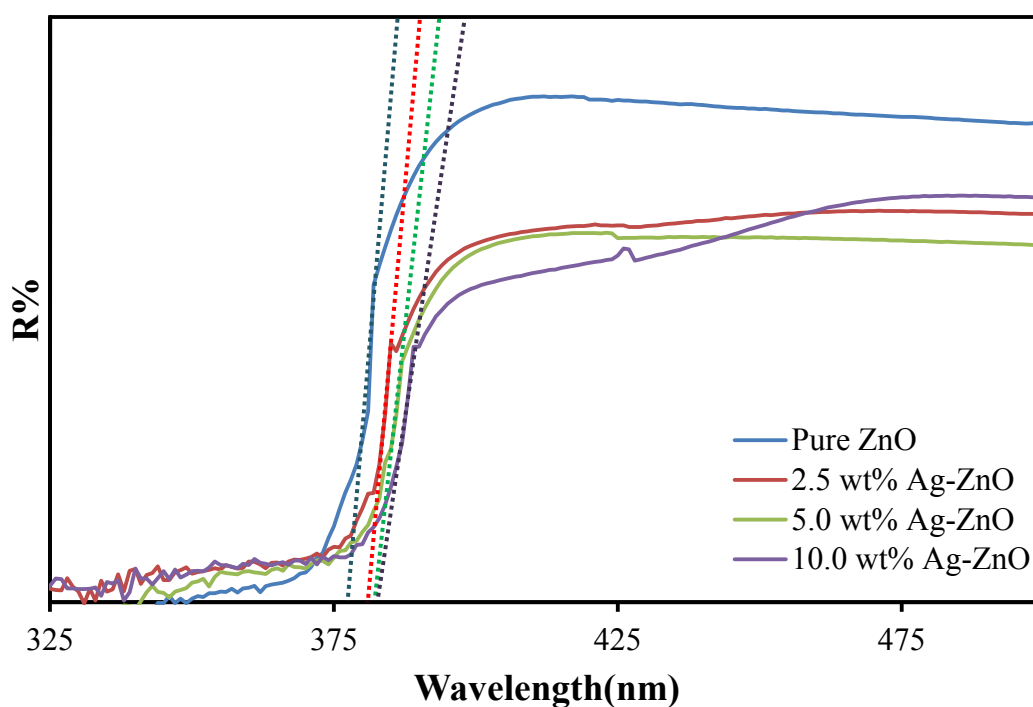


Figure 4.5: UV-Vis DRS Spectra Pure ZnO and Ag-ZnO with Different Ag Doping Loadings.

The band gap energies were calculated according to Eq. (4.4) (Tayade, Bajaj and Jasra, 2011):

$$E_g = hc/\lambda = 1240/\lambda \quad (4.4)$$

Where:

E_g = band gap energy, eV

h = Planck's constant (4.135667×10^{15} eVs)

c = velocity of light (3×10^8 m/s)

λ = absorption onset wavelength, nm

By applying Eq. (4.4), the measured band gap energy of pure ZnO, 2.5 wt% Ag-ZnO, 5.0 wt% Ag-ZnO and 10.0 wt% Ag-ZnO were 3.27 eV, 3.25 eV, 3.23 eV and 3.22 eV, respectively. The band gap measurement results directed that all Ag-ZnO samples had a lower band gap in contrast with the pure ZnO. It demonstrated that Ag-ZnO samples can absorb UV radiation as well as visible region of the solar light, thus deduced that Ag-ZnO could also be a promising photocatalyst in sunlight photocatalysis. These findings were in agreement with previous literature reports (Patil, et al., 2016; Liang, et al., 2015).

4.1.5 Photoluminescence Analysis

Figure 4.6 shows the PL spectra of ZnO and Ag-ZnO with different Ag wt% when excited at 325 nm. It was observed that pure ZnO had the highest PL intensity, while 5.0 wt% Ag-ZnO had the lowest PL intensity among all samples. Tao, et al. (2016) reported that a higher emission peak would aid in rapid recombination charge carrier action, whereas lower emission peak would indicate lower recombination charge carrier occurrence. Their study explained that the low emission peak would often link to the wide space-charge region (SCR). It was proposed that the increased Ag loading up to 5.0 wt% onto ZnO surface lead to wider space-charge region (SCR). Since the photogenerated charge carriers were separated at a large electric field, the recombination of h_{VB}^+ and e_{CB}^- pairs would be reduced. Furthermore, Ag dopant had a stronger capacity to capture the e_{CB}^- and accelerate the interfacial charge transfer thus prolonged lifetime of photogenerated charge carriers which ultimately aid in photocatalytic efficiency (Bechambi, Najjar and Sayadi, 2016; Liu, Wei and Gao, 2015). On the contrary, when Ag loading exceeded the optimal ratio such as 10.0 wt% Ag-ZnO, the PL intensity increased. This phenomenon could be attributed to the formation of Ag clusters which lead to weaken of Ag NPs attachment with micro/nanoflowers ZnO and ultimately, increase occurrence of recombination of photogenerated charge carriers (Liu, et al., 2012; Zhang, et al., 2014).

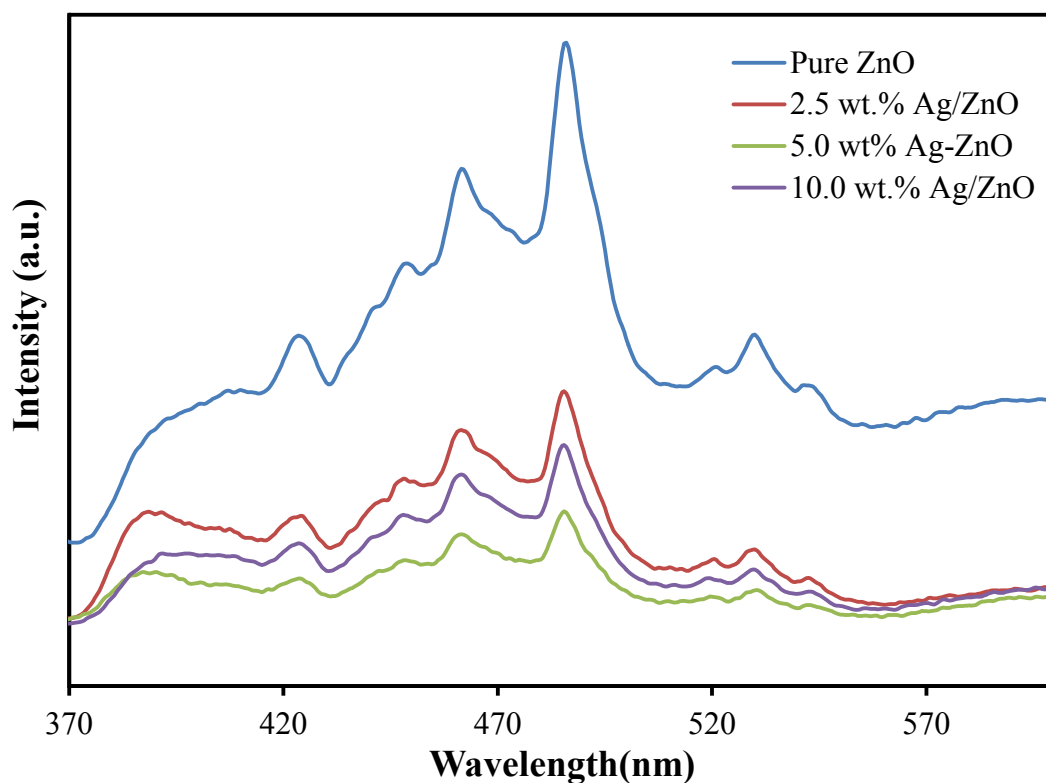


Figure 4.6: PL Spectra of Pure ZnO and Ag-ZnO with Different Ag Loadings.

4.2 Photoactivity of Photocatalyst under the UV-Vis Light Irradiation

The photocatalytic performances of the developed photocatalysts were evaluated by the degradation of FG dye in aqueous solution under UV-Vis light irradiation. Figure 4.7 presents the results of conducted photocatalytic test on eight various conditions towards the removal of FG dye. During the experiment, the six photocatalyst were compared under similar condition and it was resulted to 5.0 wt% Ag-ZnO sample exhibited highest photocatalytic degradation activities compared to other Ag-ZnO samples under 240 min. The results showed the photocatalytic degradation of FG dye with difference Ag-ZnO photocatalysts followed the order: 5.0 wt% Ag-ZnO (93.15% degradation efficiency) > 10.0 wt% Ag-ZnO (85.94% degradation efficiency) > 2.5 wt% Ag-ZnO (83.77% degradation efficiency). Furthermore, 5.0 wt% Ag-ZnO performed better than as-synthesized pure ZnO with only 80.04% degradation efficiency under similar conditions. The as-synthesized 5.0 wt% Ag-ZnO also exhibited higher photocatalytic degradation compared to commercially produced

photocatalyst such as commercial ZnO and commercial TiO₂ with photocatalytic degradation efficiency of 70.56% and 62.17%, respectively.

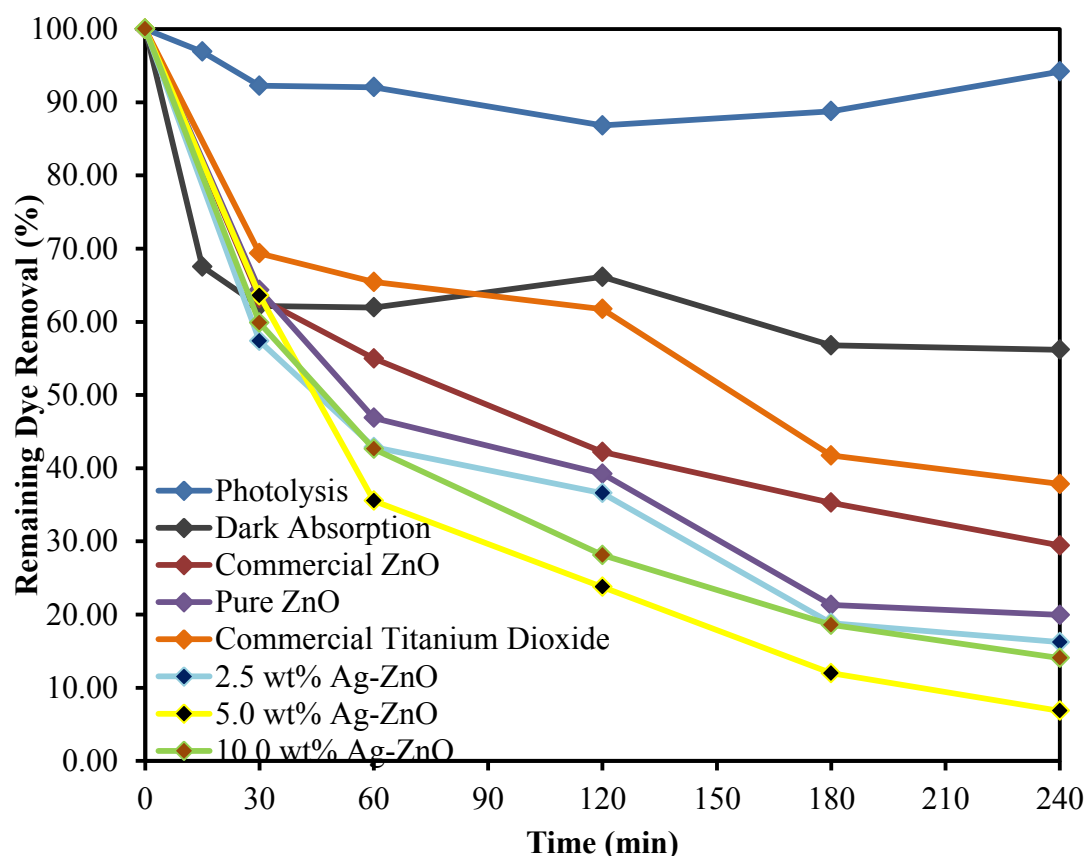


Figure 4.7: Preliminary Photocatalysis Studies Using Various Photocatalytic Conditions ([FG] = 5.0 mg/L; [Photocatalyst] = 1 g/L; pH = 6.65).

Additional comparative studies with 5.0 wt% Ag-ZnO sample were also conducted to evaluate the purity of photocatalytic activities. The results of the additional studies displayed that the FG dye concentration hardly decreased when irradiated with UV-Vis irradiation without the presence of photocatalyst as the photocatalytic efficiency was only 5.81%. It was concluded that the FG dye was stable during photolysis process. In contrary, the FG dye was degraded 43.82% under dark absorbance. It was determined that the high dark absorption dye degradation was due to the high electrostatic attraction between FG dye molecules with the surface of the photocatalyst. Similar results of photolysis and dark absorption

condition were reported (Akhil, et al., 2016; Subash, et al., 2012a; Subash, et al., 2012b). Akhil, et al. (2016) stated that less than 2% of photocatalytic degradation of MB occurred during photolysis within 120 min. Their study confirmed that the MB dye was stable under photolysis condition. Meanwhile, Subash, et al. (2012a) demonstrated that 50.0% of adsorption of Reactive Red 120 dye under pH 7 within 30 min by Zr-Ag-ZnO during dark absorption due to its high electrostatic attraction between positively charged Zr-Ag-ZnO and negatively charged Reactive Red 120 dye. Another studies conducted by Subash, et al. (2012b) also stated that the high electrostatic attraction between the Ce-Ag-ZnO photocatalyst and Naphthol blue black dye molecules at pH 9 had increase the absorption capability of Ce-Ag-ZnO and allowed it to degrade 29.0% of the dye within 30 min.

Figure 4.8a displays the UV-Vis absorption spectra of FG dye degradation using 5.0 wt% Ag-ZnO. The results showed that the characteristic FG absorption peak at 624 nm gradually diminished under UV-Vis irradiation of 240 min. Additionally, there was no new absorption peak appearing in the absorption spectra and thus indicated that the reaction intermediates was not present at the end of the photocatalysis process (Sohrabnezhad and Seifi, 2016; Hou, 2015). The change of color for FG dye degradation over 5.0 wt% Ag-ZnO is shown in Figure 4.8b. It exhibited that the FG dye color was changed from dark sea green color to colorless after photocatalytic treatment with 5.0 wt% Ag-ZnO. The result was supported by other earlier reports such as Miao, et al. (2016), Zhou, et al. (2015) and Sinha, Ahmaruzzaman and Bhattacharjee (2014). This concluded that the FG dye was degraded over the surface of 5.0 wt% Ag-ZnO.

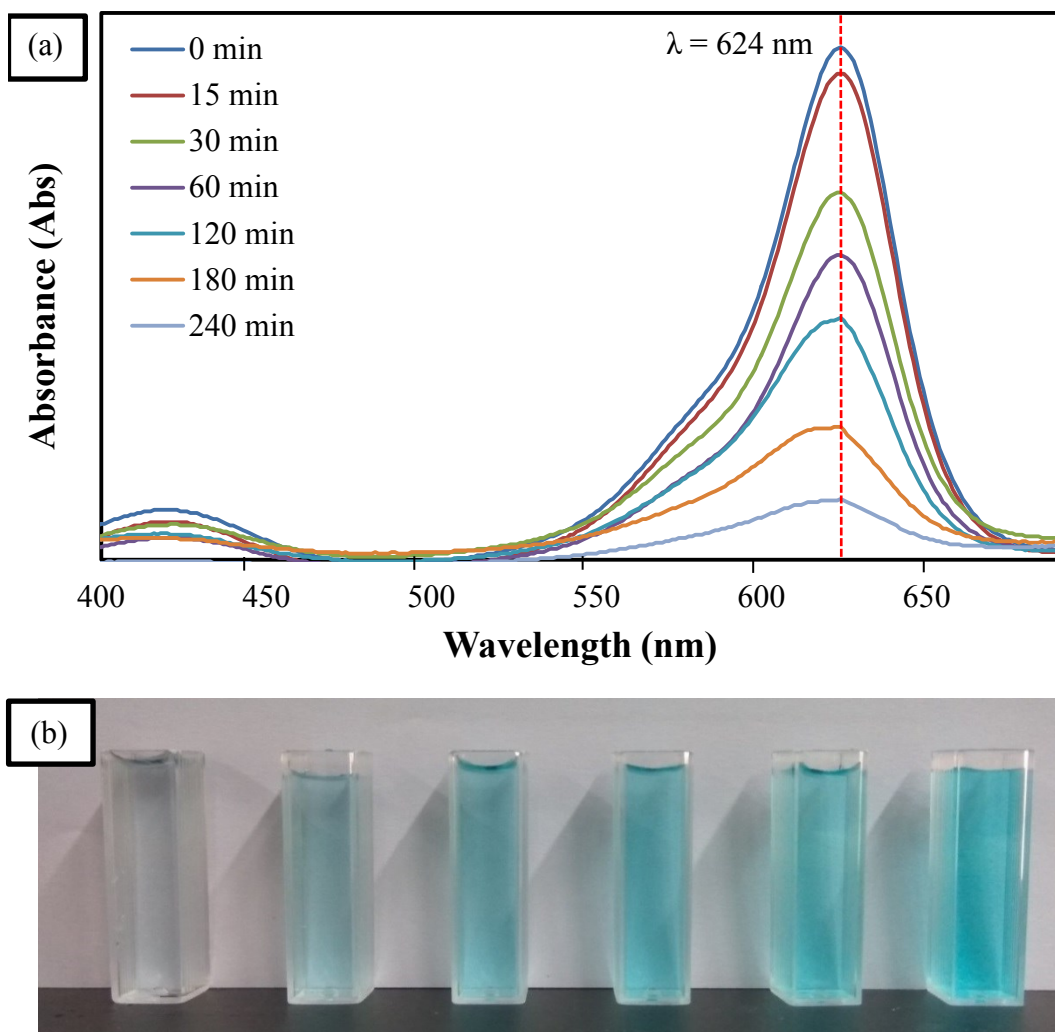


Figure 4.8: (a) Absorption Spectra of Photocatalytic Degradation of FG Dye over Time at Optimized Conditions and (b) Color Change for Photocatalytic Degradation of FG Dye over Time Using 5.0 wt% Ag-ZnO ([FG] = 5 mg/L; pH = 6.65; [5.0 wt% Ag-ZnO] = 1.0 g/L).

The photocatalytic enhancement of as-synthesized pure ZnO compared to commercial ZnO and commercial TiO₂ was mainly attributed to its modified 3D shape. The morphological modification to 3D shape of the photocatalyst also aided in the photocatalytic reaction as specified by Xing, et al. (2011) where their synthesized 30 mg/L of 3D quasi-flower like ZnO had degraded MeO completely within 60 min in comparison with commercial ZnO and commercial TiO₂. They deduced that the 3D shape of the photocatalyst reduce occurrence of aggregation and would lead to increase of surface area of the photocatalyst exposed to the dye molecules, thus reduction in photocatalysis efficiency.

On the contrary, Ag-ZnO performed better photocatalytic activity than pure ZnO as attachment of Ag dopant onto the photocatalyst had instigated low band gap and low photogenerated charge carrier recombination efficiency which further enhanced the photocatalysis reaction. Such improvement was reported similar to supplementary literature reports. Yildirim, Unalan and Durucan (2013) demonstrated that the pure ZnO with band gap 3.241 eV had a lower photocatalytic degradation of 84.1% in relation to Ag-ZnO with band gap of 3.207 eV which had completely degraded 1g/L MeO dye under 120 min. The low band gap of the as-synthesized photocatalyst allowed easier e_{CB}^- transfer from VB to CB and thus increased production of photogenerated charge carrier which ultimately increased the photocatalytic activities. According to Liang, et al. (2015), their as-produced Ag-ZnO was able to remove 79% of 10 mg/L RhB at 150 min which was greater than pure ZnO (21%) as Ag-ZnO had the lower PL intensity compared to pure ZnO. Thus, this enabled the photocatalyst to trap more e_{CB}^- and increase the separation of h_{VB}^+ and e_{CB}^- pairs for photocatalytic reaction improvement.

Among the synthesized Ag-ZnO samples, 5.0 wt% Ag-ZnO had the highest photocatalytic degradation efficiency as it had the optimal Ag loading in the Ag-ZnO. The result showed was consistent with the PL analysis as 5.0 wt% Ag-ZnO had the lowest recombination of photogenerated charge carriers compared to other Ag-ZnO samples. When the Ag wt% is above the optimal loading, the active sites on the surface of Ag-ZnO would reduce as the UV-Vis irradiation was partly shielded and would decrease the e_{CB}^- utilization in the photocatalytic activities, thus reducing the photocatalytic degradation of FG dye (Liang, et al., 2015). Similarly to literature reports done by Cheng, et al. (2013) had exhibited that the increased Ag wt% above the optimal Ag loading of 4.82 wt% pompon-like Ag-ZnO towards 0.025mM of MeO dye had reduced its photocatalytic degradation efficiency from 99.1% to 94.6% under 120 min. They deduced that the increased of Ag wt% above the optimal loading had shielded the photocatalyst from the UV light irradiation and ultimately decrease the photocatalytic efficiency. It was concluded that the synthesized 5.0 wt% Ag-ZnO outperform the pure ZnO, commercial ZnO, commercial TiO₂ and other Ag loading ZnO due to its 3D shape, low band gap, low photogenerated charge carrier recombination efficiency and optimal Ag loading.

The sedimentation test was done to evaluate the ability of particle separation. Figure 4.9 shows the sedimentation test over time with different photocatalysts. The result showed that 5.0 wt% Ag-ZnO had the fastest sedimentation ability as its supernatant was not relatively turbid after 30 min sedimentation. The sedimentation ability was mainly attributed to the density of the photocatalyst. Since 5.0 wt% Ag-ZnO (5.79 g/cm^3) had the heaviest density as compared to commercial TiO_2 (4.23 g/cm^3), commercial ZnO (5.61 g/cm^3) and pure ZnO (5.75 g/cm^3), it would fall fastest as reported in other studies (Karunakaran, Rajeswari and Gomanthisankar, 2011; Tekumalla, et al., 2016; Vyas, Mishra and Gandhi, 2013).

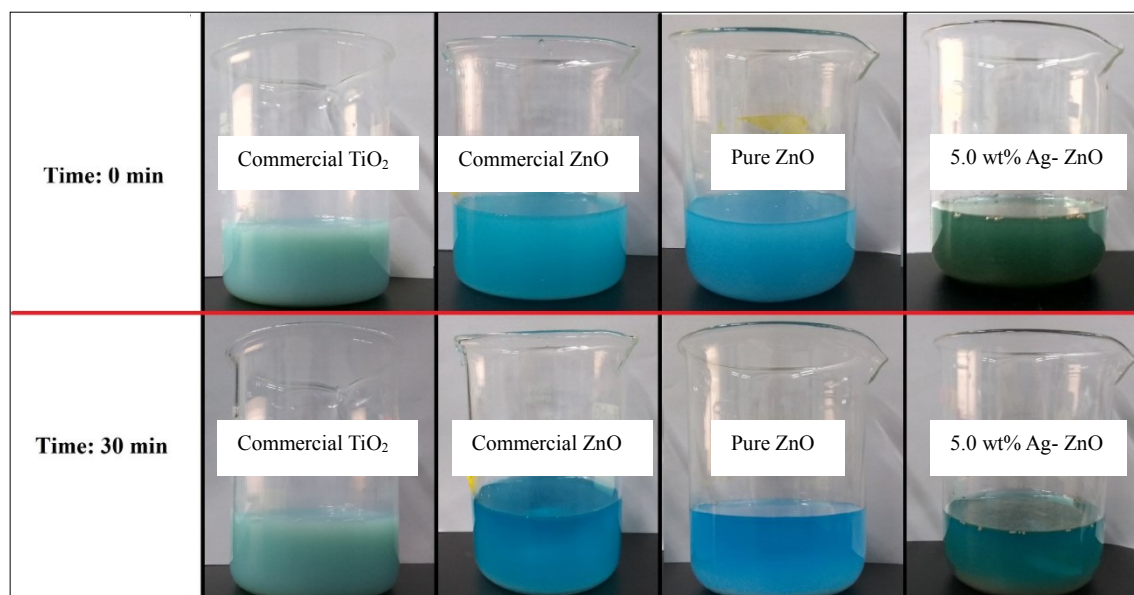


Figure 4.9: Sedimentation Test of Commercial TiO_2 , Commercial ZnO, Pure ZnO and 5.0 wt% Ag-ZnO over Time.

4.3 Process Parameters

4.3.1 Initial Dye Concentration

The dependency of the photocatalytic degradation of FG dye on initial dye concentration was investigated in the presence of 1 g/L 5.0 wt% Ag-ZnO and natural pH (pH 6.65). The effect of initial dye concentrations on the photocatalytic degradation process was evaluated by varying the initial dye concentration from 2.5 ppm to 20.0 ppm. Figure 4.10 displays the effect of initial dye concentration on the photocatalytic activities of FG dye. It was noted that the degradation percentage at low FG dye concentration of 2.5 ppm (100.00% degradation efficiency) was higher than 5.0 ppm (86.08% degradation efficiency), 10.0 ppm (51.51% degradation efficiency) and 20.0 ppm (40.49% degradation efficiency) of FG dye solution.

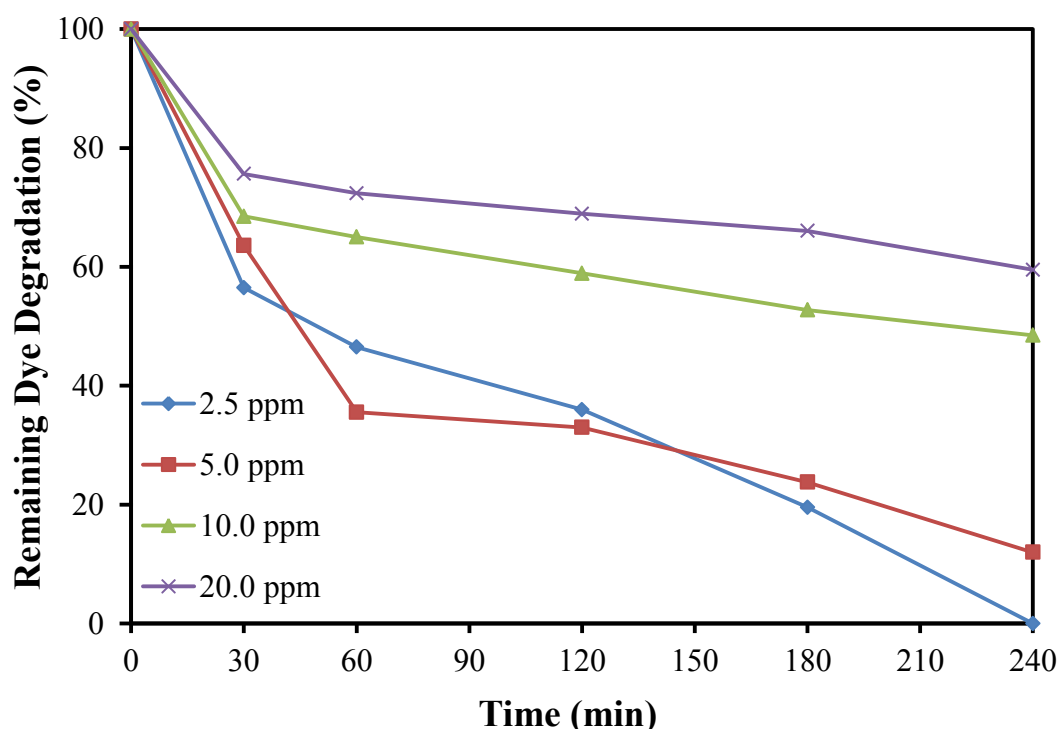


Figure 4.10: Effect of Initial Dye Concentration on the Photocatalytic Degradation of FG Dye ([5.0 wt% Ag-ZnO] = 1.0 g/L; pH = 6.65).

The low dye concentration of 2.5 ppm of FG dye demonstrated good photocatalytic activities compared to other higher initial dye concentration as less pollutant were required to be degraded in low dye concentration. When there is less pollutant to be degraded, the degradation efficiency would be high. Similar studies stated by Subash, et al. (2013) explained the presence of less pollutants to be degraded allow better photocatalytic degradation which their results displays low concentration of 1×10^{-4} M Acid Black 1 dye was degraded at highest photocatalytic efficiency with 3 g/L $\text{WO}_3\text{-Ag-ZnO}$ under 30 min compared to other higher dye concentration. Furthermore, low initial dye concentration allowed less interference of FG dye molecules towards light photons. Under low concentration of FG dye, it would allow more photons to reach to the surface of the photocatalyst for production of photogenerated e_{CB}^- thus amplifying the photocatalytic efficiency (Chamjangali and Boromund, 2013). Wang, et al. (2014) studies showed that increase of 0.02 mM of RhB dye had reduced photocatalytic degradation to 79.6% compared to photocatalytic degradation of 98.5% with 0.01 mM of RhB dye as the excess initial dye concentration had increases the probability between RhB dye and light photons and thus lead to reduction of photocatalytic activity.

In addition, the intermediate products produced during the dye-oxidation would compete with the FG dye molecules for available Ag-ZnO active sites. The decrease of initial dye concentration would reduce the competition occurrence between intermediates products and FG dye molecules and thus allow the complete degradation of FG dye. Similar to Panda, Sahoo and Mohapatra (2011) studies, the photocatalytic degradation of MeO reduced from 70% to 58% when initial dye concentration increase from 0.7 mg/mL to 0.8 mg/mL. They deduced that the intermediate products was the main attribution to their result as the intermediate products competed with MeO dye molecules for available Fe(III) active sites of the $\text{Fe}_2\text{O}_3\text{-SiO}_2$ composite.

The complete photocatalytic degradation of 2.5 mg/L of FG dye under 240 min was due to its lower amount of FG dye molecules in the system compared to other varied initial dye concentration. Low presence of FG dye molecules would lessen competition occurrence with O_2 and OH^- ions on the surface of photocatalyst. A study done by Khatee, et al. (2014) detailed that their study had a high degradation

efficiency of 67% Acid Red 17 dye at low dye concentration of 2.5 ppm as less amount of dye molecules were occupied at the active sites of the photocatalyst. Their study concluded that the unoccupied active site of the photocatalyst would then generate $\bullet\text{OH}$ radicals from O_2 and OH^- ions and ultimately lead to higher photocatalytic degradation of Acid Red 17 dye molecules. Consequently, the ideal initial dye concentration selected should be 2.5 ppm as it performed the best degradation efficiency towards FG dye molecules as compared to other initial dye concentration.

4.3.2 Solution pH Effect

The influence of solution pH on the photocatalytic degradation of FG dye was studied by varying the solution pH from 2.00 to 9.00 using HNO_3 and NaOH under constant initial dye concentration of 2.5 ppm. Figure 4.11 presents result of the solution pH effect on the FG dye photocatalytic degradation. The outcome exhibited that natural pH of 6.65 could completely remove FG dye within 240 min. At acidic pH of 2.00 and 4.00, the FG degradation efficiency was 43.54% and 74.30%, respectively. On the other hand, the dye degradation efficiency of alkaline pH (pH 9.00) was 61.29% by 240 min. The neutral pH only achieved 68.05% of FG dye degradation at same time period. Thus, the best performing solution pH for photocatalytic degradation reaction using as-synthesized 5.0 wt% Ag-ZnO was natural pH at constant initial dye concentration.

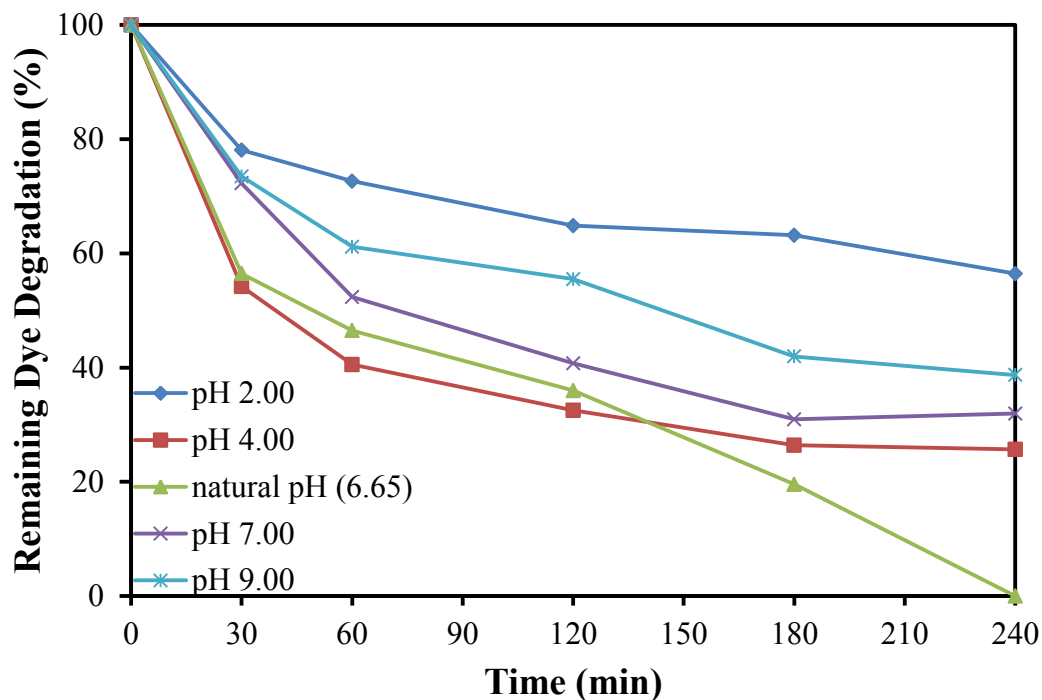


Figure 4.11: Effect of Solution pH on the Photocatalytic Degradation of FG Dye ([5.0 wt% Ag-ZnO] = 1.0 g/L; [FG] = 2.5 ppm).

It was observed that the increase of pH from pH 2.00 to 6.65 (natural pH) increased the photocatalytic degradation of FG dye and then decreased after pH 6.65. The observation was mainly attributed to the competition due to dissociation ions from pH adjusters with FG dye molecules. The generation of NO_3^- ions from HNO_3 dissociation might have absorbed on the surface of 5.0 wt% Ag-ZnO, thus reduced in OH^- ions availability (Devi and Reddy, 2010). According to Umar and Aziz (2013), more OH^- ions would be required for photocatalytic degradation of FG dye as other OH^- ions could react with other non-targeted compounds due to its non-selective nature, therefore reduce the photocatalytic degradation efficiency.

However in natural pH, the photocatalyst was able to perform best as there is no addition of pH adjuster in the system. Thus, the natural pH would had the highest photocatalytic degradation efficiency compared to other varied pH solution as it has the least competition between dye molecules and dissociated ions from pH adjuster. Meanwhile, FG dye degradation efficiency dropped in alkaline condition as NaOH

was introduced into the solution. Na^+ and OH^- ions dissociated from NaOH are most likely to be absorbed on the photocatalyst surface and ultimately, reduce the photocatalytic degradation. Furthermore, alkaline pH medium would cause electrostatic repulsion between dye molecules and surface of photocatalyst thus reducing the contact between them. This study concluded that the natural pH was best used for optimum photocatalytic degradation of FG dye.

A comparison study was also conducted between the present study and literature report. The results are shown in Table 4.1. Modification of the ZnO morphologies was seen to improve the photocatalytic degradation efficiency when compared with present study and Sun, et al. (2010) studies. In this present study, the modified 3D micro/nanoflowers 5.0 wt% Ag-ZnO was able to degrade 100.0% of FG dye within 240 min while 2D diamond-like Sn-ZnO produced from Sun, et al. (2010) studies only managed to degrade 87.0% of MB dye within 600 min. Furthermore, the synthesis method of ZnO also affected the photocatalytic degradation of dye. As reported by Chen, et al. (2013), as-produced 3D coral-like Au-ZnO had photocatalytic degradation performance of 82.1% within 600 min which was lower than this present study despite 3D morphologies modification. The lower performance of 3D coral-like Au-ZnO was mainly attributed to its hydrothermal synthesis method as hydrothermal method would produce bigger photocatalyst size (8 μm), thus decrease surface to volume ratio of the photocatalyst and ultimately reduce the availability of active site for photocatalytic degradation process. On the contrary, co-precipitation method in the present study would synthesize a smaller particle size ranging from 700 nm to 3.5 μm diameter. The comparison of Yang, et al. (2010) study and present study was also done to investigate the Ag dopant effect towards the photocatalytic reaction. The as-synthesized 5.0 wt% Ag-ZnO in the present study performed better with low power light irradiation than Yang, et al. (2010) photocatalyst due to the presence of Ag dopant. The photocatalyst used in the present study resulted in reduction of recombination of photogenerated charge carriers and thus improved photocatalytic reaction. It is concluded that, the present study had better photocatalytic degradation efficiency due to its 3D morphological modification, co-precipitation synthesis method and Ag dopant attachment.

Table 4.1: Comparison Survey of the Degradation of Dye by UV-Vis Light Photocatalysis.

Photocatalyst	Dye	ZnO Synthesis Method	Experimental condition				Degradation efficiency (%)	References	
			[Dye] (mg/L)	[Photocatalyst] (g/L)	Solution pH	Source of light			Time (min)
			Cd-ZnO	MB	Sol-gel	10.0			0.04
Coral-like Au-ZnO	Orange II	Hydrothermal	10.0	1.50	7.00	8 W pen-ray lamp	600	82.1	Chen, et al. (2013)
Dumbbell- shaped ZnO	MB	Microwave heating	15.0	1.00	7.00- 8.00	300 W Hg lamp	75	99.6	Yang, et al. (2010)
Eu-ZnO	MeO	Co-precipitation	10.0	1.00	6.20	100 W Hg lamp	180	95.3	Zong, et al. (2014)
Pd-ZnO	MeO	Sol-gel	10.0	1.00	7.00	300 W Hg lamp	60	48.2	Zhong, et al. (2012)
Sn-ZnO	MB	Microwave heating	40.0	0.33	6.70	Sunlight irradiation	600	87.0	Sun, et al. (2010)
Flower-like Ag-ZnO	FG	Co-precipitation	2.5	1.00	6.65	45 W fluorescent light	240	100.0	Present study

4.4 Mineralization Study

Figure 4.12 presents the variations of FG dye in terms of photocatalytic degradation and photocatalytic mineralization in the presence of 5.0 wt% Ag-ZnO micro/nanoflowers under UV-Vis irradiation. As shown, FG dye was photocatalytic mineralized at 100.0% within 240 min through COD reduction similarly to photocatalytic degradation efficiency of 100.0% at identical conditions. The result further deduced that the successful conversion of harmful FG dye molecules to harmless inorganic product.

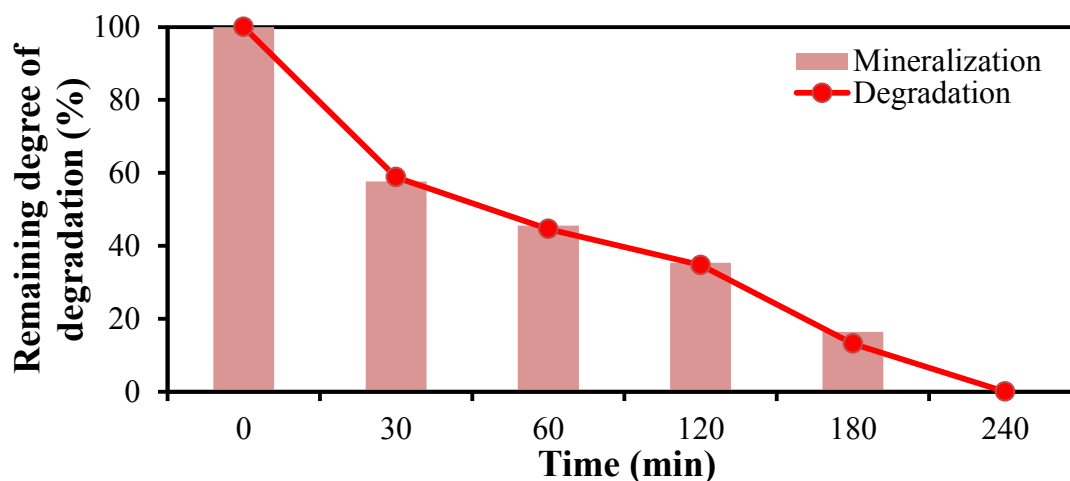


Figure 4.12: Photocatalytic Mineralization and Degradation of FG Dye ([5.0 wt% Ag-ZnO] = 1.0 g/L; [FG] = 2.5 ppm; pH = 6.65).

The outcome of the mineralization study was in line with other research works. Korake, et al. (2014) stated that the 100 mg/L of metasytox was degraded 90% with 2 g/dm³ of 0.5 mol% La-ZnO nanorods while obtaining COD mineralization of 85% within 150 min under similar condition. Their study showed that the photocatalytic degradation occurred at the same time with photocatalytic mineralization. Similarly, Shinde, Bhosale and Rajpure (2012) also displayed that the COD mineralization of 85.8% Acid Orange 7 while photocatalytic degradation of 99.5% during photocatalytic reaction with Ag-ZnO within 120 min under sunlight illumination. Therefore, the 5.0 wt % Ag-ZnO exhibited good photocatalytic activity in degradation and mineralization of FG dye.

4.5 Detection of Free Radicals

The role of active species such as $\bullet\text{OH}$ radicals, $\bullet\text{O}_2^-$ radicals and photogenerated $h_{\nu\text{B}}^+$ was investigated during the photocatalytic degradation of FG dye using 5.0 wt% Ag-ZnO. With the application of radical scavengers, the photocatalytic degradation process would be partially suppressed and degradation of FG dye would reduce. The importance of radical species was understood corresponding to the degree of suppression in the FG dye degradation induced by the radical scavengers. In this study, the radical scavenger such as isopropanol, BQ and KI are used for $\bullet\text{OH}$, $\bullet\text{O}_2^-$ and $h_{\nu\text{B}}^+$ radicals quenching, respectively (Yang, et al., 2015; Halliwell and Gutteridge, 2015; Van Doorslaer, et al., 2012). The result of the photocatalytic degradation of FG dye after 240 min of UV-Vis irradiation is displayed in Figure 4.13.

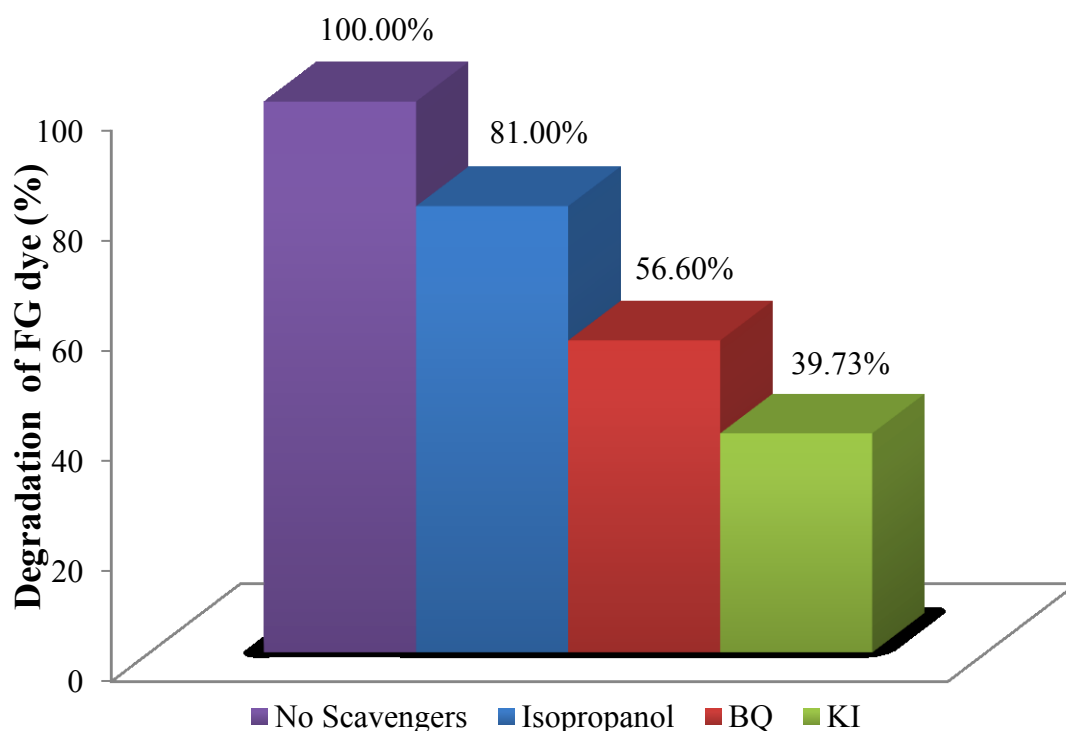


Figure 4.13: Effect of Radical Scavengers on the Photocatalytic Degradation of FG Dye ([5.0 wt% Ag-ZnO] = 1.0 g/L; [FG] = 2.5 ppm; pH = 6.65).

The degradation efficiency of FG dye solution declined as compared to without radical scavenger loaded condition in the presence of isopropanol, which the degradation dropped from 100.00% to 81.00%. This indicated that the $\bullet\text{OH}$ radicals played a minor role in the photocatalysis reaction of FG dye. Meanwhile, the introduction of BQ into the system had reduced the photocatalytic degradation performance to 56.60%. It was then deduced that the $\bullet\text{O}_2^-$ radicals played important roles in the photocatalytic reaction of FG dye. The addition of KI had significantly hindered the degradation efficiency of FG dye as degradation efficiency of only 39.73% was achieved. It was suggested that the h_{VB}^+ also played significant parts in the photocatalytic mechanism similarly to the $\bullet\text{O}_2^-$ radicals. The inclusive scavenging results matched with earlier literature reports (Fageria, Gangopadhyay and Pande, 2014; Liu, et al., 2015; Sampaio, et al., 2016).

A plausible mechanism of photocatalytic degradation of FG dye under UV-Vis light illumination could be proposed similar to other research works (Cai, et al., 2013; Liu, Wei and Gao, 2015; Mohammadzadeh, et al., 2015). As mentioned in Section 2.3.1, photocatalytic process started when Ag-ZnO adsorbed $h\nu$ with equal or greater than its band gap energy. Next, photogenerated charge carriers were produced and the e_{CB}^- were trapped by Ag^+ ions as shown in Eqs. (4.5) and (4.6). The separation efficiency of the photogenerated charge carriers was then enhanced. The h_{VB}^+ produced would further react with electron donors to form $\bullet\text{OH}$ radicals. At the same time, the trapped e_{CB}^- foraged by O_2 would produce $\bullet\text{O}_2^-$ radicals which lead to $\bullet\text{OH}$ radicals, $\text{HO}_2^{\bullet-}$, and H_2O_2 generation. The reactions could be illustrated from Eqs. (4.6) to (4.12). At the end, the produced radicals degraded the FG dye into harmless products as presented from Eqs. (4.13) to (4.15). From the proposed mechanism, the h_{VB}^+ and $\text{O}_2^{\bullet-}$ radicals participated major parts of photocatalytic reaction, while $\bullet\text{OH}$ took part in minor extent in photocatalytic reaction mechanism. Figure 4.14 illustrates photocatalytic mechanism Ag-ZnO under UV-Vis light irradiation.



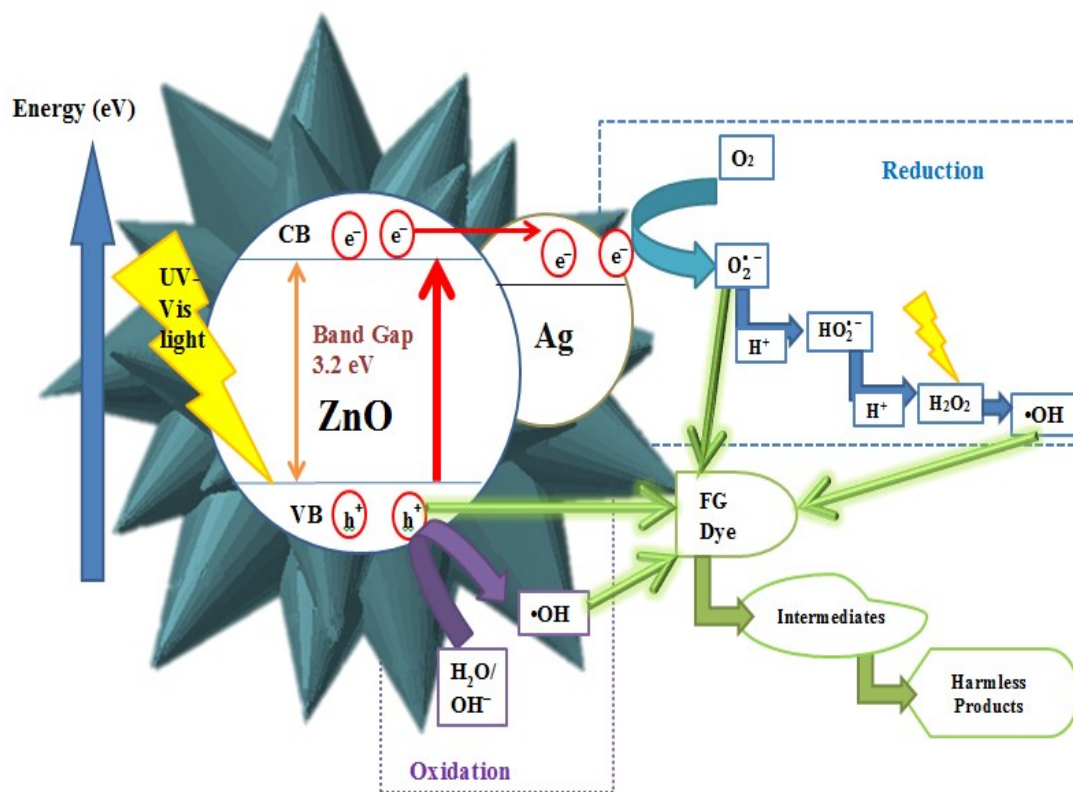
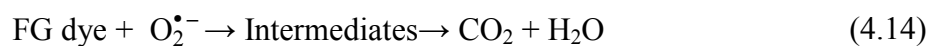
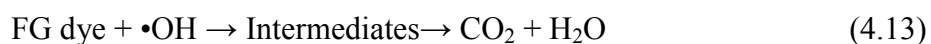


Figure 4.14: Schematic Diagram of Proposed UV-Vis Photocatalytic Mechanism of FG Dye over 5.0 wt% Ag-ZnO Photocatalyst.

4.6 Antibacterial Study

4.6.1 Screening for Antibacterial Response

The screening for antibacterial response towards *E.coli* was tested for 180 min in different conditions. Figure 4.15 displays compilation of viable or survived *E.coli* colonies in petri dish under different conditions at specified time intervals of the experiment. It was noted that the colonies without membrane lysis can be seen as darker pigments in the figure. Drastic reduction of darker pigments was observed for petri dish which contain 5.0 wt% Ag-ZnO and illuminated by UV-Vis light over time. This indicated that the 5.0 wt% Ag-ZnO had good photokilling ability towards *E.coli*. At the end of treatment, the petri dish containing bacteria in contact with 5.0 wt% Ag-ZnO did not have any dark pigments which indicated 1×10^7 colonies of *E.coli* were disinfected. The order of photocatalytic condition with good antibacterial response is as follows: 5.0 wt% Ag-ZnO > pure ZnO > dark absorption > photolysis. The results of the photocatalytic disinfection of *E.coli* were aligned with the photocatalytic degradation of FG dye.

Similar findings can be observed by other literature reports (Li, et al., 2011; Pant, et al., 2012; Zhu, et al., 2016). Li, et al. (2011) reported that the UV light aided Ag-TiO₂ reduce the viable Gram-negative *Pseudomonas putida* bacterial cell percentage more than UV light aided commercial TiO₂, dark absorption of Ag-TiO₂ and UV light within 180 min. Furthermore, the findings from Pant, et al. (2012) also demonstrated that the nanoflowers Ag-TiO₂/ZnO had the best antimicrobial effect towards *E.coli* compared to TiO₂/ZnO with UV radiation and Ag-TiO₂/ZnO without UV radiation. Zhu, et al. (2016) also presented that the 1.0 mol% Ag-MgO had the highest inactivation of 10^7 CFU *E.coli*/mL under 25 min in comparison to pure MgO and photolysis condition.

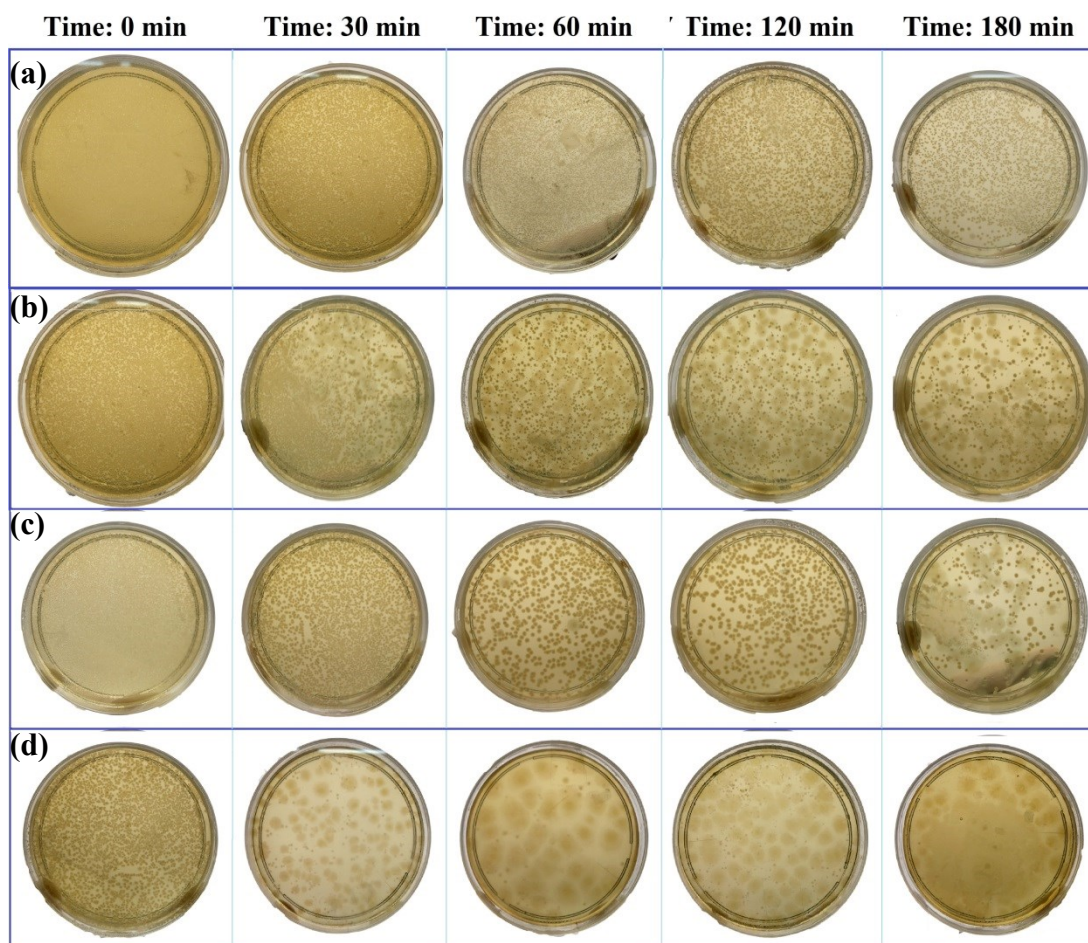


Figure 4.15: Screening for Antibacterial Response under (a) Photolysis, (b) Dark Absorption and Photocatalytic Activities with (c) Pure ZnO and (d) 5.0 wt% Ag-ZnO over Time.

It was deduced that the diminishing number of viable *E.coli* in photocatalytic disinfection upon using 5.0 wt% Ag-ZnO was due to presence of generated reactive oxygen species from photocatalyst with aid from UV-Vis irradiation as reported by Matai, et al. (2014). Examples of proposed ROS involved in the antibacterial response are $\bullet\text{OH}$, $\text{HO}_2^{\bullet-}$ and $\text{O}_2^{\bullet-}$. ROS can also be generated inside the bacterial cell due to impeded electronic transport along the respiratory chain in the disintegrated plasma membrane and could cause intracellular oxidative stress towards the bacterial cell membrane (Song, et al., 2016). Huang, et al. (2015) also reported that the ROS could cause lethal attack to the cell if close contact between the photocatalysis and bacteria was established. The bacteria with damaged membrane would then leach its intracellular components and ultimately die. According to earlier literature reports on antibacterial response such as Karunakaran, Rajeswari and Gomathisankar (2011)

and Ibănescu, et al. (2014), 5.0 wt% Ag-ZnO was able to produce more ROS due to attachment of Ag which would imply more damage to the bacterial membrane and ultimately reduce the viability of *E.coli* colonies. Therefore, it was concluded that ROS was mainly responsible for the antibacterial response from 5.0 wt% Ag-ZnO.

4.6.2 Membrane Integrity Assay

To confirm the postulation of bacterial membrane leakage due to antibacterial response of different conditions, the membrane integrity assay analysis was executed. If membrane lysis occurred, the DNA would be leached out from the bacterial cell. Leached DNA components showed a strong absorption at 260 nm where it was measured by an UV-Vis spectrophotometer at 260 nm (Dasgupta and Ramalingam, 2016; Meghana, et al., 2015; Xia, et al., 2016). Figure 4.16 presents the absorbance of leaked DNA components over time in different conditions. The figure displayed that the highest absorbance of DNA components at 180 min belonged to 5.0 wt% Ag-ZnO at 0.115 abs followed by pure ZnO (0.092 abs) > dark absorption (0.054 abs) > photolysis (0.005 abs).

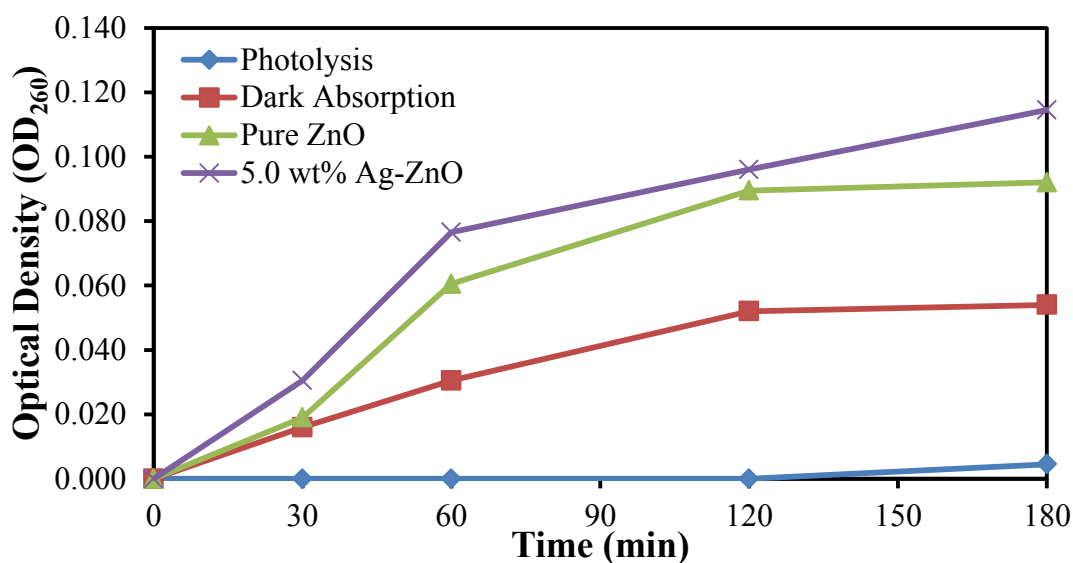


Figure 4.16: Membrane Integrity Assay Analysis under Different Conditions.

The result from the membrane integrity assay was in accordance with other literature reports (Zijno, et al., 2015; Deokar, et al., 2013). Cells exposed to 6.4 $\mu\text{g/mL}$ of ZnO had 3-fold DNA absorbance increase compared to photolysis and dark absorbance condition as stated by Zijno, et al. (2015) study. They deduced that the increase of DNA absorbance was due to the generation of ROS which induced oxidative stress towards the bacterial membrane. Moreover, Deokar, et al. (2013) also reported that the measured leaked DNA absorbance for *E.coli* indicated alteration and punctured bacterial lipid membrane components. Furthermore, despite presence of high oxidative stress from ROS, the DNA components was not reduced easily as DNA-binding proteins protected the DNA components by condensing it into a stable state (Carré, et al., 2014; Calhoun and Kwon, 2010). The DNA components were altered instead of reduced in absorbance as stated by Xu, et al. (2017). Therefore, the measurement of DNA absorbance was not affected by DNA decomposition reaction. Thus, it was suggested that 5.0 wt% Ag-ZnO caused more membrane lysis compared to other conditions as it had the most DNA absorbance leaked in the system. The result was in agreement with the screening test in the previous section.

E.coli was classified as a Gram-negative bacteria and it consisted of two cellular membranes which were the outer and inner membranes as identified by Gupta (2008). The outer membranes of the Gram-negative bacteria consisted of lipopolysaccharide and phospholipid bilayer layers which made up of fatty acid molecules. The damage of cell outer membrane was done by lipid peroxidation process due to presence of $\text{O}_2^{\bullet-}$ radicals in the photocatalytic reaction (Thabet, et al., 2014; Premanathan, et al., 2011; Krishnamoorthy, et al., 2012; Tsai, et al., 2010). Dalrymple, et al. (2010) explained that lipid peroxidation started during the reaction of unsaturated fatty acids and $\text{O}_2^{\bullet-}$ radicals in the presence of O_2 to form $\text{HO}_2^{\bullet-}$ radical. The $\text{HO}_2^{\bullet-}$ radicals would then react with lipid molecules in the phospholipid and lipopolysaccharide layer. After the reaction, a chain of reaction of biomolecules oxidation was formed. Next, the inner membrane comprises of peptidoglycan layer and cytoplasmic membrane would later broke down due to oxidative stress caused by ROS thus leading to the leakage of protein nucleotides (Chong, et al., 2010; Xia, et al., 2013; Veneiri, et al., 2016). Figure 4.17 displays the overall inactivation action of

ROS generated from 5.0 wt% Ag-ZnO towards the inner and outer membranes of *E.coli*.

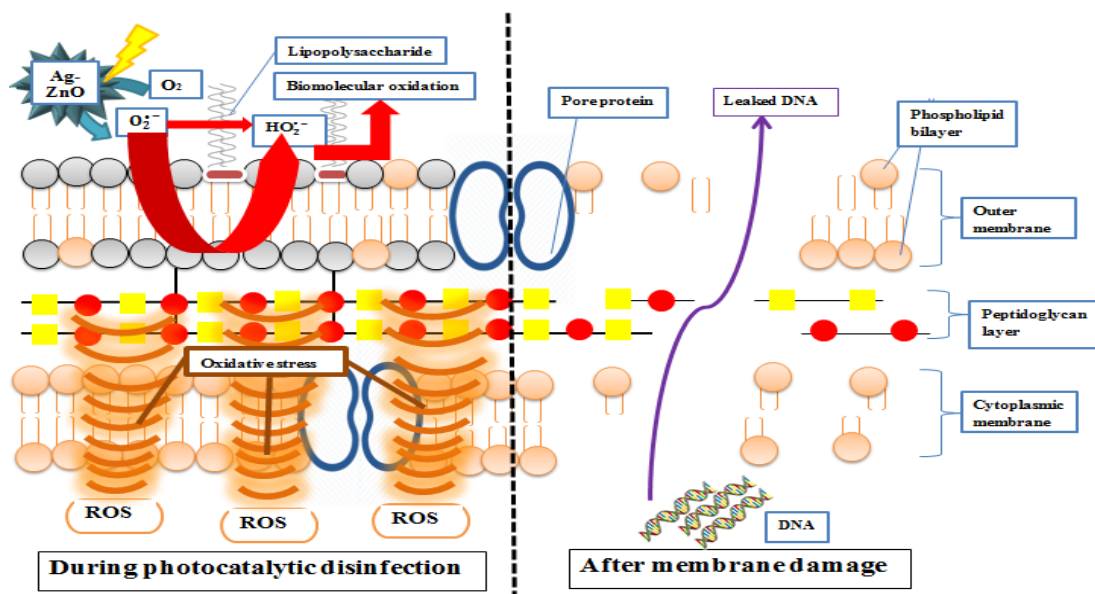


Figure 4.17: Schematic Diagram of Photocatalytic Disinfection Mechanism of *E.coli* under UV-Vis illumination.

Table 4.2 shows the comparison studies on photocatalytic disinfection with other photocatalyst. The antibacterial response can be enhanced with morphological modification. Karunakaran, Rajeswari and Gomanthisankar (2011) study deduced that its produced Ag-ZnO had no definite shape and resulted to agglomeration of the photocatalyst particles and ultimately reduction of antibacterial response towards *E.coli*. In comparison to Karunakaran, Rajeswari and Gomanthisankar (2011) study, modified 3D flower-like shape Ag-ZnO produced in this study had a better antibacterial response performance as 3D shape could prevent agglomeration of particles. At the same time, the attachment of Ag onto the photocatalyst also enhanced the antibacterial response performance towards *E.coli*. As-synthesized ZnO from Zyoud, et al. (2016) reduced lower in log number of *E.coli* CFU/mL than the present study as as-produced photocatalysts from the present study have Ag attachment to its photocatalyst. It was deduced that, the present study had better antibacterial response efficiency due to its 3D morphological modification and Ag dopant attachment.

Table 4.2: Comparison Survey of the Antibacterial Response of *E.coli* by UV-Vis Light Photocatalysis.

Photocatalyst	Experimental condition				Log CFU/mL reduction	References
	[<i>E.coli</i>] (CFU/mL)	[Photocatalyst] (g/L)	Source of light	Time (min)		
Ag/TiO ₂ /ZnO nanoflowers	1.00 x 10 ⁷	0.40	100 W UV light	120	10 ⁷	Pant, et al. (2012)
0.1 at% Ag-ZnO	1.00 x 10 ¹³	0.80	8 W mercury lamp	10	10 ¹	Karukaran, Rajeswari and Gomanthisankar (2011)
Ag-ZnO/g-C ₃ N ₄	1.00 x 10 ⁶	0.20	100 W UV light	120	10 ³	Adhikari, et al. (2015)
Pd-ZnO	4.00 x 10 ⁷	1.00	10 W UV laser beam	10	10 ⁶	Khalil, Gondal and Dastageer (2011)
Se-ZnO	9.00 x 10 ⁶	0.55	40 W tungsten lamp	60	10 ²	Dutta, Nenavathu and Talukar (2014)
ZnO	7.37 x 10 ⁵	2.00	Solar simulator	90	10 ¹	Zyoud, et al. (2016)
5.0 wt% flower-like Ag-ZnO	1.50 x 10 ⁷	1.00	45 W compact fluorescent lamp	180	10 ⁷	Present study

CHAPTER 5

CONCLUSION AND RECOMMENDATIONS

5.1 Conclusion

In summary, 3D flower-like Ag-ZnO micro/nanostructures were successfully synthesized by low temperature co-precipitation and photodeposition methods. The as-synthesized photocatalyst was characterized by XRD, EDX, FESEM, UV-Vis absorption and PL analysis. The XRD analysis proved that the synthesized Ag-ZnO possessed high crystallinity. FESEM demonstrated that the produced Ag-ZnO had a 3D flower-like shape and varied in sizes from 700 nm to 3.5 μm . Furthermore, the EDX analysis confirmed that Ag, Zn and O elements were present in the photocatalyst. UV-Vis absorption analysis determined that the band gap of 5.0 wt% Ag-ZnO was 3.23 eV. This deduced that the 5.0 wt% Ag-ZnO can be activated under UV-Vis irradiation. Moreover, PL analysis determined that the Ag-ZnO had a lower emission peak compared to pure ZnO, which implied lower recombination of photogenerated charge carriers.

A comparison study was executed using different Ag loadings of Ag-ZnO, pure ZnO, commercial ZnO and commercial TiO₂. It was observed that the as-produced 5.0 wt% Ag-ZnO exhibited superior photocatalytic activity compared to 2.5 wt% Ag-ZnO, 10.0 wt% Ag-ZnO, pure ZnO, commercial ZnO and commercial

TiO₂. The 93.15% photocatalytic degradation of 5 ppm FG dye was achieved by 5.0 wt% Ag-ZnO while 10.0 wt% Ag-ZnO, 2.5 wt% Ag-ZnO, pure ZnO, commercial ZnO and commercial TiO₂ managed to degrade 85.94%, 83.77%, 80.04%, 70.56%, 62.17%, respectively under 240 min. Besides that, the sedimentation test was conducted to evaluate the ability of particle separation. It was demonstrated that the 5.0 wt% Ag-ZnO micro/nanoparticles were able to settle within 30 min and formed a layer at the bottom compared to pure ZnO, commercial ZnO and commercial TiO₂. This feature would allow the reusability and separation of the 5.0 wt% Ag-ZnO in the wastewater treatment sector.

Two parameters were tested under the UV-Vis irradiation including the initial dye concentration and solution pH for the degradation of FG dye. Under initial dye concentration of 2.5 ppm and pH 6.65, complete photocatalytic degradation of FG dye was achieved under 240 min. Mineralization study was also conducted to determine the extent of mineralization of 5.0 wt% Ag-ZnO under optimized conditions. The complete photocatalytic mineralization of FG dye was also attained within 240 mins. Furthermore, the investigation of active species roles using radical scavenger had demonstrated that $\bullet\text{O}_2^-$ and $h\nu_B^+$ radicals participated major parts of photocatalytic reaction while $\bullet\text{OH}$ played a minor extent in photocatalytic reaction mechanism of FG dye degradation.

Furthermore, the screening for antibacterial response was tested under 180 min with 5.0 wt% Ag-ZnO and pure ZnO under UV-Vis light illumination. Drastic reduction of 10^7 *E.coli* colonies was observed with presence of 5.0 wt% Ag-ZnO under UV-Vis light over time compared to pure ZnO. Membrane integrity assay was also conducted to determine the bacterial membrane leakage postulation. The result observed showed that 5.0 wt% Ag-ZnO produced the highest leaked DNA absorbance of 0.115 abs compared to pure ZnO. This showed that the 5.0 wt% Ag-ZnO had good antibacterial properties towards *E.coli* under the UV-Vis illumination. In summary, the 5.0 wt% Ag-ZnO was an effective and promising photocatalyst for organic pollutants and antibacterial treatments.

5.2 Recommendations

Upon completion of the present study, several fundamental and engineering aspects should be focus in the future photocatalytic studies.

1. The study should be given focus on synthesizing porous 3D flower-like ZnO micro/nanostructures as they are able to improve the adsorption of dye and bacteria.
2. The produced photocatalyst could be tested using solar light irradiation as the light source as this light source is free, abundant and clean energy source which would further bring benefit to photocatalysis technology.
3. The Ag-ZnO photocatalyst should be evaluated using real wastewater as mixtures of dyes and bacteria are present in the wastewater.

REFERENCES

- Adhikari, S.P., Pant, H.R., Kim, J.H., Kim, H.J., Park, C.H. and Kim, C.S., 2015. One pot synthesis and characterization of Ag-ZnO/g-C₃N₄ photocatalyst with improved photoactivity and antibacterial properties. *Colloids and Surface A: Physicochemical and Engineering Aspects*, 482, pp. 477-484.
- Aguilar, K., Garvín, A. and Ibarz, A., 2016. Effect of the concentration on the kinetic model of the photo-degradation of 5-hydroxymethylfurfural by UV irradiation. *Journal of Food Engineering*, 191, pp. 67-76.
- Ahmad, S., Shafie, S., Ab Kadir, M. and Ahmad, N., 2013. On the effectiveness of time and date-based sun positioning solar collector in tropical climate: a case study in northern peninsular Malaysia. *Renewable and Sustainable Energy Reviews*, 28, pp. 635-642.
- Akhigbe, L., Ouki, S. and Saroj, D., 2016. Disinfection and removal performance for *Escherichia coli* and heavy metals by silver-modified zeolite in a fixed bed column. *Chemical Engineering Journal*, 295, pp. 92-98.
- Akhil, K., Jayakumar, J., Gayathiri, G., Khan, S.S., 2016. Effect of various capping agents on photocatalytic, antibacterial and antibiofilm activities of ZnO nanoparticles. *Journal of Photochemistry and Photobiology, B: Biology*, 160, pp. 32-42.
- Akurati, K., 2008. *Synthesis of TiO₂ based nanoparticles for photocatalytic applications*. Göttingen: Cuvillier Verlag Gottingen Publisher.
- Al-Hardan, N., Abdullah, M., Ahmed, N., Yam, F. and Abdul Aziz, A., 2012. UV photodetector behavior of 2D ZnO plates prepared by electrochemical deposition. *Superlattices and Microstructures*, 51, pp. 765-771.

- Alley, E., 2007. *Water quality control handbook*. New York: McGraw-Hill.
- American Water Works Association and American Society of Civil Engineers, 2012. *Water Treatment Plant Design*. New York: McGraw-Hill Companies, Inc.
- Amin, K., Hameid, H. and Elsttar, A., 2010. Effect of food azo dyes tartrazine and carmoisine on biochemical parameters related to renal, hepatic function and oxidative stress biomarkers in young male rats. *Food and Chemical Toxicology*, 48, pp. 2994-2999.
- Amornpitoksuk, P., Suwanboon, S., Sangkanu, S., Sukhoom, A. and Muensit, N., 2012. Morphology, photocatalytic and antibacterial activities of radial spherical ZnO nanorods controlled with a diblock copolymer. *Superlattices and Microstructures*, 51, pp. 103-113.
- Anpo, M., 2010. *Environmentally benign photocatalysts: applications of titanium oxide-based materials*. London: Springer International Publishing.
- Antonopoulou, M., Evgenidou, E., Lambropoulou, D. and Konstantinou, I., 2014. A review on advanced oxidation processes for the removal of taste and odor compounds from aqueous media. *Water Research*, 53, pp. 215-234.
- Ariffin, M. and Sulaiman, S., 2015. Regulating sewage pollution of Malaysian rivers and its challenges. *Procedia Environmental Sciences*, 30, pp. 168-173.
- Asano, T., Burton, F. and Leverence, H., 2007. *Water reuse: Issues, Technology, and Applications*. New York: McGraw-Hill.
- Barudin, N.H.A., Sreekantan, S., Ong, M.T. and Lai, C.W., 2014. Synthesis, characterization and comparative study of nano-Ag-TiO₂ against Gram-positive and Gram-negative bacteria under fluorescent light. *Food Control*, 46, pp. 480-487.
- Bechambi, O., Najjar, W. and Sayadi, S., 2016. The nonylphenol degradation under UV irradiation in the presence of Ag-ZnO nanorods: effect of parameters and degradation pathway. *Journal of the Taiwan Institute of Chemical Engineers*, 60, pp. 496-501.

- Belgiorno, V., Naddeo, V. and Rizzo, L., 2011. *Water, wastewater and soil treatment by advanced oxidation processes*. Italy: Sanitary Environmental Engineering Division (SEED) Publication.
- Berg, H.C., 2004. *E.coli in motion*. New York: Bertelsmann Springer Science and Business Media.
- Bitton, G., 2005. *Wastewater Microbiology*. New Jersey: John Wiley & Sons, Inc.
- Bordbar, M., Forghani-Pilerood, S., Yeganeh-Faal, A. and Khodadadi, B., 2016. Effect of morphology on the photocatalytic behavior of ZnO nanostructures: low temperature sonochemical synthesis of Ni doped ZnO nanoparticles. *Journal of Nanostructures*, 6, 190-198.
- Borges, M.E., Sierra, M., Cuevas, E., Garcia, R.D. and Esparza, P., 2016. Photocatalysis with solar energy: sunlight-responsive photocatalyst based on TiO₂ loaded on a natural material for wastewater treatment. *Solar Energy*, 135, pp. 527-535.
- Cai, Y., Fan, H., Xu, M., and Li, Q., 2013. Rapid photocatalytic activity and honeycomb Ag/ZnO heterostructures via solution combustion synthesis. *Colloids and Surfaces A: Physicochemical and Engineering Aspects*, 436, pp. 787-795.
- Cai, A., Du, L., Wang, Q., Chang, Y., Wang, X. and Guo, X., 2016. Kelp-inspired N-I-doped ZnO photocatalysts with highly efficient catalytic activity. *Materials Science in Semiconductor Processing*, 43, pp. 25-33.
- Calhoun, L.N. and Kwon, Y.M., Structure, function and regulation of DNA-binding protein Dps and its role in acid and oxidative stress resistance in *Escherichia coli*: a review. *Journal of Applied Microbiology*, 110, pp. 375-386.
- Cao, D., Xiao, X., Wu, Y., Ma, X., Wang, M., Wu, Y. and Du, D., 2013. Role of electricity production in the anaerobic decolorization of dye mixture by exoelectrogenic bacterium *Shewanella oneidensis* MR-1. *Bioresource Technology*, 136, pp. 176-181.
- Cao, W., Chen, L. and Qi, Z., 2015. Microwave-assisted synthesis of

- Ag/Ag₂SO₄/ZnO nanostructures for efficient visible-light-driven photocatalysis. *Journal of Molecular Catalysis A: Chemical*, 401, pp. 81-89.
- Carré, G., Hamon, E., Ennahar, S., Estner, M., Lett, M., Horvatovich, P., Gies, J., Keller, V., Keller, N. and Andre, P., 2014. TiO₂ photocatalysis damages lipids and proteins in *Escherichia coli*. *Applied and Environmental Microbiology*, 80, pp. 2573-2581.
- Cauda, V., Pugliese, D., Garino, N., Sacco, A., Bianco, S., Bella, F., Lamberti, A. and Gerbaldi, C., 2014. Multi-functional energy conversion and storage electrodes using flower-like zinc oxide nanostructures. *Energy*, 65, pp. 639-646.
- Chakma, S., Das, L. and Moholkar, V., 2015. Dye decolorization with hybrid advanced oxidation processes comprising sonolysis/fenton-like/photo-ferrioxalate systems: a mechanistic investigation. *Separation and Purification Technology*, 156, pp. 596-607.
- Chamjangali, M.A. and Boroumand, S., 2013. Synthesis of flower-like Ag-ZnO nanostructure and its application in the degradation of methyl orange. *Journal of Brazil Chemical Society*, 24, pp. 1329-1338.I
- Chandrasena, G.I., Pham, T., Payne, E.G., Deletic, A. and McCarthy, D.T., 2014. *E.coli* removal in laboratory scale stormwater biofilters: Influence of vegetation and submerged zone. *Journal of Hydrology*, 519, pp. 814-822.
- Chang, J., Ahmad, M., Wlodarski, W. and Waclawik, E., 2013. Self-assembled 3D ZnO porous structures with exposed reactive {0001} facets and their enhanced gas sensitivity. *Sensors*, 13, pp. 8445-8460.
- Chen, C.C., Yu, B., Liu, P., Liu, J. and Wang, L., 2011. Investigation of nano-sized ZnO particles fabricated by various synthesis routes. *Journal of Ceramic Processing Research*, 12, pp. 420-425.
- Chen, P., Lee, G., Davies, S., Masten, S., Amutha, R. and Wu, J., 2013. Hydrothermal synthesis of coral-like Au/ZnO catalyst and photocatalytic degradation of Orange II dye. *Materials Research Bulletin*, 48, pp. 2375-2382.

- Cheng, M., Zeng, G., Huang, D., Lai, C., Xu, P., Zhang, C. and Liu, Y., 2016. Hydroxyl radicals based advanced oxidation processes (AOPs) for remediation of soils contaminated with organic compounds: a review. *Chemical Engineering Journal*, 284, pp. 582-598.
- Cheng, Y., An, L., Lan, J., Gao, F., Tan, R., Li, X. and Wang, G., 2013. Facile synthesis of pompon-like ZnO-Ag nanocomposites and their enhanced photocatalytic performance. *Materials Research Bulletin*, 48, pp. 4287-4293.
- Cheremisinoff, N.P., 2002. *Handbook of water and wastewater treatment technologies*. Woburn: Butterworth-Heinemann.
- Chu, P. and Liu, X., 2008. *Biomaterials fabrication and processing handbook*. Boca Raton: CRC Press/Taylor & Francis.
- Cui, J., Sun, J., Liu, X., Li, J., Ma, X. and Chen, T., 2014. Fabrication of hierarchical flower-like porous ZnO nanostructures from layered $\text{ZnC}_2\text{O}_4 \cdot 3\text{Zn}(\text{OH})_2$ and gas sensing properties. *Applied Surface Science*, 308, pp. 17-23.
- Cui, J., Li, Y., Liu, L., Chen, L., Xu, J., Ma, J., Fang, G., Zhu, E., Wu, H., Zhao, L., Wang, L. and Huang, Y., 2015. Near-infrared plasmonic-enhanced solar energy harvest for highly efficient photocatalytic reactions. *Nano Letters*, 15, pp. 6295-6301.
- Dalrymple, O.K., Stefanakos, E., Trotz, M.A. and Goswami, D.Y., 2010. A review of the mechanism and modeling of photocatalytic disinfection. *Applied Catalysis B: Environmental*, 98, pp. 27-38.
- Das, S., Sinha, S., Suar, M., Yun, S.I., Mishra, A. and Tripathy, S.K., 2015. Solar-photocatalytic disinfection of *Vibrio cholerae* by using Ag-ZnO core-shell structure nanocomposites. *Journal of Photochemistry and Photobiology B: Biology*, 142, pp. 68-76.
- Dasgupta, N. and Ramalingam, C., 2016. Silver nanoparticle antimicrobial activity explained by membrane rupture and reactive oxygen generation. *Environmental Chemical Letter*, 14, pp. 477-485.

- Deng, Q., Duan, X., Ng, D., Tang, H., Yang, Y., Kong, M., Wu, Z., Cai, W. and Wang, G., 2012. Ag nanoparticle decorated nanoporous ZnO microrods and their enhanced photocatalytic activities. *ACS Applied Material Interfaces*, 4, pp. 6030-6037.
- Deokar, A.R., Lin, L.Y., Chang, C.C. and Ling, Y.C., 2013. Single-walled carbon nanotubes coated antibacterial paper: preparation and mechanistic study. *Journal of Materials Chemistry B*, 9, pp. 2639-2646.
- Department of Environmental Ministry of Natural Resources and Environment, 2010. PU(A) 434 Environmental requirements: a guide for investors. Putrajaya: Department of Environmental Ministry of Natural Resources and Environment.
- Dermenci, K., Genc, B., Ebin, B., Olmez-Hanci, T. and Gürmen, S., 2014. Photocatalytic studies of Ag/ZnO nanocomposite particles produced via ultrasonic spray pyrolysis method. *Journal of Alloys and Compounds*, 586, pp. 267-273.
- Devi, L.G. and Reddy, K.M., 2010. Enhanced photocatalytic activity of silver metallized TiO₂ particles in the degradation of an azo dye methyl orange: characterization and activity at different pH values. *Applied Surface Science*, 256, pp. 3116-3121.
- Ding, Y., Zhou, P. and Tang, H., 2016. Visible-light photocatalytic degradation of bisphenol A on NaBiO₃ nanosheets in a wide pH range: a synergistic effect between photocatalytic oxidation and chemical oxidation. *Chemical Engineering Journal*, 291, pp. 149-160.
- Dong, X., Yang, P., Liu, Y., Jia, C., Wang, D., Wang, J., Chen, L. and Che, Q., 2016. Morphology evolution of one-dimensional ZnO nanostructures towards enhanced photocatalysis performance. *Ceramics International*, 42, pp. 518-526.
- Dutta, R.K., Nenavathu, B.P. and Talukdar, S., 2014. Anomalous, antibacterial activity and dye degradation by selenium doped ZnO nanoparticles. *Colloids and Surfaces B: Biointerfaces*, 114, pp. 218-224.
- Elango, M., Deepa, M., Subramanian, R. and Musthafa, A.M., 2017. Synthesis, characterization of polyindole/Ag-ZnO nanocomposite and its antibacterial

- activity. *Journal of Alloys and Compounds*, 696, pp. 391-401.
- Erkurt, H. and Arshad, M., 2010. *Biodegradation of azo dyes*. Berlin: Springer Publishing Company.
- Esparza-González, S.C., Sánchez-Valdésa, S., Ramírez-Barróna, S.N., Loera-Ariasd, M.J., Bernalb, J., Iván Meléndez-Ortiz, H. and Betancourt-Galindo, R., 2016. Effects of different surface modifying agents on the cytotoxic and antimicrobial properties of ZnO nanoparticles. *Toxicology in Vitro*, 37, pp. 134-141.
- Fagan, R., McCormack, D., Hinder, S. and Pillai, S., 2016. Photocatalytic properties of g-C₃N₄-TiO₂ heterojunctions under UV and visible light conditions, *Materials*, 9, pp. 286.
- Fageria, P., Gangopadhyay, S. and Pande, S., 2014. Synthesis of ZnO/Au and ZnO/Ag nanoparticles and their photocatalytic application using UV and visible light. *The Royal Society of Science*, 4, pp. 24962-24972.
- Fakhri, A., Pourmand, M., Khakpour, R. and Behrouz, S., 2015. Structural, optical, photoluminescence and antibacterial properties of copper-doped silver sulfide nanoparticles. *Journal of Photochemistry and Photobiology B: Biology*, 149, pp. 78-83.
- Fatin, S.O., Lim, H.N., Tan, W.T. and Huang, N.M., 2012. Comparison of photocatalytic activity and cyclic voltammetry of zinc oxide and titanium dioxide nanoparticles toward degradation of methylene blue. *International Journal of Electrochemical Science*, 7, pp. 9074-9084.
- Gautam, S., Shandilya, P., Priya, B., Singh, V.P., Raizada, P., Rai, Radheshyam, Valente, M.A. and Singh, P., 2017. Superparamagnetic MnFe₂O₄ dispersed over graphitic carbon sand composite and bentonite as magnetically recoverable photocatalyst for antibiotic mineralization. *Separation and Purification Technology*, 172, pp. 498-511.
- Ghaly, A.E., Ananthashankar, R., Alhattab, M. and Ramakrishnan V.V., 2013. Production, characterization and treatment of textile effluents: a critical review.

- Journal of Chemical Engineering and Process Technology*, 5, pp. 1-19.
- Gomez-Solís, C., Ballesteros, J., Torres-Martínez, L., Juárez-Ramírez, I., Díaz Torres, L., Elvira Zarazua-Morin, M. and Lee, S., 2015. Rapid synthesis of ZnO nano-corncoobs from Nital solution and its application in the photodegradation of methyl orange. *Journal of Photochemistry and Photobiology A: Chemistry*, 298, pp. 49-54.
- Gupta, P.K., 2008. *Cell and Molecular Biology*. Rastogi Publication: New Delhi.
- Güy, N., Çakar, S. and Özacar, M., 2016. Comparison of palladium/zinc oxide photocatalysts prepared by different palladium doping methods for congo red degradation. *Journal of Colloid and Interface Science*, 466, pp. 128-137.
- Halliwell, B. and Gutteridge, J., 2015. *Free radicals in biology and medicine*. Oxford: Clarendon Press.
- Hales, D., 2015. *An invitation to health: the power of now*. Montreal: Cengage Learning Solutions.
- Hedje, M. and Ulm, R., 2012. UV-B photoreceptor-mediated signaling in plants. *Trends in Plant Science*, 938, pp. 1-8.
- Hernández-Ramírez, A. and Medina-Ramírez, I., 2015. *Photocatalytic semiconductors: synthesis, characterization, environmental applications*. New York: Springer International Publishing.
- Hou, X., 2015. Facile fabrication and enhanced photocatalytic properties of ZnO/Au nanocomposites through a mild wet-chemistry route. *Materials Letters*, 140, pp. 39-42.
- Hu, Z.S., Hung, F.Y., Chen, K.J., Chang, S.J., Hsieh, W.K., Liao, T.Y. and Chen, T.P., 2013. Recovery of thermal-degraded ZnO photodetector by embedding nano silver oxide nanoparticles. *Applied Surface Science*, 279, pp. 31-35.
- Huang, J., Wu, Y., Gu, C., Zhai, M., Yu, K., Yang, M. and Liu, J., 2010. Large-scale synthesis of flowerlike ZnO nanostructure by a simple chemical solution route and its gas-sensing property. *Sensors and Actuators B: Chemical*, 146, pp. 206-

212.

Huang, J., Wu, Y., Gu, C., Zhai, M., Sun, Y. and Liu, J., 2011. Fabrication and gas-sensing properties of hierarchically porous ZnO architectures. *Sensors and Actuators B: Chemical*, 155, pp. 126-133.

Huang, J., Wu, Y., Gu, C., Zhai, M., Yu, K., Yang, M. and Liu, J., 2012. Large-scale synthesis of flowerlike ZnO nanostructure by a simple chemical solution route and its gas-sensing property. *Sensors and Actuators B: Chemical*, 146, pp. 206-212.

Huang, G., Xia, D., An, T., Ng, T.W., Yip, H.Y., Li, G., Zhao, H. and Wong, P.K., 2015. Dual roles of capsular extracellular polymeric substances in photocatalytic inactivation of *Escherichia coli*: comparison of *E.coli* BW25113 and isogenic mutants. *Applied and Environmental Microbiology*, 81, pp. 5174-5183.

Huebschen, G., Altpeter, I., Tschuncky, R. and Herrmann, H., 2016. *Materials characterization using nondestructive evaluation (NDE) methods*. Cambridge: Elsevier Science.

Hunge, Y.M., Mahadik, M.A., Moholkar, A.V. and Bhosale, C.H., 2017. Photoelectrocatalytic degradation of oxalic acid using WO₃ and stratified WO₃/TiO₂ photocatalysts under sunlight illumination. *Ultrasonics Sonochemistry*, 35, pp. 233-242.

Ibănescu, M., Musat, V., Textor, T., Badilita, V. and Mahlig, B., 2014. Photocatalytic and antimicrobial Ag/ZnO nanocomposites for functionalization of textile fabrics. *Journal of Alloys and Compounds*, 610, pp. 244-249.

Ingram, P., 1999. *Biomedical applications of microprobe analysis*. San Diego: Academic Press.

Jagadish, C. and Pearton, S., 2006. *Zinc oxide bulk, thin films and nanostructures*. Amsterdam: Elsevier.

Jing, Q., Fu, W., Li, W., Yang, H., Li, M., Ma, J., Zhou, X., Sun, M., Zhao, H., Zhang, Y., Zhao, W., Zhang, L. and Chen, H., 2012. Synthesis of snowflake-like

- multi-layered ZnO with controllable pore size and its photocatalytic property. *Applied Surface Science*, 258, ppt. 3604-3610.
- Kanematsu, H. and Barry, D.M., 2015, *Biofilm and materials science*. Switzerland: Springer International Publishing.
- Kansal, S., Sood, S., Umar, A. and Mehta, S., 2013. Photocatalytic degradation of Eriochrome Black T dye using well-crystalline anatase TiO₂ nanoparticles. *Journal of Alloys and Compounds*, 581, pp. 392-397.
- Kanukaran, C., Rajeswari, V. and Gomathisankar, P., 2011. Enhanced photocatalytic and antibacterial activities of sol-gel synthesized ZnO and Ag-ZnO. *Materials Science in Semiconductor Processing*, 14, pp. 133-138.
- Kayaci, F., Vempati, S., Ozgit-Akgun, C., Biyikli, N. and Uyar, T., 2014. Enhanced photocatalytic activity of homoassembled ZnO nanostructures on electrospun polymeric nanofibers: a combination of atomic layer deposition and hydrothermal growth. *Applied Catalysis B: Environmental*, 156-157, pp.173-183.
- Khalil, A., Gondal, M.A. and Dastageer, M.A., 2011. Augmented photocatalytic activity of palladium incorporated ZnO nanoparticles in the disinfection of *Escherichia coli* microorganism from water. *Applied Catalysis A: General*, 402, pp. 162-167.
- Khan, F., Baek, S.H., Lee, J.Y. and Kim, J.H., 2015. Work function tuning and fluorescence enhancement of hydrogen annealed Ag-doped Al-rich zinc oxide nanostructures using a sol-gel process. *Journal of Alloys and Compounds*, 647, pp. 566-572.
- Khaparde, R. and Acharya, S., 2016. Effect of isovalent dopants on photodegradation ability of ZnS nanoparticles. *Spectrochimica Acta Part A: Molecular and Biomolecular Spectroscopy*, 163, pp. 49-57.
- Khatee, A., Darvishi, R., Soltani, C., Hanifeh, Y., Safarpour, M., Ranjbar, H.G. and Joo, S.W., 2014. Synthesis and characterization of Dysprosium-doped ZnO nanoparticles for photocatalysis of a textile dye under visible light irradiation.

Industrial and Engineering Chemistry Research, 53, pp. 1924-1932.

Korake, P.V., Sridharkrishna, R., Hankare, P.P. and Garadkar, K.M., 2012. Photocatalytic degradation of phosphamidon using Ag-doped ZnO nanorods. *Toxicological & Environmental Chemistry*, 94, pp. 1075-1085.

Korake, P.V., Dhabbe, R.S., Kadam, A.N., Gaikwad, Y.B. and Garadkar, K.M., 2014. Highly active lanthanum doped ZnO nanorods for photodegradation of metasytox. *Journal of Photochemistry and Photobiology B: Biology*, 130, pp. 11-19.

Kornacki, J.L., 2010. *Principles of microbiological troubleshooting in the industrial food processing environment*. New York: Springer Science and Business Media.

Kőrösia, L., Prato, M., Scarpellini, A., Kovács, J., Dömötör, D., Kovács, T. and Papp, S., 2016. H₂O₂-assisted photocatalysis on flower-like rutile TiO₂ nanostructures: rapid dye degradation and inactivation of bacteria. *Applied Surface Science*, 365, pp. 171-179.

Krishnamoorthy, K., Veerapandian, M., Zhang, L., Yun, K. and Kim, S.J., 2012. Antibacterial efficiency of graphene nanosheets against pathogenic bacteria via lipid peroxidation. *Journal of Physical Chemistry C*, 116, pp. 17280-17287.

Kumar, R., Rana, D., Umar, A., Sharma, P., Chauhan, S. and Chauhan, M., 2015. Ag-doped ZnO nanoellipsoids: potential scaffold for photocatalytic and sensing applications. *Talanta*, 137, pp. 204-213.

Kurbanov, S., Jeon, H., Shaymardanov, Z., Rakhimov, R. and Kang, T., 2016. Photoluminescence from porous textured ZnO films grown by chemical bath deposition. *Journal of Luminescence*, 170, pp. 168-173.

Kuriakose, S., Choudhary, V., Satpati, B. and Mohapatra, S., 2014. Enhanced photocatalytic activity of Ag-ZnO hybrid plasmonic nanostructures prepared by a facile wet chemical method. *Beilstein Journal Nanotechnology*, 5, pp. 639-650.

Kusic, H., Koprivanac, N. and Bozic, A., 2013. Environmental aspects on the photodegradation of reactive triazine dyes in aqueous media. *Journal of*

Photochemistry and Photobiology A: Chemistry, 252, pp. 131-144.

- Lai, Y., Meng, M. and Yu, Y., 2010. One-step synthesis, characterizations and mechanistic study of nanosheets-constructed fluffy ZnO and Ag/ZnO spheres used for Rhodamine B photodegradation. *Applied Catalysis B: Environmental*, 100, pp. 491-501.
- Lam, S.M., Sin, J.C., Abdullah, A.Z. and Mohamed, A.R., 2012. Degradation of wastewaters containing organic dyes photocatalysed by zinc oxide: a review. *Desalination and Water Treatment*, 41, pp. 131-169.
- Lam, S.M., Sin, J.C., Abdullah, A.Z. and Mohamed, A.R., 2013, ZnO nanorods surface-decorated by WO₃ nanoparticles for photocatalytic degradation of endocrine disruptors under a compact fluorescent lamp. *Ceramics International*, 39, pp. 2343-2352.
- Lavand, A. and Malghe, Y.S., 2015. Visible light photocatalytic degradation of 4-chlorophenol using C/ZnO/CdS nanocomposite. *Journal of Saudi Chemical Society*, 19, pp. 471-478.
- Lee, J., Khoa, N., Kim, S., Kim, E. and Hahn, S., 2015. Fabrication of Au/GO/ZnO composite nanostructures with excellent photocatalytic performance. *Materials Chemistry and Physics*, 164, pp. 29-35.
- Lee, K.M., Lai, C.W., Ngai, K.S. and Juan, J.C., 2016. Recent developments of zinc oxide based photocatalyst in water treatment technology: a review. *Water Research*, 88, pp. 428-448.
- Lemma, S.M., Esposito, A., Mason, M., Brusetti, L., Cesco, S. and Scampicchio, M., 2015. Removal of bacteria and yeast in water and beery by nylon nanofibrous membrane. *Journal of Food Engineering*, 157, pp. 1-6.
- Lewinsky, A.A., 2007. *Hazardous materials and wastewater*. New York: Nova Science Publishers.
- Li, M., Noriega-Trevino, M.E., Nino-Martinez, N., Marambio-Jones, C., Wang, J., Damoiseaux, R., Ruiz, F. and Hoek, E.M.V., 2011. Synergistic bactericidal

- activity of Ag-TiO₂ nanoparticles in both light and dark condition. *Environmental Science and Technology*, 45, pp. 8989-8995.
- Li, Q., Tan, X., Zheng, X., Tang, W. and Yang, J., 2015a, A novel method for the determination of Fast Green in grape wine based on resonance Rayleigh scattering. *Journal of Molecular Structure*, 1100, pp. 14-20.
- Li, Y., Liu, J.C., Lian, X.X., Lu, T. and Zhao, F.X., 2015b. Morphology, photoluminescence and gas sensing of Ce-doped ZnO microspheres. *Transactions of Nonferrous Metal Society of China*, 25, pp. 3657-3663.
- Li, R., Song, X., Huang, Y., Fang, Y., Jia, M. and Ma, W., 2016a. Visible-light photocatalytic degradation of azo dyes in water by Ag₃PO₄: an unusual dependency between adsorption and the degradation rate on pH value. *Journal of Molecular Catalysis A: Chemical*, 421, pp. 57-65.
- Li, J., Sun, S., Qian, C., He, L., Chen, K., Zhang, T., Chen, Z. and Ye, M., 2016b. The role of adsorption in photocatalytic degradation of ibuprofen under visible light irradiation by BiOBr microspheres. *Chemical Engineering Journal*, 297, pp. 139-147.
- Li, F., Kang, Y., Chen, M., Liu, G., Lv, W., Yao, K., Chen, P. and Huang, H., 2016c. Photocatalytic degradation and removal mechanism of ibuprofen via monoclinic BiVO₄ under simulated solar light. *Chemosphere*, 150, pp. 139-144.
- Liang, Y., Guo, N., Li, L., Li, R., Ji, G. and Gan, S., 2015, Fabrication of porous 3D flower-like Ag/ZnO heterostructure composites with enhanced photocatalytic performance. *Applied Surface Science*, 332, pp. 32-39.
- Lin, W.H., Wu, J.J., Mitch, M., Chou, C., Chang, Y.M. and Yoshimura, M., 2014. Charge transfer in Au nanoparticle–nonpolar ZnO photocatalysts illustrated by surface-potential-derived three-dimensional band diagram. *The Journal of Physical Chemistry*, 118, ppt. 19814-19821.
- Lin, Q., Gao, M., Chang, J. and Ma, H., 2016. Adsorption properties of crosslinking carboxymethyl cellulose grafting dimethyldiallylammonium chloride for cationic

and anionic dyes. *Carbohydrate Polymers*, 151, pp. 283-294.

Liu, H., Shao, G., Zhao, J., Zhang, Z., Zhang, Y., Liang, J., Liu, X., Jia, H. and Xu, B., 2012. Worm-like ag/zno core-shell heterostructural composites: fabrication, characterization, and photocatalysis. *Journal of Physical Chemical C*, 116, pp. 16182-16190.

Liu, Y., Li, Q., Zhang, J.T., Sun, W.Z., Gao, S. and Shang, J.K., 2014. PdO loaded TiO₂ hollow sphere composite photocatalyst with a high photocatalytic disinfection efficiency on bacteria. *Chemical Engineering Journal*, 249, pp. 63-71.

Liu, H., Hu, Y., Zhang, Z., Liu, X., Jia, H. and Xu, B., 2015. Synthesis of spherical Ag/ZnO heterostructural composites with excellent photocatalytic activity under visible and UV irradiation. *Applied Surface Science*, 355, pp. 644-652.

Liu, Y., Wei, S. and Gao, W., 2015. Ag/ZnO heterostructures and their photocatalytic activity under visible light: effect of reducing medium. *Journal of Hazardous Materials*, 287, pp. 59-68.

Liu, J., Zhao, Y., Ma, J., Dai, Y., Li, J. and Zhang, J., 2016a. Flower-like ZnO hollow microspheres on ceramic mesh substrate for photocatalytic reduction of Cr(VI) in tannery wastewater. *Ceramics International*, 42, pp. 15968-15974

Liu, Y., He, X., Fu, Y. and Dionysiou, D., 2016b. Degradation kinetics and mechanism of oxytetracycline by hydroxyl radical-based advanced oxidation processes. *Chemical Engineering Journal*, 284, pp. 1317-1327.

Liu, J., Hu, Z., Peng, Y., Huang, H., Li, Y., Wu, M., Ke, X., Tendeloo, G. and Su, B., 2016c. 2D ZnO mesoporous single-crystal nanosheets with exposed {0001} polar facets for the depollution of cationic dye molecules by highly selective adsorption and photocatalytic decomposition. *Applied Catalysis B: Environmental*, 181, pp. 138-145

López-Muñoz, M., Arencibia, A., Segura, Y. and Raez, J., 2017. Removal of As(III) from aqueous solutions through simultaneous photocatalytic oxidation and

- adsorption by TiO₂ and zero-valent iron. *Catalysis Today*, 280, pp. 149-154.
- Lofrano, G., 2012. *Emerging compounds removal from wastewater*. Dordrecht: Springer.
- Lu, Y., Wang, L., Wang, D., Xie, T., Chen, L. and Lin, Y., 2011. A comparative study on plate-like and flower-like ZnO nanocrystals surface photovoltage property and photocatalytic activity. *Materials Chemistry and Physics*, 129, pp. 281-287.
- Lu, J., Wang, H., Peng, D., Chen, T., Dong, S. and Chang, Y., 2016. Synthesis and properties of Au/ZnO nanorods as a plasmonic photocatalyst. *Physica E: Low-dimensional Systems and Nanostructures*, 78, pp. 41-48.
- Ma, Q.L., Xiong, R., Zhai, B.G. and Huang, Y.M., 2015. Ultrasonic synthesis of fern-like ZnO nanoleaves and their enhanced photocatalytic activity. *Applied Surface Science*, 324, pp. 842-848.
- Malato, S., Fernández-Ibáñez, P., Maldonado, M., Blanco, J. and Gernjak, W., 2009. Decontamination and disinfection of water by solar photocatalysis: recent overview and trends. *Catalysis Today*, 147, pp. 1-59.
- Martin, D., 2015. *Investigation into high efficiency visible light photocatalysts for water reduction and oxidation*. Tokyo: Springer Japan.
- Matai, I., Sachdev, A., Dubey, P., Kumar, S.U., Bhushan, B. and Gopinath, P., 2014. Antibacterial activity and mechanism of Ag-ZnO nanocomposite on *S. aureus* and GFP-expressing antibiotic resistant *E.coli*. *Colloids and Surfaces B: Biointerfaces*, 115, pp. 359-367.
- Meenakshi, G., Sivasamy, A., Josephine, G.A. and Kavithaa, S., 2016. Preparation, characterization and enhanced photocatalytic activities of zinc oxide nanorods/silicon carbide composite under UV and visible light irradiations. *Journal of Molecular Catalysis A: Chemical*, 411, pp. 167-178.
- Meghana, S., Kabra, P., Chakraborty, S. and Padmavathy, N., 2015. Understanding the pathway of antibacterial activity of copper oxide nanoparticles. *Royal Society*

- of Chemistry Advances*, 5, pp. 12293-12299.
- Miao, Y., Zhang, H., Yuan, S., Jiao, Z. and Zhu, X., 2016. Preparation of flower-like ZnO architectures assembled with nanosheets for enhanced photocatalytic activity. *Journal of Colloid and Interface Science*, 462, pp. 9-18.
- Milazzo, G., 1979. *Studies in environmental science 9: energetics and technology of biological elimination of wastes*. Rome: Elsevier Scientific Publishing Company.
- Mittal, A., Kaur, D. and Mittal, J., 2009. Batch and bulk removal of a triarylmethane dye, Fast Green FCF, from wastewater by adsorption over waste materials. *Journal of Hazardous Materials*, 163, pp. 568-577.
- Mohamed, R., McKinney, D., Kadi, M., Mkhaliid, I. and Sigmund, W., 2016. Platinum/zinc oxide nanoparticles: enhanced photocatalysts degrade malachite green dye under visible light conditions. *Ceramics International*, 42, pp. 9375-9381.
- Mohammadzadeh, S., Olya, M.E., Arabi, A.M., Shariati, A. and Nikou, M.R.K., 2015. Synthesis, characterization and application of ZnO-Ag as a nanophotocatalyst for organic compounds degradation, mechanism and economic study. *Journal of Environmental Sciences*, 35, pp. 194-207.
- Moussavi, G., Hossaini, H., Jafari, S. and Farokhi, M., 2014. Comparing the efficacy of UVC, UVC/ZnO and VUV processes for oxidation of organophosphate pesticides in water. *Journal of Photochemistry and Photobiology A: Chemistry*, 290, pp. 86-93.
- Muñoz-Fernandez, L., Sierra-Fernandez, A., Milošević, O. and Rabanal, M., 2016. Solvothermal synthesis of Ag/ZnO and Pt/ZnO nanocomposites and comparison of their photocatalytic behaviours on dyes degradation. *Advanced Powder Technology*, 27, pp. 983-993.
- Nawaz, M. and Ahsan, M., 2014. Comparison of physico-chemical, advanced oxidation and biological techniques for the textile wastewater treatment. *Alexandria Engineering Journal*, 53, pp. 717-722.

- Ochei, J., 2008. *Medical laboratory science: theory and practice*. New Delhi: Tata McGraw-Hill Publishing Company Limited.
- Odeh, M., Ferhod, S. and Lafta, J., 2012. Modification of the photocatalytic activity of zinc oxide by doping silver. *International Journal of Science and Research*, 3, pp. 2133-2138
- Panda, D. and Tseng, T.Y., 2013. One-dimensional ZnO nanostructures: fabrication, optoelectronic properties, and device applications. *Journal of Material Science*. 48, pp. 6849-6877.
- Panda, N., Sahoo, H. and Mohapatra, S., 2010. Decolourization of methyl orange using fenton-like mesoporous Fe₂O₃-SiO₂ composite. *Journal of Hazardous Materials*, 185, pp. 359-365.
- Pant, H.R., Pant, B., Sharman, R.K., Amargargal, A., Kim, H.J., Park, C.H., Tijing, L.D. and Kim, C.S., 2012. Antibacterial and photocatalytic properties of Ag/TiO₂/ZnO nano-flowers prepared by facile one-pot hydrothermal process. *Ceramics International*, 39, pp. 1503-1510.
- Pant, B., Park, M., Kim, H.Y. and Park, S.J., 2016. Ag-ZnO photocatalyst anchored on carbon nanofibers: synthesis, characterization, and photocatalytic activities. *Synthetic Metals*, 220, pp. 533-537.
- Park, J., Mahmud, I., Shin, H., Park, M., Ranjkesh, A., Lee, D. and Kim, H., 2016. Effect of surface energy and seed layer annealing temperature on ZnO seed layer formation and ZnO nanowire growth. *Applied Surface Science*, 362, pp. 132-139.
- Parsons, S., 2004. *Advanced oxidation processes for water and wastewater treatment*. London: International Water Association (IWA) Publication.
- Paschoalino, F., Paes Paschoalino, M., Jordão, E. and de Figueiredo Jardim, W., 2012. Evaluation of TiO₂, ZnO, CuO and Ga₂O₃ on the photocatalytic degradation of Phenol using an annular-flow photocatalytic reactor. *Open Journal of Physical Chemistry*, 2, pp. 135-140.
- Patil, S., Mali, M., Tamboli, M., Patil, D., Kulkarni, M., Yoon, H., Kim, H., Al-

- Deyab, S., Yoon, S., Kolekar, S. and Kale, B., 2016. Green approach for hierarchical nanostructured Ag-ZnO and their photocatalytic performance under sunlight. *Catalysis Today*, 260, pp. 126-134.
- Perlman, D., and Laskin, A.I., 1981. *Advances in Applied Microbiology*. New Jersey: Academic Press, Inc.
- Podporska-Caroll, J., Myles, A., Quilty, B., McCormack, D.E., Fagan, R., Hinder, S.J., Dionysiou, D.D. and Pillai, S.C., 2017. Antibacterial properties of F-doped ZnO visible light photocatalyst. *Journal of Hazardous Materials*, 324, pp. 39-47.
- Premanathan, M., Karthikeyan, K., Jeyasubramanian, K. and Manivannan, G., 2011. Selective toxicity of ZnO nanoparticles towards Gram-positive bacteria cancer cells by apoptosis through lipid peroxidation. *Nanomedicine: Nanotechnology, Biology, Medicine*, 7, pp. 184-192.
- Qian, X., Yue, D., Tian, Z., Reng, M., Zhu, Y., Kan, M., Zhang, T. and Zhao, Y., 2016. Carbon quantum dots decorated Bi₂WO₆ nanocomposite with enhanced photocatalytic oxidation activity for VOCs. *Applied Catalysis B: Environmental*, 193, pp. 16-21.
- Rauf, M., Meetani, M. and Hisaindee, S., 2011. An overview on the photocatalytic degradation of azo dyes in the presence of TiO₂ doped with selective transition metals. *Desalination*, 276, pp. 13-27.
- Ravichandran, K., Sathish, P., Snega, S., Karthika, K., Rajkumar, P.V., Subha, K. and Sakthivel, B., Improving the antibacterial efficiency of ZnO nanopowders through simultaneous anionic (F) and cationic (Ag) doping. *Powder Technology*, 274, pp. 250-257.
- Ravishankar, T., Manjunatha, K., Ramakrishnappa, T., Nagaraju, G., Kumar, D., Sarakar, S., Anandakumar, B., Chandrappa, G., Reddy, V. and Dupont, J., 2014. Comparison of the photocatalytic degradation of trypan blue by undoped and silver-doped zinc oxide nanoparticles. *Materials Science in Semiconductor Processing*, 26, pp. 7-17.
- Redha, Z.M., Yusuf, H.A., Ahmed, H.A., Fielden, P.R., Goddard, N.J. and Baldock,

- S.J. A miniaturized injection-moulded flow-cell with integrated conducting polymer electrodes for on-line electrochemical degradation of azo dye solutions. *Microelectronic Engineering*, 169, pp. 16-23.
- Rodríguez, R., Espada, J., Pariente, M., Melero, J., Martínez, F. and Molina, R., 2016. Comparative life cycle assessment (LCA) study of heterogeneous and homogenous Fenton processes for the treatment of pharmaceutical wastewater. *Journal of Cleaner Production*, 124, pp. 21-29.
- Saharan, P., Chaudhary, G., Lata, S., Mehta, S. and Mor, S., 2015. Ultra-fast and effective treatment of dyes from water with the synergistic effect of Ni doped ZnO nanoparticles and ultrasonication. *Ultrasonics Sonochemistry*, 22, pp. 317-325.
- Salema, V., Marin, E., Martinez-Arteaga, R., Ruano-Gallego, D., Fraile, S., Margolles, Y., Teira, X., Gutierrez, C., Bodelon, G. and Fernandez, L.A., 2013. Selection of single domain antibodies from immune libraries displayed on the surface of *E.coli* cells with two β -domains of opposite topologies. *PloS one*, 8, pp. 75126-75143.
- Salma, A., Thoröe-Boveleth, S., Schmidt, T. and Tuerk, J., 2016. Dependence of transformation product formation on pH during photolytic and photocatalytic degradation of ciprofloxacin. *Journal of Hazardous Materials*, 313, pp. 49-59.
- Samadi, M., Zirak, M., Naseri, A., Khorashadizade, E. and Moshfegh, A., 2016, Recent progress on doped ZnO nanostructures for visible-light photocatalysis. *Thin Solid Films*, 605, pp. 2-19. *Plos One*, 8, pp 1-18.
- Sampaio, M.J., Lima, M.J., Baptista, D.L., Silva, A.M.T., Silva, C.G. and Faria, J.L., (in press). Ag-loaded ZnO materials for photocatalytic water treatment. *Chemical Engineering Journal*. (Accepted for publication 25 May 2016).
- Saravanan, R., Karhikeyan, N., Gupta, V.K., Thirumal, E., Thangadurai, P., Narayanan, V. and Stephen, A., 2013. ZnO/Ag nanocomposite: an efficient catalyst for degradation studies of textile effluents under visible light. *Materials Science and Engineering C*, 33, pp. 2235-2244.

- Saravanan, R., Mansoob Khan, M., Gupta, V., Mosquera, E., Gracia, F., Narayanan, V. and Stephen, A., 2015. ZnO/Ag/CdO nanocomposite for visible light-induced photocatalytic degradation of industrial textile effluents. *Journal of Colloid and Interface Science*, 452, pp. 126-133.
- Schneider, J., Bahnemann, D., Ye, J., Puma, G. and Dionysiou, D., 2016. *Photocatalysis*. Cambridge: Royal Society of Chemistry.
- Sharma, V., McKone, H.T. and Markow, P.G., 2011. A global perspective on the history, use, and identification of synthetic food dyes. *Journal of Chemical Education*, 88, pp. 24-28.
- Shinde, S.S., Bhosale, C.H. and Rajpure, K.Y., 2012. Oxidative degradation of acid orange 7 using Ag-doped zinc oxide thin films. *Photochemistry and Photobiology B: Biology*, 117, pp. 262-268.
- Shojaei, A.F. and Golriz, F., 2015. High photocatalytic activity in nitrate reduction by using Pt/ZnO nanoparticles in the presence of formic acid as hole scavenger. *Bulgarian Chemical Communications*, 47, pp. 509-514.
- Silva, C., Sampaio, M., Carabineiro, S., Oliveira, J., Baptista, D., Bacsa, R., Machado, B., Serp, P., Figueiredo, J., Silva, A. and Faria, J., 2014, Developing highly active photocatalysts: gold-loaded ZnO for solar phenol oxidation. *Journal of Catalysis*, 316, pp. 182-190.
- Sincero, A.P.S. and Sincero, G.A., 2003. *Physical-Chemical Treatment of Water and Wastewater*. Boca Raton: 2003.
- Sinha, T., Ahmaruzzaman, M. and Bhattacharjee, A., 2014. A simple approach for the synthesis of silver nanoparticles and their application as a catalyst for the photodegradation of methyl violet 6B dye under solar irradiation. *Journal of Environmental Chemical Engineering*, 2, pp. 2269-2279.
- Sohrabnezhad, S. and Seifi, A., 2016. The green synthesis of Ag/ZnO in montmorillonite with enhanced photocatalytic activity. *Applied Surface Science*, 366, pp. 33-40.

- Song, M.Y., Jurng, J.S., Park, Y.K. and Kim, B.C., 2016. An aptamer cocktail-functionalized photocatalyst with enhanced antibacterial efficiency towards target bacteria. *Journal of Hazardous Materials*, 318, pp. 247-254.
- Souza, R., Freitas, T., Domingues, F., Pezoti, O., Ambrosio, E., Ferrari-Lima, A. and Garcia, J., 2016. Photocatalytic activity of TiO₂, ZnO and Nb₂O₅ applied to degradation of textile wastewater. *Journal of Photochemistry and Photobiology A: Chemistry*, 329, pp. 9-17.
- Spellman, F.R., 2011. *Spellman's standard handbook for wastewater operators*. Boca Raton: CRC Press.
- Subash, B., Krishnakumar, B., Swaminathan, M. and Shanthi, M., 2012a. Highly efficient, solar active, and reusable photocatalyst: Zr-loaded Ag-ZnO for reactive red 120 dye degradation with synergistic effect and dye-sensitized mechanism. *Langmuir*, 29, pp. 939-949.
- Subash, B., Krishnakumar, B., Velmurugan, R., Swaminathan, M. and Shanthi, M., 2012b. Synthesis of Ce co-doped Ag-ZnO photocatalyst with excellent performance for NBB dye degradation under natural sunlight illumination. *Catalysis Science and Technology*, 2, pp. 2319-2326.
- Subash, B., Krishnakumar, B., Swaminathan, M. and Shanthi, M., 2013. Enhanced photocatalytic performance of WO₃ loaded Ag-ZnO for acid black 1 degradation by UV-A light. *Journal of Molecular Catalysis A: Chemical*, 366, pp. 54-63.
- Sun, J., Dong, S., Feng, J., Yin, X. Zhao, X., 2010. Enhanced sunlight photocatalytic performance of Sn-doped ZnO for methylene blue degradation. *Journal of Molecular Catalysis A: General*, 335, pp. 145-150.
- Suzuki, H., Araki, S. and Yamamoto, H., 2015. Evaluation of advanced oxidation processes (AOP) using O₃, UV, and TiO₂ for the degradation of phenol in water. *Journal of Water Process Engineering*, 7, pp. 54-60.
- Tahir, H., Hamed, U., Sultan, M. and Jahanzeb, Q., 2010. Batch adsorption technique for the removal of malachite green and fast green dyes by using montmorillonite clay as adsorbent. *African Journal of Biotechnology*, 9, pp. 8206-

8214.

- Talebian, N. and Zare, E., 2014. Structure and antibacterial property of nano-SiO₂ supported oxide ceramic. *Ceramics International*, 40, pp. 281-287.
- Tankhiwale, R. and Bajpai, S.K., 2012. Preparation, characterization and antibacterial application of ZnO-nanoparticles coated polyethylene films for food packaging. *Colloids and Surfaces B: Biointerfaces*, 90, pp. 16-20.
- Tao, J., Gong, Z., Yao, G., Cheng, Y., Zhang, M., Lv, J., Shi, S., He, G., Jiang, X., Chen, X. and Sun, Z., 2016. Enhanced optical and photocatalytic properties of Ag quantum dots-sensitized nanostructured TiO₂/ZnO heterojunctions. *Journals of Alloys and Compounds*, 688, pp. 605-612.
- Tayade, R., Bajaj, H. and Jasra, R., 2011. Photocatalytic removal of organic contaminants from water exploiting tuned bandgap photocatalysts. *Desalination*, 275, pp. 160-165.
- Tekumalla, S., Farhan, N., Srivatsan, T.S. and Gupta, M., 2016. Nano-ZnO particles' effect in improving the mechanical response of Mg-3Al-0.4Ce alloy. *Metals*, 6, pp. 276-286.
- Thabet, S., Simonet, F., Lemaire, M., Guillard, C. and Cotton, P., 2014. Impact of photocatalysis on fungal cells: depiction of cellular and molecular effects on *Saccharomyces cerevisiae*. *Applied and Environmental Microbiology*, 80, pp. 7527-7535.
- Tokumura, M., Sugawara, A., Raknuzzaman, M., Habibullah-Al-Mamun, M. and Masunaga, S., 2016. Comprehensive study on effects of water matrices on removal of pharmaceuticals by three different kinds of advanced oxidation processes. *Chemosphere*, 159, pp. 317-325.
- Tsai, T., Chang, H., Chang, K., Liu, Y. and Tseng, C., 2010. A comparative study of the bactericidal effect of photocatalytic oxidation by TiO₂ on antibiotic-resistant and antibiotic-sensitive bacteria. *Journal of Chemical Technology and Biotechnology*, 85, pp. 1642-1653.

- Udom, I., Ram, M., Stefanakos, E., Hepp, A. and Goswami, D., 2013. One dimensional-ZnO nanostructures: synthesis, properties and environmental applications. *Materials Science in Semiconductor Processing*, 16, pp. 2070-2083.
- Ujang, Z., Henze, M., 2006. *Municipal Wastewater Management in Developing Countries*. London, International Water Association Publishing.
- Umar, A., Chauhan, M., Chauhan, S., Kumar, R., Kumar, G., Al-Sayari, S., Hwang, S. and Al-Hajry, A., 2011. Large-scale synthesis of ZnO balls made of fluffy thin nanosheets by simple solution process: structural, optical and photocatalytic properties. *Journal of Colloid and Interface Science*, 363, pp. 521-528.
- Umar, M. and Aziz, H.A., 2013. *Photocatalytic degradation of organic pollutants in water*. Rijeka: INTECH Open Access Publisher.
- Van Doorslaer, X., Heynderickx, P., Demeestere, K., Debevere, K., Van Langenhove, H. and Dewulf, J., 2012. TiO₂ mediated heterogeneous photocatalytic degradation of moxifloxacin: Operational variables and scavenger study. *Applied Catalysis B: Environmental*, 111-112, pp. 150-156.
- Veneiri, D., Tournas, F., Gounaki, I., Binas, V., Zachopoulos, A., Kiriakidis, G. and Mantzavinos, D., 2016. Inactivation of *Staphylococcus aureus* in water by means of solar photocatalysis using metal doped TiO₂ semiconductors. *Journal of Chemical Technology and Biotechnology*, 92, pp. 43-51.
- Vyas, J., Mishra, M. and Gandhi, V., 2013. Photocatalytic degradation of alizarin cyanine green G, reactive red 195 and reactive black 5 using UV/TiO₂ process. *Material Science Forum*, 764, pp. 284-292.
- Wang, J.M., Li, C, Zhuang, H. and Zhang, J.H., 2013. Photocatalytic degradation of methylene blue and inactivation of Gram-negative bacteria by TiO₂ nanoparticles in aqueous suspension. *Food Control*, 34, pp. 372-377.
- Wang, Y.Z., Xue, X.X. and Yang, H., 2014. Preparation and characterization of carbon or/and boron-doped titania nano-materials with antibacterial activity. *Ceramics International*, 40, pp. 12533-12537.

- Wang, X., Wan, X., Xu, X. and Chen, X., 2014. Facile fabrication of highly efficient AgI/ZnO heterojunction and its application of methylene blue and rhodamine B solution degradation under natural sunlight. *Applied Surface Science*, 321, pp. 10-18.
- Wang, L., Hou, X., Li, F., He, G. and Li, L. 2015. Hybrid ZnO/Ag nanocomposites: fabrication, characterization, and their visible-light photocatalytic activity. *Materials Letters*, 161, pp. 368-371.
- Wu, D., Yue, S.T., Wang, W., An, T.C., Li, G.Y., Yip, H.Y., Zhao, L.J. and Wong, P.K., 2016. Boron doped BiOBr nanosheets with enhanced photocatalytic inactivation of Escherichia coli. *Applied Catalysis B: Environmental*, 192, pp. 35-45.
- Xia, D., Ng, T.W., An, T., Li, G., Li, Y., Yip, H.Y., Zhao, H., Lu, A. and Wong, P., 2013. A recyclable mineral catalyst for visible-light driven photocatalytic inactivation of bacteria: natural magnetic sphalerite. *Environment Science Technology*, 47, pp. 11166-11173.
- Xia, D., An, T., Li, G., Wang, W., Zhao, H. and Wong, P.K., 2016. Synergistic photocatalytic inactivation mechanisms of bacteria by graphene sheets grafted plasmonic Ag AgX (X= Cl, Br, I) composite photocatalyst under visible light irradiation. *Water Research*, 99, pp. 149-161.
- Xiang, Y., Fang, J. and Shang, C., 2016. Kinetics and pathways of ibuprofen degradation by the UV/chlorine advanced oxidation process. *Water Research*, 90, pp. 301-308.
- Xing, Z., Geng, B., Li, X., Jiang, H., Feng, C. and Ge, T., 2011. Self-assembly fabrication of 3D porous quasi-flower-like ZnO nanostrip clusters for photodegradation of an organic dye with high performance. *Crystal Engineering Communications*, 13, pp. 2137-2142.
- Xu, C., Li, J., Yang, L., Shi, F., Yang, L. and Ye, M., 2017. Antibacterial activity and a membrane damage mechanism of Lachnum YM30 melanin against *Vibrio parahaemolyticus* and *Staphylococcus aureus*. *Food Control*, 73, pp. 1445-1451.

- Yang, L., Dong, S., Sun, J., Feng, J., Wu, Q. and Sun, S., 2010. Microwave-assisted preparation, characterization and photocatalytic properties of a dumbbell-shaped ZnO photocatalyst. *Journal of Hazardous Materials*, 179, pp. 438-443.
- Yang, Z., Du, X., Zhong, W., Yin, Y., Xu, M., Au, C. and Du, Y., 2011. The synthesis of novel ZnO microcrystals through a simple solvothermal method and their optical properties. *Journal of Alloys and Compounds*, 509, pp. 3403-3408.
- Yang, C., Li, Q., Tang, L., Xin, K., Bai, A. and Yu, Y., 2015. Synthesis, photocatalytic activity, and photogenerated hydroxyl radicals of monodisperse colloidal ZnO nanospheres. *Applied Surface Science*, 357, pp. 1928-1938.
- Yang, P., Shi, W., Wang, H. and Liu, H., 2016. Screening of freshwater fungi for decolorizing multiple synthetic dyes. *Brazilian Journal of Microbiology*, 118, pp. 1-7.
- Yildirim, Ö.A., Unalan, H.E. and Durucan, C., 2013. Highly efficient room temperature synthesis of silver-doped zinc oxide (ZnO: Ag) nanoparticles: structural, optical, and photocatalytic properties. *Journal of the American Ceramic Society*, 96, pp. 766-773.
- Yu, H., Fan, H., Wang, X., Wang, J. and Cheng, P., 2015. Synthesis of flower-like ZnO nanostructures by sonochemical route and their photocatalytic activity. *Optic - International Journal for Light and Electron Optics*, 126, pp. 4397-4400.
- Zhang, Y., Xu, J., Xu, P., Zhu, Y., Chen, X. and Yu, W., 2010. Decoration of ZnO nanowires with Pt nanoparticles and their improved gas sensing and photocatalytic performance. *Nanotechnology*, 21, p. 285501.
- Zhang, D. and Zeng, F., 2011. Visible light-activated cadmium-doped ZnO nanostructured photocatalyst for the treatment of methylene blue dye. *Journal of Material Sciences*, 47, pp. 2155-2161.
- Zhang, P., Shao, C., Zhang, Z., Zhang, M., Mu, J., Guo, Z. and Liu, Y., 2011. In situ assembly of well-dispersed Ag nanoparticles (AgNPs) on electrospun carbon nanofibers (CNFs) for catalytic reduction of 4-nitrophenol. *Nanoscale*, 3, pp.

3357-3363.

- Zhang, Y., Wang, Q., Xu, J. and Ma, S., 2012. Synthesis of Pd/ZnO nanocomposites with high photocatalytic performance by a solvothermal method. *Applied Surface Science*, 258, pp. 10104-10109.
- Zhang, H., Liu, H., Dong, H., Liu, X., Jia, H. and Xu, B., 2014. Synthesis of spindle-like Ag/ZnO heterostructure composites with enhanced photocatalytic performance. *Superlattices and Microstructures*, 65, pp. 134-145.
- Zhang, X., Jiang, J. and Shi, W., 2014. Three-dimensional hierarchical ZnO nanostructures with controllable building units: hydrothermal synthesis, growth process and photocatalytic activities for organic dyes. *Micro & Nano Letters*, 9, 509-513.
- Zhang, W., Ding, L., Luo, J., Jaffrin, M. and Tang, B., 2016a. Membrane fouling in photocatalytic membrane reactors (PMRs) for water and wastewater treatment: a critical review. *Chemical Engineering Journal*, 302, pp. 446-458.
- Zhang, X., Wang, L., Liu, C., Ding, Y., Zhang, S., Zeng, Y., Liu, Y. and Luo, S., 2016b. A bamboo-inspired hierarchical nanoarchitecture of Ag/CuO/TiO₂ nanotube array for highly photocatalytic degradation of 2,4-dinitrophenol. *Journal of Hazardous Materials*, 313, pp. 244-252.
- Zhang, Y., Xu, J., Wang, Q., Pan, Z., Ma, S. and Chen, Q., 2016c. Preparation and properties of ZnO loaded with uniform Ag nanoparticles. *Materials Research Bulletin*, 73, pp. 119-124.
- Zhong, J., Li, J., He, X., Zeng, J., Lu, Y., Hu, W. and Lin, K., 2012. Improved photocatalytic performance of Pd-doped ZnO. *Current Applied Physics*, 12, pp. 998-1001.
- Zhou, H., Zhang, H., Wang, Y., Miao, Y., Gu, L. and Jiao, Z., 2015. Self-assembly and template-free synthesis of ZnO hierarchical nanostructures and their photocatalytic properties. *Journal of Colloid and Interface Science*, 448, pp. 367-373.

- Zhou, S., Zhang, S., Liu, F., Liu, J., Xue, J., Yang, D. and Chang, C., 2016. ZnO nanoflowers photocatalysis of norfloxacin: effect of triangular silver nanoplates and water matrix on degradation rates. *Journal of Photochemistry and Photobiology A: Chemistry*, 328, pp. 97-104.
- Zhu, X., Wu, D., Wang, W., Tan, F., Wong, P.K., Wang, X., Qiu, X. and Qiao, X., 2016a. Highly effective antibacterial activity and synergistic effect of Ag-MgO nanocomposite against *Escherichia coli*. *Journal of Alloys and Compounds*, 684, pp. 282-290.
- Zhu, J., Liu, S., Yang, Q., Xu, P., Ge, J. and Guo, X., 2016b. Fabrication of flower-like Ag@AgCl/Bi₂WO₆ photocatalyst and its mechanism of photocatalytic degradation. *Colloids and Surfaces A: Physicochemical and Engineering Aspects*, 489, pp. 275-281.
- Zijno, A., Angelis, I.D., Berardia, B.D., Andreoli, C., Russo, M.T., Pietraforte, D., Scorza, G., Degan, P., Ponti, J., Rossi, F. and Barone, F., 2015. Different mechanisms are involved in oxidative DNA damage and genotoxicity induction by ZnO and TiO₂ nanoparticles in human colon carcinoma cells. *Toxicology in Vitro*, 29, pp. 1503-1512.
- Zong, Y., Li, Z., Wang, X., Ma, J. and Men, Y., 2014. Synthesis and high photocatalytic activity of Eu-doped ZnO nanoparticles. *Ceramics International*, 40, pp. 10375-10382
- Zyoud, A., Dwikat, M., Al-Shakhshir, S., Ateeq, S., Shteirwi, J., Zu'bi, A., Helaf, M.H.S., Campet, G., Park, D.H., Kwon, H.S., Kim, T.W., Kharoof, M., Shawahna, R. and Hilal, H.S., 2016. Natural dye-sensitized ZnO nano-particles as photo-catalyst in complete degradation of *E.coli* bacteria and their organic content. *Journal of Photochemistry and Photobiology A: Chemistry*, 328, pp. 207-216.

APPENDICES

Appendix A: National Water Quality Standards.

National Water Quality Standards For Malaysia

PARAMETER	UNIT	CLASS					
		I	IIA	IIB	III	IV	V
Ammoniacal Nitrogen	mg/l	0.1	0.3	0.3	0.9	2.7	> 2.7
Biochemical Oxygen Demand	mg/l	1	3	3	6	12	> 12
Chemical Oxygen Demand	mg/l	10	25	25	50	100	> 100
Dissolved Oxygen	mg/l	7	5-7	5-7	3-5	< 3	< 1
pH	-	6.5-8.5	6-9	6-9	5-9	5-9	-
Colour	TCU	15	150	150	-	-	-
Electrical Conductivity*	µS/cm	1000	1000	-	-	6000	-
Floatables	-	N	N	N	-	-	-
Odour	-	N	N	N	-	-	-
Salinity	‰	0.5	1	-	-	2	-
Taste	-	N	N	N	-	-	-
Total Dissolved Solid	mg/l	500	1000	-	-	4000	-
Total Suspended Solid	mg/l	25	50	50	150	300	300
Temperature	°C	-	Normal + 2 °C	-	Normal + 2 °C	-	-
Turbidity	NTU	5	50	50	-	-	-
Faecal Coliform**	count/100 ml	10	100	400	5000 (20000) _a	5000 (20000) _a	-
Total Coliform	count/100 ml	100	5000	5000	50000	50000	> 50000

Notes

* = At hardness 50 mg/l CaCO₃

** = Maximum (unbracketed) and 24-hour average (bracketed) concentrations

N = Free from visible film sheen, discoloration and deposits

Source : EQR2006

Water Classes And Uses

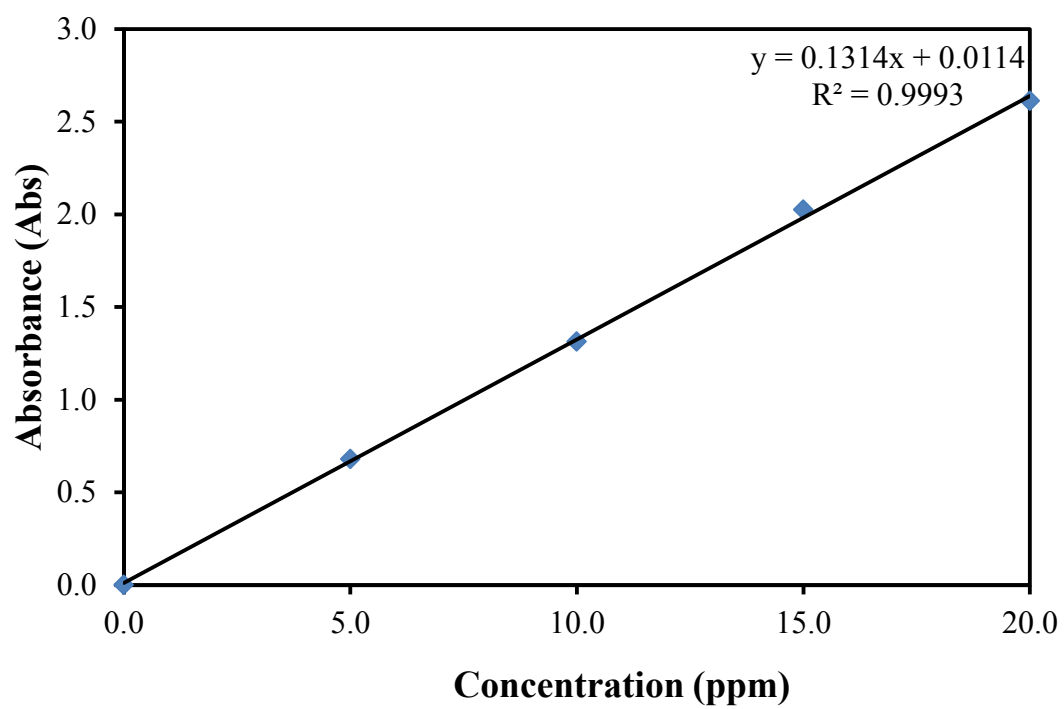
CLASS	USES
Class I	Conservation of natural environment. Water Supply I - Practically no treatment necessary. Fishery I - Very sensitive aquatic species.
Class IIA	Water Supply II - Conventional treatment. Fishery II - Sensitive aquatic species.
Class IIB	Recreational use body contact.
Class III	Water Supply III - Extensive treatment required. Fishery III - Common, of economic value and tolerant species, livestock drinking.
Class IV	Irrigation
Class V	None of the above.

Source : EQR2006

**Appendix B: Malaysian Environmental Quality (Industrial Effluents)
Regulation 2009 Fifth Schedule [Paragraph 11(1)(a)].**

**ACCEPTABLE CONDITIONS FOR DISCHARGE OF INDUSTRIAL EFFLUENT FOR MIXED EFFLUENT OF
STANDARDS A AND B**

	Parameter (1)	Unit (2)	Standard	
			A (3)	B (4)
(i)	Temperature	°C	40	40
(ii)	pH Value	-	6.0-9.0	5.5-9.0
(iii)	BOD ₅ at 20°C	mg/L	20	40
(iv)	Suspended Solids	mg/L	50	100
(v)	Mercury	mg/L	0.005	0.05
(vi)	Cadmium	mg/L	0.01	0.02
(vii)	Chromium, Hexavalent	mg/L	0.05	0.05
(viii)	Chromium, Trivalent	mg/L	0.20	1.0
(ix)	Arsenic	mg/L	0.05	0.10
(x)	Cyanide	mg/L	0.05	0.10
(xi)	Lead	mg/L	0.10	0.5
(xii)	Copper	mg/L	0.20	1.0
(xiii)	Manganese	mg/L	0.20	1.0
(xiv)	Nickel	mg/L	0.20	1.0
(xv)	Tin	mg/L	0.20	1.0
(xvi)	Zinc	mg/L	2.0	2.0
(xvii)	Boron	mg/L	1.0	4.0
(xviii)	Iron (Fe)	mg/L	1.0	5.0
(xix)	Silver	mg/L	0.1	1.0
(xx)	Aluminium	mg/L	10	15
(xxi)	Selenium	mg/L	0.02	0.5
(xxii)	Barium	mg/L	1.0	2.0
(xxiii)	Fluoride	mg/L	2.0	5.0
(xxiv)	Formaldehyde	mg/L	1.0	2.0
(xxv)	Phenol	mg/L	0.001	1.0
(xxvi)	Free Chlorine	mg/L	1.0	2.0
(xxvii)	Sulphide	mg/L	0.50	0.50
(xxviii)	Oil and Grease	mg/L	1.0	10
(xxix)	Ammoniacal Nitrogen	mg/L	10	20
(xxx)	Colour	ADMI*	100	200

Appendix C: Calibration Curve on the FG Dye at Natural pH.

PUBLICATION

Lam, S.M., Quek, J.A. and Sin, J.C., 2017. Surfactant-free synthesis of ZnO micro/nanoflowers with efficient photocatalytic antibacterial performance. *Materials Letters*, 195, pp. 34-36.